

THE ROLE OF STRATOSPHERIC PATHWAY IN LINKING ARCTIC SEA ICE  
LOSS TO THE MID-LATITUDE CIRCULATION

A Dissertation

Submitted to the Faculty

of

Purdue University

by

Bithi De

In Partial Fulfillment of the

Requirements for the Degree

of

Doctor of Philosophy

August 2019

Purdue University

West Lafayette, Indiana

**THE PURDUE UNIVERSITY GRADUATE SCHOOL**  
**STATEMENT OF DISSERTATION APPROVAL**

Dr. Yutian Wu, Co-Chair

Lamont-Doherty Earth Observatory, Columbia University

Dr. Wen-wen Tung, Co-Chair

Department of Earth, Atmospheric, and Planetary Sciences

Dr. Alexander Gluhovsky

Department of Earth, Atmospheric, and Planetary Sciences

Dr. Daniel R. Chavas

Department of Earth, Atmospheric, and Planetary Sciences

Dr. Robert L. Nowack

Department of Earth, Atmospheric, and Planetary Sciences

Dr. Harshvardhan Harshvardhan

Department of Earth, Atmospheric, and Planetary Sciences

Dr. Xiangdong Zhang

International Arctic Research Center, University of Alaska-Fairbanks

**Approved by:**

Dr. Daniel Cziczo

Head of the Department of Earth, Atmospheric, and Planetary Sciences

In loving memory of my  
grandpa Harishankar De and teacher Chandrasekhar Dey.

## ACKNOWLEDGMENTS

I sincerely thank my supervisors, Dr. Yutian Wu and Dr. Wen-wen Tung, for their guidance and constant support in various ways. I am grateful to Dr. Yutian Wu for her patience, encouragement and attention to detail that has helped me to grow as an independent researcher. I extend gratitude to Dr. Wen-wen Tung for her exceptional assistance in last two years as my co-advisor in Purdue.

I would like to thank my committee members, Dr. Alexander Gluhovsky, Dr. Harshvardhan Harshvardhan, Dr. Robert L. Nowack and Dr. Daniel R. Chavas from Purdue University as well as Dr. Xiangdong Zhang from University of Alaska Fairbanks for being available at different stages of my research and agreeing to serve on my thesis committee. I am also thankful to Dr. Lorenzo M. Polvani and Dr. Mingfang Ting at Lamont-Doherty Earth Observatory, Columbia University for insightful discussion.

I would like to thank fellow researchers in the department of Earth-Atmospheric-Planetary Sciences (EAPS) at Purdue University for enormous help in learning and to continue my work successfully. My thank goes to all administrative and computing staff members at Purdue University for their much needed support.

These acknowledgments would not be complete without thanking my parents. I can not thank them enough for their constant support and encouragement over the years. I am also grateful to my extended family, in-laws and friends. Finally, I am deeply thankful and grateful to my husband, Sandip, for always being there for me. His continued support and understanding helped me immensely as I completed my thesis.

## TABLE OF CONTENTS

	Page
LIST OF TABLES . . . . .	vii
LIST OF FIGURES . . . . .	viii
ABBREVIATIONS . . . . .	xiii
ABSTRACT . . . . .	xiv
1 INTRODUCTION . . . . .	1
1.1 Background . . . . .	1
1.2 Motivations . . . . .	4
1.2.1 Stratospheric influence in linking AA to the mid-latitude cir- culation . . . . .	4
1.2.2 Dynamical linkage between Barents-Kara Sea sea ice loss and a colder Siberia . . . . .	6
1.2.3 Impacts of regional Arctic amplification on the mid-latitudes . .	7
1.3 Outline . . . . .	9
2 ROBUSTNESS OF THE STRATOSPHERIC PATHWAY IN LINKING THE BARENTS-KARA SEA SEA ICE VARIABILITY TO THE MID-LATITUDE CIRCULATION IN CMIP5 MODELS . . . . .	11
2.1 Introduction . . . . .	11
2.2 Data and Methods . . . . .	14
2.2.1 Observations . . . . .	14
2.2.2 CMIP5 models . . . . .	15
2.2.3 Diagnostics . . . . .	17
2.3 Results . . . . .	19
2.3.1 Prolonged response in tropospheric circulation . . . . .	19
2.3.2 Dynamics of troposphere-stratosphere coupling . . . . .	23
2.3.3 Missing mid-winter Eurasian cooling . . . . .	28
2.4 Conclusions and Discussion . . . . .	31
3 ROLE OF THE STRATOSPHERIC PATHWAY IN LINKING THE BARENTS- KARA SEA SEA ICE LOSS TO A COLDER SIBERIA . . . . .	35
3.1 Introduction . . . . .	35
3.2 Data and Methodology . . . . .	37
3.2.1 Numerical Model . . . . .	37
3.2.2 Experimental design . . . . .	38
3.2.3 Observations . . . . .	39

	Page
3.2.4	Diagnostics . . . . . 39
3.3	Results . . . . . 41
3.3.1	Colder Siberia in response to BKS SIC retreat . . . . . 41
3.3.2	Mechanism of Siberian cooling . . . . . 44
3.3.3	Role of stratosphere-troposphere coupling . . . . . 46
3.4	Conclusions and Discussion . . . . . 48
4	ARE MID-LATITUDE CIRCULATION RESPONSES LINEARLY ADDITIVE TO REGIONAL ARCTIC AMPLIFICATION? INSIGHTS FROM AN IDEALIZED ATMOSPHERIC GENERAL CIRCULATION MODEL . . 50
4.1	Introduction . . . . . 50
4.2	Data and Methods . . . . . 52
4.2.1	Observations . . . . . 52
4.2.2	Numerical Model . . . . . 53
4.2.3	Experimental Design . . . . . 53
4.3	Results . . . . . 57
4.3.1	Simulated atmospheric circulation response to regional AA . . . 57
4.3.2	Non-linearity and stratosphere-troposphere coupling . . . . . 59
4.3.3	Variation of non-linearity with forcing magnitude . . . . . 61
4.4	Conclusions and Discussion . . . . . 62
5	CONCLUSIONS AND FUTURE DIRECTIONS . . . . . 65
	REFERENCES . . . . . 71
A	SUPPLEMENTARY ILLUSTRATIVE MATERIAL . . . . . 81

## LIST OF TABLES

Table	Page
2.1 Horizontal resolution, model top height and vertical resolution of the high-top models from CMIP5 archive analyzed in this study. . . . .	15
2.2 Horizontal resolution, model top height and vertical resolution of the low-top models from CMIP5 archive analyzed in this study. . . . .	16

## LIST OF FIGURES

Figure	Page
1.1 Schematic of stratospheric polar vortex. The blue curve shows the circumpolar stratospheric polar vortex and the red curve shows the circumpolar tropospheric polar vortex in boreal winter. Adapted from Waugh et al. (2017). . . . .	3
1.2 Schematic of climatological zonal-mean zonal wind in January (winter) and July (summer). The diamonds mark the hemispheric maximum of the zonal wind at each pressure level and the approximate edge of the polar vortex for that hemisphere. Adapted from Waugh et al. (2017). . . . .	3
1.3 The regional mask around the Arctic provided by the National Snow and Ice Data Center (NSIDC). It includes Arctic Ocean, Barents and Kara Seas, Greenland Sea, Baffin Bay/Davis Strait/Labrador Sea, Gulf of St. Lawrence, Hudson Bay, Canadian Archipelago, Bering Sea, and Sea of Okhotsk. Adapted from Ahn et al. (2014). . . . .	8
2.1 Regression of 700 hPa zonal wind anomaly (in m/s per 1 standard deviation of BKS SIC loss) during February on the normalized BKS SIC variability in the previous November and December in (a) high-top models and (b) low-top models (color shadings and white contours with contour interval of 0.04 m/s), respectively. The dashed black line indicates the climatological jet position. The BKS region is highlighted in thick black box. The dots imply that at least 80% of the models agree on sign of change. (c) and (d) are similar to (a) and (b) but for 500 hPa geopotential height (color shadings and white contour with contour interval of 0.5m) during February in lower panel. . . . .	18
2.2 Monthly evolution of zonal mean zonal wind (in m/s per 1 standard deviation of BKS SIC loss) averaged between 50°–70°N from November to April, due to BKS SIC loss in November and December in (a) high-top models and (b) low-top models (color shadings). The red circles represent minimum value for each pressure level. The black dots indicate that at least 80% models agree on sign of change. . . . .	20

Figure	Page	
2.3	Similar to Fig. 2.1 but for 100mb eddy heat flux (color shadings, in $K \cdot m/s$ per 1 standard deviation of SIC loss) in December in (a) high-top models and (b) low-top models, respectively. The black contours (with a contour interval of $4 K \cdot m/s$ ) indicate climatological poleward heat flux where positive values are solid while negative values are dashed. (c), (d) and (e), (f) are similar to (a) and (b) but for wave-1 and wave-2 100mb eddy heat flux response (color shadings), respectively. The black contours have an interval of $1 K \cdot m/s$ in (c), (d), (e) and (f). . . . .	22
2.4	Wave-1 geopotential height regression (per 1 standard deviation of BKS SIC loss) at 500 mb (color shadings) and 50mb (black contours with contour interval of 0.5 m) during December (a and b) and February (c and d), respectively. Contour interval is 0.5 m. Positive values in contours are solid brown while negative values are dashed blue and the zero contour is omitted. The solid brown dot and solid blue dot represent the maxima and minima at $60^\circ N$ , as an example, at 500mb. The solid red dot and solid black dot represent the corresponding maxima and minima at 50mb, respectively. . . . .	24
2.5	Similar to Fig. 2.4 but for wave-2 geopotential height regression (in color shadings and black contours with contour interval of 0.25 m). Note the difference in colorbar from Figure 2.4. . . . .	26
2.6	Similar to Fig. 2.1 but for surface air temperature (color shadings) and 500 hPa geopotential height (black contours) during February in (a) high-top and (b) low-top models. Positive values in geopotential height are solid while negative values are dashed. Contour interval is 0.5 m. The regions to construct the Ural mountain ridge anomaly and the Eurasia cold anomaly are highlighted in thick black and green boxes, respectively. (c) Scatter plot of 500 hPa geopotential height anomaly over $60^\circ-80^\circ N$ and $30^\circ-90^\circ E$ versus Eurasia SAT (ECI) over $40^\circ-60^\circ N$ and $80^\circ-120^\circ E$ during February associated with BKS SIC loss in the previous November and December in high-top models (in blue) and low-top models (in red). The numbers represent the corresponding models listed in Tables 2.1 and 2.2. The multi-model mean is shown as asterisk in blue for high-top and red for low-top, respectively. The correlation coefficient ( $r$ ) and p-value are shown in the legend for high-top and low-top models, respectively. . . .	29

Figure	Page
3.1 Regression of surface air temperature (color shadings, units: K/1 standard deviation of BKS SIC loss) and geopotential height at 500 hPa (contours, units: m/1 standard deviation of BKS SIC loss) during JF onto normalized BKS SIC index in November. Positive values in contours are solid black while negative values are dashed black and the zero contour is omitted. The black box highlights the BKS area over 70°–82°N and 10°–110°E. The stipplings indicate that the temperature response is significant at 95% confidence level using the students <i>t</i> -test. . . . .	40
3.2 Responses of surface air temperature (color shadings, units: K) and geopotential height at 500 hPa (contours, units: gpm, contour interval 40gpm) in (a) BKS_FL, (b) BKS_TP and (c) BKS_SP experiments, respectively. Positive values in contours are solid black line while negative values are dashed black line and the zero contour is omitted. The black box highlights the area corresponding to the ridge near the Ural mountains over 60°–80°N and 30°–90°E and the purple box highlights the area corresponding to maximum Siberia cooling over 48°–65°N and 60°–130°E. No extrapolation is performed when the pressure level is outside of the range of surface pressure.	42
3.3 Same as Fig. 3.2 except wind vectors at 850 hPa are shown instead of geopotential heights. . . . .	43
3.4 Decomposition of temperature budget analysis following Rodwell and Hoskins (2001). Red text indicates the dominate terms. . . . .	44
3.5 Horizontal temperature advection response at 850 hPa in BKS_FL run (a), and its dynamic (d) and thermodynamic components (g). (b, e, h) and (c, f, i) are the same as (a, d, g) but for BKS_TP run and BKS_SP run, respectively. The area, where the pressure level is outside of the range of surface pressure, is masked. . . . .	45
3.6 Dynamic component of horizontal temperature advection response at 850 hPa in BKS_FL run (a), and its zonal (d) and meridional components (g). (b, e, h) and (c, f, i) are the same as (a, d, g) but for BKS_TP run and BKS_SP run, respectively. The area, where the pressure level is outside of the range of surface pressure, is masked. . . . .	47
4.1 Spatial structure of the prescribed heating rate (color shadings and black contours, with contour interval 0.4 K/day) at the lowest model level for $Q_0 = 3.5$ K/day. . . . .	55

Figure	Page	
4.2	Response of zonal mean zonal wind (color shadings and contours, with contour interval of 1 m/s upto -/+ 6 m/s and 2 m/s beyond that) in the FULL runs with a heating magnitude of 3.5 K/day in (a) ESC, (b) BDL, (c) BKS, (d) ALL experiments. (e) is the sum of the circulation responses to individual regional forcings and (f) is the difference between (d) and (e). Black dots represent the climatological location of jet maximum. Stippling denotes the regions that are statistically significant at the 95% confidence level using a two-sided <i>t</i> -test. . . . .	56
4.3	Response of EP flux (vector) and EP flux divergence (color shading, units: m/s/day) for the vertical component in (a) ESC, (b) BDL, (c) BKS, respectively. The EP flux is multiplied by the square root of 1000/pressure (hPa) to better demonstrate the waves in the stratosphere. Note that the vectors above 100hPa have been further magnified by a factor of 8 in ESC and by a factor of 6 for BDL and BKS. . . . .	58
4.4	Similar to fig. 4.2 but for no-vortex configuration. . . . .	60
4.5	(a) Absolute value of percentage of non-linearity in zonal mean zonal wind response as obtained with 3.5 K/day forcing magnitude in FULL run. The ratio percentage is calculated as residual (Fig. 2f) divided by ALL (Fig. 2d). The values in the denominator (ALL) that lie between -0.2 and +0.2 m/s are shown in gray contours with contour interval of 0.1 m/s, where negative values are shown in dashed line, positive values are shown in solid line and zero value is shown in black. Black dots represent the climatological location of the jet maxima. (b) Similar to (a) except for the no-vortex runs. (c) Relation between the forcing magnitude and non-linearity ratio at 700hPa, 50°N (red dots, also in Fig. 3ab) and 20hPa, 50°N (blue dots, also in Fig. 3ab in dark blue dots), respectively, in FULL run. The corresponding values using no-vortex configuration are shown in squares. . . . .	64
A.1	Multi-model spread in monthly BKS SIC among the high-top (in light red) and low-top (in light blue) models and in the observations (black line). . .	81
A.2	Response of 700mb zonal wind anomaly (in m/s per 1 standard deviation of BKS SIC loss) in winter months in observations due to BKS SIC loss in the previous November and December. The sign is reversed for the normalized BKS SIC to emphasize the SIC loss. The dashed black line indicates the climatological jet position. The BKS region is highlighted in thick black box. The dots indicate that the responses are statistically significant at the 95% confidence level.. . . .	82

Figure	Page
A.3 Response in jet speed (in m/s per 1 standard deviation of BKS SIC loss) over the region with the strongest weakening ( $45^{\circ} - 90^{\circ}\text{N}$ and $315^{\circ} - 360^{\circ}\text{E}$ ) vs. climatological jet latitude (in $^{\circ}\text{N}$ ) and climatological jet speed (in m/s) over the North Atlantic sector ( $45^{\circ} - 90^{\circ}\text{N}$ and $270^{\circ} - 360^{\circ}\text{E}$ ) in (a) upper panel and (b) lower panel, respectively. The numbers represent the corresponding high-top models (in blue) and low-top models (in red) listed in Tables 2.1 and 2.2. The multi-model mean is shown as star in blue for high-top and in red for low-top, respectively. The correlation coefficient ( $r$ ) and p-value are shown in the legend for high-top and low-top models, respectively . . . . .	83
A.4 Response of detrended surface air temperature (SAT) (in K per 1 standard deviation of SIC loss) during Dec. and Jan. associated with concurrent SIC loss in Dec. and Jan. (DJ) over the (a) ESC and (b) BDL regions, respectively. (c) shows the SAT response during Nov. due to SIC loss over BKS in Nov (N). The black box highlights the (a) ESC, (b) BDL and (c) BKS area, respectively. The dots indicate that the response is statistically significant at the 95% confidence level using t-test. . . . .	84
A.5 Vertical profile of zonal mean of prescribed heating rate with a forcing magnitude of 3.5 K/day over ESC, BDL and BKS, respectively. Contour interval is 0.2 K/day. . . . .	85
A.6 Response of detrended zonal mean zonal wind anomaly (in m/s per 1 standard deviation of SIC loss) during Dec-Jan-Feb associated with SIC loss in (a) Dec-Jan over ESC, (b) Dec-Jan over BDL and (c) Nov over BKS, respectively, in both color shadings and contours. . . . .	86
A.7 Similar to Fig. 4.5 (a) except for forcing magnitude of (a) 2.5 K/day, (b) 3 K/day, (c) 4 K/day and (d) 4.5 K/day, respectively. . . . .	87

## ABBREVIATIONS

AA	Arctic Amplification
SIC	Sea Ice Concentration
CMIP5	Coupled Model Intercomparison Project Phase 5
BKS	Barents-Kara Sea
ESC	East Siberia and Chukchi Sea
BDL	Baffin Bay - David Strait and Labrador Sea
WACS	Warm Arctic Cold Siberia (or Continents)
EP flux	Eliassen Palm flux
NAO	North Atlantic Oscillation
NAM	Northern Annular Mode
AO	Arctic Oscillation
NH	Northern Hemisphere
AGCM	Atmospheric General Circulation Model
SC-WACCM4	Specified Chemistry Whole Atmosphere Community Climate Model version 4
CAM4	Community Atmosphere Model version 4

## ABSTRACT

De, Bithi Ph.D., Purdue University, August 2019. The Role of Stratospheric Pathway in Linking Arctic Sea Ice Loss to the Mid-latitude Circulation . Major Professors: Yutian Wu and Wen-wen Tung.

Rapid melting of sea ice and an increased warming have been observed over the Arctic since 1990s and is expected to continue in future climate projections. Possible linkage between the Arctic sea ice and the Northern Hemisphere mid-latitude circulation has been studied previously but is not yet fully understood. This dissertation investigates the influence of the Arctic on the mid-latitudes and the underlying dynamical mechanisms. Specifically, we hypothesize that the stratosphere and its coupling with the troposphere play an important role in amplifying and extending the mid-latitude circulation response to arctic warming.

First, we assess the robustness of the stratospheric pathway in linking the sea ice variability, specifically over the Barents-Kara Sea (BKS), in late autumn and early winter to the mid-latitude circulation in the subsequent winter using an ensemble of global climate model simulations. We analyze two groups of models from the Coupled Model Intercomparison Project phase 5 (CMIP5) archive, one with a well-resolved stratosphere (high-top models) and the other with a poorly-resolved stratosphere (low-top models) to distinguish the role of the stratospheric pathway. It has been found that, collectively, high-top models are able to capture the persistent mid-latitude circulation response in the subsequent winter. The response in low-top models is, however, weaker and not as long-lasting most likely due to lack of stratospheric variability. Diagnosis of eddy heat flux reveals that stronger vertical wave propagation leads to a stronger response in stratospheric polar vortex in high-top models. The results robustly demonstrate that multi-model ensemble of CMIP5

high-top models are able to capture the prolonged impact of sea ice variability on the mid-latitude circulation and outperforms the low-top models in this regard.

We further explore the dynamical linkage between the BKS sea ice loss and the Siberian cold anomalies using a comprehensive Atmospheric General Circulation Model (AGCM), with a well-resolved stratosphere, with prescribed sea ice loss over BKS region. Decomposition of dynamic and thermodynamic components suggests a dynamically induced warm Arctic cold Siberia pattern in the winter following sea ice loss over the BKS in late autumn. Specifically, the results show that the meridional component of the horizontal temperature advection, from the Arctic into the Siberia, dominates in driving a cold temperature anomaly. Additionally, we conduct targeted experiments in order to quantitatively measure the role of the stratospheric pathway. We find that the stratosphere plays a critical role in the tropospheric circulation anomaly characterized by an intensified ridge-trough pattern that is attributable for the enhanced meridional temperature advection from the Arctic into the Siberia.

Next, we extend our study to investigate the sensitivity to geographical location of Arctic sea ice loss and associated warming in modulating the atmospheric circulation. In particular, we assess the linear additivity of the regional Arctic sea ice loss and Arctic Amplification (AA), using a simplified dry dynamical core model. We find that the responses to regional AA over three key regions of the Arctic, i.e. Barents-Kara Sea, East Siberia-Chukchi sea and Baffin Bay-Labrador Sea, separately, show similar equatorward shift of the tropospheric jet but differences in the stratospheric polar vortex. In addition, responses to regional Arctic Amplification are not linearly additive and the residual resembles a positive Northern Annular Mode-like structure. Additional targeted experiments further diagnose the role of the stratosphere in the non-linearity. It is found that the stratosphere-troposphere coupling plays an important role in driving the non-linear circulation response to regional AA.

The findings of our research leads to a systematic understanding of the role of the stratospheric pathway in modulating the mid-latitude circulation response to Arctic sea ice loss and accompanied surface warming. Our study suggests that the repre-

sentation of the stratosphere in climate models plays an important role in correctly simulating the mid-latitude circulation response and could be accountable for the some of the discrepancies among recent studies. Additionally, the result indicates that studying the regional sea ice loss might not provide the full picture of pan-Arctic sea ice melting and caution the use of regional sea ice to explain the recent trend.

# 1. INTRODUCTION

## 1.1 Background

Rapid sea ice loss accompanied with amplified warming over the Arctic has been observed in the past few decades (Screen and Simmonds, 2010). In particular, the Arctic warming is more than twice faster compared to the global average and the trend is expected to continue in global climate model projections (Collins and Coauthors, 2013; Serreze and Barry, 2011). The enhanced response of the Arctic to greenhouse gas forcing is widely known as the Arctic Amplification (AA).

Specifically, the exposed open ocean water absorbs more solar radiation, and therefore, an increase in surface to atmosphere heat fluxes amplifies the near surface warming. Several intertwined factors such as enhanced atmospheric and oceanic transport, cloud cover and long wave radiation feedback, increased black carbon aerosol concentration (Cohen et al., 2014; Collins and Coauthors, 2013; Gong et al., 2017; Pithan and Mauritsen, 2014; Serreze and Barry, 2011, and references therein) may have also contributed in shaping the remarkable warming trend.

In correspondence with the AA, an increasing frequency of extreme weather events across North America and Europe, such as extreme cold snaps, heavy snow fall, intense flooding, has gained scientific and socio-economic attention. A potential influence of the Arctic warming on the mid-latitude weather, specifically via atmospheric circulation, has been suggested by numerous observational and modeling studies (see review papers Barnes and Screen, 2015; Cohen et al., 2014; Vihma, 2014, and references therein). There is a growing recognition that the consequences of the dramatic sea ice melting and AA are not confined within the Arctic itself and are critically important to the global climate system, such as persistent regional weather systems leading to extreme floods, droughts, heat waves or cold spells are likely to increase due

to AA (Francis et al., 2018). Nevertheless, how the AA can impact the mid-latitudes remains inconclusive due to incomplete understanding of how the interaction mechanism works (Francis, 2017; Screen et al., 2018b).

The dynamics of the Arctic and mid-latitude linkage is complex and it is hard to disentangle among several contributing factors (Overland et al., 2016). Considerable diversities exist in the previous modeling investigations (Screen et al., 2018b) in terms of inconsistent results. The majority of the studies have detected a negative North Atlantic Oscillation (NAO) or Northern Annular Mode (NAM) like pattern due to sea ice loss (Bader et al., 2011, references therein).

It has also been suggested that the recently observed cold winter extremes over the mid-latitudes are attributable to the declining sea ice and associated AA (Francis and Vavrus, 2012; Kug et al., 2015; Mori et al., 2014). More importantly, an equatorward shift of the mid-latitude jet stream associated with a weakening of the stratospheric polar vortex have been widely documented (Jaiser et al., 2013; Kim et al., 2014; Sun et al., 2015; Zhang et al., 2017). At the same time, others have argued that the AA has no significant influence on the NAO variability (Screen et al., 2013) or in driving extreme cold events over the mid-latitudes in the recent few decades (McCusker et al., 2016; Screen et al., 2015; Sun et al., 2016). Additionally, the small sample of years in observations makes it challenging to distinguish robust conclusion.

The sea ice loss and AA can influence the atmospheric circulation via a tropospheric pathway and a stratospheric pathway (Sun et al., 2015). The transient eddy feedback has been attributable in setting up the tropospheric adjustment to the meridional temperature gradient and baroclinic instability (Screen et al., 2018a; Wu and Smith, 2016, and references therein). The stratospheric pathway, on the other hand, is composed of a two-way dynamical coupling mechanism that modulates the winter-time stratospheric polar vortex, resulting in a downward influence on the tropospheric circulation (Simpson et al., 2019).

A schematic of circumpolar stratospheric and tropospheric polar vortex during boreal winter is shown in Figure 1.1 (adapted from Waugh et al. (2017)). Note that,

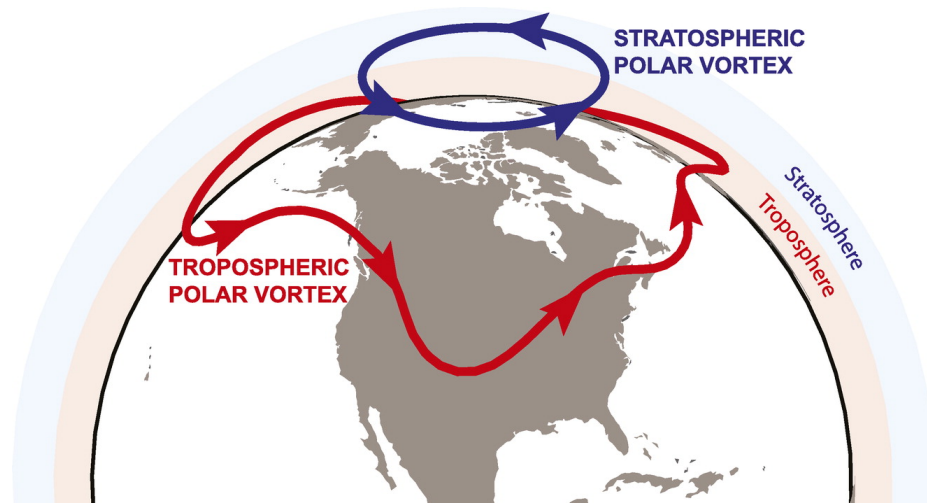


Figure 1.1. Schematic of stratospheric polar vortex. The blue curve shows the circumpolar stratospheric polar vortex and the red curve shows the circumpolar tropospheric polar vortex in boreal winter. Adapted from Waugh et al. (2017).

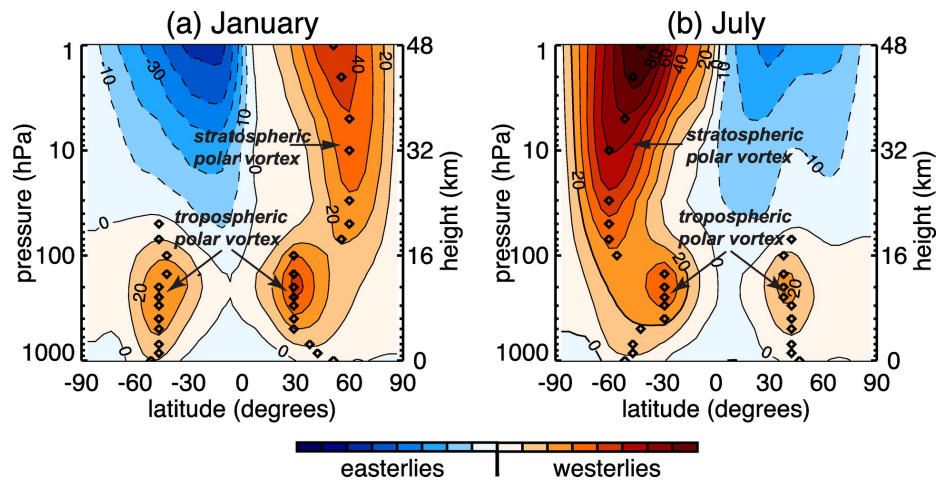


Figure 1.2. Schematic of climatological zonal-mean zonal wind in January (winter) and July (summer). The diamonds mark the hemispheric maximum of the zonal wind at each pressure level and the approximate edge of the polar vortex for that hemisphere. Adapted from Waugh et al. (2017).

the tropospheric polar vortex exists year around while the stratospheric polar vortex is a dominant circulation feature of the boreal winter (Fig. 1.2). The variability of the stratospheric polar vortex and its impact on the large-scale tropospheric circulation in boreal winter has been increasingly recognized in last two decades (e.g. Baldwin and Dunkerton, 2001; Waugh et al., 2017). In particular, Thompson and Wallace (1998) discovered that the variability in the stratospheric polar vortex is followed by tropospheric circulation anomalies that spans over the hemispheric scale. The stratosphere-troposphere coupling works in a two-way mechanism: planetary scale Rossby waves emanating from the troposphere can propagate upward into the stratosphere, decelerate the stratospheric zonal wind via wave-mean flow interaction, which in turn affects the tropospheric circulation via downward influence mechanism (Lee and Black, 2015, and references therein). It has also been suggested that the coupling between the stratosphere and the troposphere is an important source of predictability of the surface weather regimes on seasonal to sub-seasonal scale (e.g. Gerber et al., 2012, and references therein). Understanding to what extent AA affects the stratospheric polar vortex, and further downward influence on the tropospheric circulation is the major focus of the thesis.

Therefore, it is crucial to better understand how the dynamics of the Arctic and mid-latitude teleconnection works. The key purpose of this dissertation is to diagnose 1) what is the robust response of the atmospheric circulation to the Arctic sea ice loss and AA, and 2) what is the underlying mechanism, specifically what is the role of the stratospheric pathway in linking the Arctic to the midlatitudes.

## **1.2 Motivations**

### **1.2.1 Stratospheric influence in linking AA to the mid-latitude circulation**

Previously, Wu and Zhang (2010) found a lagged response in the tropospheric circulation to autumn sea ice concentration (SIC) using observations. This delayed time scale of about 2-4 months, when SIC leads the circulation, is much longer than

the timescale of the troposphere. The underlying dynamics of the delayed response is not well understood following the previously hypothesized linkage mechanisms between the Arctic and the mid-latitudes such as change in atmospheric circulation and a wavier jet stream (Cohen et al., 2014).

Recent studies have suggested that in addition to the tropospheric pathway, the stratospheric pathway might be attributable in linking the Arctic sea ice loss, especially over the Barents and Kara Sea (BKS), with the mid-latitude circulation (Kim et al., 2014; Nakamura et al., 2016; Sun et al., 2015). The proposed mechanism argues that increased planetary-scale waves, forced by reduced sea ice in late autumn, can vertically propagate into the stratosphere and weaken the stratospheric polar vortex (Jaiser et al., 2013; Kim et al., 2014). The anomalous stratospheric circulation can persist for 1-2 months and later migrate downward resulting in a negative NAM-like pattern near the surface, and thus, a prolonged circulation response in the subsequent winter (Kim et al., 2014; Nakamura et al., 2016; Zhang et al., 2017).

In order to diagnose the wave-mean flow interaction, associated with the troposphere-stratosphere coupling, Eliassen Palm flux (EP flux) has been widely used (Edmon et al., 1980). In a spherical-pressure coordinate, the quasi-geostrophic EP flux is written as  $\vec{F} = [F_\phi, F_p]$ , where  $F_\phi = -a \cos \phi \langle u^* v^* \rangle$ ,  $F_p = a f \cos \phi \frac{\langle v^* \theta^* \rangle}{\langle \theta \rangle_p}$ ,  $f$  is Coriolis parameter,  $\theta$  is potential temperature,  $u$  and  $v$  are the zonal and meridional wind velocities, angle brackets denote zonal average, and asterisk denotes deviation from zonal average. The direction of the flux vectors generally indicates the propagation of waves and the flux divergence measures the wave forcing on the zonal wind. Specifically, the upward propagation phase is characterized with enhanced planetary scale wave propagation into the stratosphere from the troposphere and the convergence of EP flux and the weakening of the stratospheric polar vortex. The downward coupling mechanism has been extensively investigated previously (for example Simpson et al., 2009).

Although the delayed impact of the BKS SIC via the stratosphere has been previously studied, it has been derived using single model simulation (Kim et al., 2014;

Nakamura et al., 2016; Zhang et al., 2017) or a limited period of observations (Yang et al., 2016). In addition, inconsistent circulation responses, such as a stronger polar vortex or a positive NAO like pattern (Cai et al., 2012; Cassano et al., 2014; Screen et al., 2013; Strey et al., 2010), due to SIC loss contradicts the hypothesis. Therefore, re-visiting the stratosphere-troposphere coupling mechanism is important for a robust understanding of how the delayed circulation response to BKS SIC works. Following Screen et al. (2018b), we advocate that ensemble of simulations from diverse coupled models can provide valuable insights into the physical mechanism, by minimizing the biases due to a specific model physics and experimental design. In this dissertation, we investigate the stratosphere-troposphere coupling mechanism using a group of high-top models with well-resolved stratosphere and a group of low-top models with poorly-resolved stratosphere. We compare the responses between the two groups through the chain of events linking the autumn BKS SIC variability to the mid-winter circulation anomaly. The consistent differences allow us to uniquely distinguish the role of the stratospheric pathway in a multi-model framework.

### **1.2.2 Dynamical linkage between Barents-Kara Sea sea ice loss and a colder Siberia**

The impacts of the Arctic sea ice loss, especially over the BKS region, on the mid-latitude circulation via a stratospheric pathway have been widely documented (De and Wu, 2018; Kim et al., 2014; Nakamura et al., 2016; Zhang et al., 2017, for example).

Although, it is still inconclusive, whether and how the rapid sea ice decline and associated surface warming over the Arctic can influence the recently emerged cold temperature anomalies over the adjacent northern continents (Shepherd, 2016), which has been referred as the “Warm Arctic Cold Siberia (or Continents)” (WACS) patterns (Overland et al., 2011). A potential linkage between the rapid sea ice decline and AA and the cold winter events has been proposed previously (Kug et al., 2015; Mori

et al., 2014; Vihma, 2014). However, the connection has been opposed by some studies suggesting that the extreme cold events are likely associated with the atmospheric natural variability (McCusker et al., 2016; Screen et al., 2015, for example). The conflicting results indicate that the relation between the Arctic and colder Siberia is still inconclusive. Additionally, to what extent the troposphere-stratosphere interaction can influence the Siberian cooling has not been explored.

Therefore, to explicitly assess the role of BKS sea ice decline on Siberian temperature, we use a comprehensive AGCM with a well resolved stratosphere and perform model experiments forced with BKS sea ice decline. We analyze the temperature budget and examine the relative contributions of the thermodynamical and dynamical components to induce the total temperature response.

Additionally, the study performs targeted experiments to explicitly quantify the role of the stratosphere-troposphere coupling in driving the large-scale circulation anomaly.

### **1.2.3 Impacts of regional Arctic amplification on the mid-latitudes**

The first two sections in this dissertation complement previously hypothesized linkage between the BKS region and the mid-latitudes by providing insights into the underlying dynamical mechanisms via a stratosphere-troposphere interaction. However, it is important to note that the atmospheric circulation response is sensitive to the geographical location and spatial pattern of the Arctic sea ice loss (Pedersen et al., 2016; Screen, 2017; Screen et al., 2018b; Sun et al., 2015). For example, a stronger stratospheric polar vortex has been found due to SIC loss confined over the Pacific sector of the Arctic in contrast to a weaker stratospheric polar vortex associated with BKS SIC loss (McKenna et al., 2018; Sun et al., 2015). Nevertheless, the majority of the existing observational and modeling studies have explored the influence of pan-Arctic and BKS sea ice loss and associated AA on the mid-latitude weather and

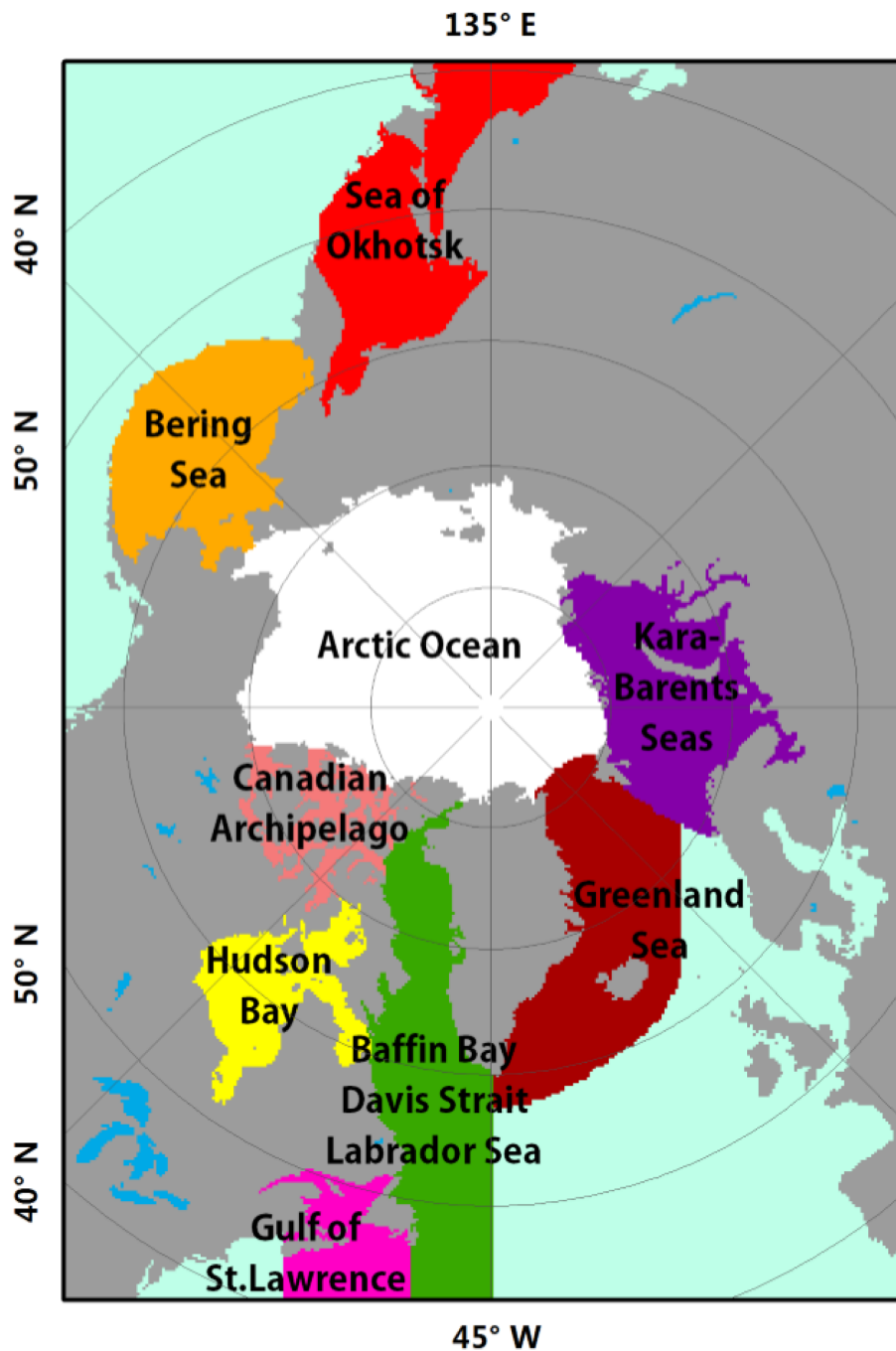


Figure 1.3. The regional mask around the Arctic provided by the National Snow and Ice Data Center (NSIDC). It includes Arctic Ocean, Barents and Kara Seas, Greenland Sea, Baffin Bay/Davis Strait/Labrador Sea, Gulf of St. Lawrence, Hudson Bay, Canadian Archipelago, Bering Sea, and Sea of Okhotsk. Adapted from Ahn et al. (2014).

climate (Kim et al., 2014; McCusker et al., 2016; Mori et al., 2014; Screen et al., 2015) and less attention has been made on sea ice loss over different locations.

Additionally, whether resolving the stratospheric pathway can explain the observed trend (Shepherd, 2016) is still complicated, primarily because the sensitivity of the atmospheric circulation response to the magnitude and geographical location of the sea ice loss (McKenna et al., 2018; Screen, 2017; Sun et al., 2016). Large internal variability in the atmospheric circulation has also been reported that makes the relation between AA and the observed trend questionable (McCusker et al., 2016; Ogawa et al., 2018). Therefore, it is necessary to explore how the impacts of the regional sea ice loss interact among themselves and thus, influence the mid-latitude atmospheric circulation.

Recently Screen (2017), in a comprehensive modeling investigation, has suggested that the response to pan-Arctic sea ice loss can not be reproduced by linear addition of regional responses, however, the underlying dynamics remains unexplained. This gap motivates us to further explore the linear additivity of atmospheric circulation response to regional AA. In this section of the dissertation, we specifically investigate the dynamical mechanisms underlying the non-linearity, using a simplified AGCM. In order to that, we focus on three key regions of the Arctic i.e. Barents-Kara Sea, Baffin Bay/Labrador Sea and East Siberia/Chukchi Sea (see fig. 1.3). In addition, we conduct additional targeted experiments to explicitly distinguish the role of stratosphere-troposphere coupling in the non-linear circulation response to regional AA.

### 1.3 Outline

The thesis is composed of 5 chapters. In chapter 2, we present that stratosphere-troposphere coupling is the key in linking Arctic sea ice loss to the mid-latitude circulation. We explore the robustness of the hypothesized dynamical mechanism using an ensemble of simulations from diverse modeling groups in the CMIP5 experiments.

The chapter 3 demonstrates that a colder Siberia is dynamically induced due to BKS SIC loss in a comprehensive AGCM. Specifically, we show an important contribution of the stratosphere-troposphere coupling in driving the cold temperature anomalies over Siberia. In chapter 4, we exhibit whether responses to the regional Arctic amplification are linearly additive in a simplified dry dynamical core model. Targeted perturbation experiments demonstrate the underlying dynamical mechanisms of non-linear responses to regional AA. Finally in chapter 5, we present the conclusion of this dissertation by summarizing the results. We also discuss about the importance of our work and possible future directions.

## 2. ROBUSTNESS OF THE STRATOSPHERIC PATHWAY IN LINKING THE BARENTS-KARA SEA SEA ICE VARIABILITY TO THE MID-LATITUDE CIRCULATION IN CMIP5 MODELS

A version of this chapter has been published in *Climate Dynamics Journal*.

Reference: De, B. & Wu, Y. *Clim Dyn* (2018). <https://doi.org/10.1007/s00382-018-4576-6>

DOI: 10.1007/s00382-018-4576-6

### 2.1 Introduction

The Arctic has experienced an unprecedented and accelerated sea ice loss and warming in the recent decades (Screen and Simmonds, 2010), which is widely known as the Arctic Amplification (AA). Global climate model simulations have projected a likelihood of further warming by the end of the current century with a doubling of near surface temperature increase over the Arctic compared to the global average (Collins and Coauthors, 2013). The AA peaks in early winter possibly due to ice-albedo feedback with retreat of sea ice in the fall. However, contributions from enhanced atmospheric moisture and oceanic transport, cloud cover and longwave radiation feedback (e.g., Cohen et al., 2014; Collins and Coauthors, 2013; Gong et al., 2017; Lu and Cai, 2009; Pithan and Mauritsen, 2014) are also important in shaping the emerging pattern.

It has been widely documented that sea ice variability, especially over the Barents and Kara Sea (BKS), could significantly alter the mid-latitude atmospheric circulation in the Northern Hemisphere (NH) (see review papers by Barnes and Screen, 2015; Cohen et al., 2014, and references therein). A majority of the studies have detected

a negative North Atlantic Oscillation (NAO) or Northern Annular Mode (NAM)-like pattern and a weakening of the stratospheric polar vortex as a result of sea ice loss. Nevertheless, considerable diversities still exist among the modeling studies (see a review paper by Screen et al., 2018b) - some authors found a positive NAO-like pattern (Screen et al., 2014) and a stronger polar vortex (Cai et al., 2012), while others suggested no significant impact on the NAO variability (Screen et al., 2013). In addition, from observations, autumn sea ice concentration (SIC) over the Arctic is found to precede the mid-latitude tropospheric circulation by about 2-4 months (Wu and Zhang, 2010). However, the dynamical mechanism that accounts for this prolonged remote impact of sea ice variability is not well understood. Previous studies (e.g., Kim et al., 2014; Nakamura et al., 2016; Sun et al., 2015; Wu and Smith, 2016) have suggested that, in addition to the tropospheric pathway, the stratospheric pathway might also be potentially important in linking the late autumn early winter sea ice loss with the mid-latitude circulation via troposphere-stratosphere coupling, and therefore could probably explain the prolonged tropospheric circulation response (Zhang et al., 2017).

Similar to the mechanism that links October snow cover over Eurasia to mid-latitude winter (Cohen et al., 2010; Smith et al., 2010), recent studies have suggested that more planetary-scale waves, forced by reduced sea ice and enhanced warming in early winter, can propagate vertically into the stratosphere, increase the polar cap geopotential height and weaken the stratospheric polar vortex (Jaiser et al., 2013; Kim et al., 2014). The anomalous stratospheric circulation can persist for about 1-2 months and later descend into the troposphere, resulting in negative NAM-like pattern near the surface (Kim et al., 2014; Nakamura et al., 2016; Sun et al., 2015).

In particular, to explore the role of the stratosphere, Sun et al. (2015) performed a set of prescribed sea ice loss experiments using the Whole Atmosphere Community Climate Model version 4 (WACCM4), a high-top model with a well-resolved stratosphere, along with identical experiments using the Community Atmosphere Model version 4 (CAM4), the low-top counterpart with a poorly-resolved stratosphere de-

veloped at National Center for Atmospheric Research (NCAR). Both the high-top and low-top models have similar physics and horizontal resolution, however, they differ in vertical extent. In that study, statistically significant negative NAM-like response was found in the tropospheric circulation in late winter in WACCM4 with future projection of pan-Arctic sea ice decline while the response was much weaker in CAM4. Therefore, they suggested that the stronger circulation response in WACCM4 is likely due to the better representation of the stratosphere. Additionally, we note that most of the modeling studies that exhibit a negative NAO or a weakened polar vortex used high-top models with realistic simulation of the stratosphere (e.g. Nakamura et al., 2016; Wu and Smith, 2016; Zhang et al., 2018). The studies that can not reproduce a tendency for the negative NAO or weakened polar vortex used low-top models with poorly represented stratosphere (Cai et al., 2012; Screen et al., 2013).

Specifically, it has been proposed that the BKS SIC retreat could induce a long lasting effect on the tropospheric circulation through the stratospheric pathway (Nakamura et al., 2016; Zhang et al., 2017). However, so far, the remote effects of BKS SIC variability via troposphere-stratosphere coupling have been studied using single climate model simulations (Kim et al., 2014; Nakamura et al., 2016; Screen, 2017; Zhang et al., 2017) and limited period of observations (Kim et al., 2014; Yang et al., 2016). Recently, it has been strongly advocated that simulations from diverse coupled models, using as many models as possible, are necessary to examine the robustness of the results (Screen et al., 2018b, and references therein). The Coupled Model Intercomparison Project phase 5 (CMIP5) experiments represent an excellent resource for multi-model study to assess the robustness of the stratospheric pathway, which has remained poorly explored in this regard. In this study, our goal is to revisit the prolonged impact of the BKS SIC variability and assess the robustness of the mechanism of the stratospheric linkage from diverse coupled model simulations. Moreover, our aim is to explicitly demonstrate the responses in planetary scale waves to SIC variability to better understand the troposphere-stratosphere coupling in multi-model ensemble settings.

Therefore, in this study, we shall use an ensemble of global climate models that participated in the CMIP5 experiments, focus on year-to-year variability and examine whether there is any significant difference between the high-top and low-top models. Earlier Charlton-Perez et al. (2013) documented that the stratospheric dynamical variability is under-represented in CMIP5 low-top models as compared to high-top models. Therefore, it is expected that differences can be seen between high-top and low-top models in their representation of the stratospheric pathway, i.e. the stratosphere-troposphere coupling that links the Arctic with the mid-latitudes. In this study, our key research questions include:

1. How well do CMIP5 models simulate the stratospheric pathway in linking the BKS SIC variability with the mid-latitude circulation?
2. Does the impact of BKS SIC variability differ between high-top and low-top models and what is the underlying mechanism?

Our study uniquely explores to what extent the circulation responses may be solely the result of BKS SIC variability via stratospheric pathway in the two groups of the models. The chapter is organized as follows. Section 2.2 discusses about the CMIP5 model outputs and diagnostics. Section 2.3 describes the prolonged impact of BKS SIC variability on the mid-latitude circulation and surface air temperature and exploits the dynamics in high-top and low-top models. Section 2.4 concludes the study. The results presented here have been published in De and Wu (2018).

## **2.2 Data and Methods**

### **2.2.1 Observations**

ERA-Interim reanalysis data produced by the European Center for Medium-Range Weather Forecasts (ECMWF) (Dee and Coauthors, 2011) has been used to represent the atmospheric circulation in Figure A2. We use the monthly 700 hPa zonal wind in  $1.5^\circ$  longitude  $\times$   $1.5^\circ$  latitude horizontal resolution for the period of 1979-2014. In

Table 2.1.  
Horizontal resolution, model top height and vertical resolution of the high-top models from CMIP5 archive analyzed in this study.

Number	Models	Resolution (lat $\times$ lon)	Lid Heights	Vertical Levels
1	CanESM2	$2.7906^\circ \times 2.8125^\circ$	1 hPa	35
2	CESM1-WACCM	$1.88^\circ \times 2.5^\circ$	$5.1 \times 10^{-6}$ hPa	66
3	GFDL-CM3	$2^\circ \times 2.5^\circ$	0.01 hPa	48
4	HadGEM2-CC	$1.25^\circ \times 1.875^\circ$	0.01 hPa	60
5	IPSL-CM5A-LR	$1.8947^\circ \times 3.75^\circ$	0.04 hPa	39
6	IPSL-CM5A-MR	$1.2676^\circ \times 2.5^\circ$	0.04 hPa	39
7	MIROC-ESM	$2.79^\circ \times 2.81^\circ$	0.0036 hPa	80
8	MIROC-ESM-CHEM	$2.79^\circ \times 2.81^\circ$	0.0036 hPa	80
9	MPI-ESM-LR	$1.8653^\circ \times 1.875^\circ$	0.01 hPa	47
10	MRI-CGCM3	$1.12148^\circ \times 1.125^\circ$	0.01 hPa	48

addition, we use monthly SIC derived from the passive microwave satellite data using bootstrap algorithm during the same time period. The SIC dataset is available in  $448 \times 304$  horizontal (25 km mesh) grid in the NASA National Snow and Ice Data Center Distributed Active Archive Center (Comiso, 2000). We focus on the year-to-year variability by removing the long-term linear trend from observations for all variables.

### 2.2.2 CMIP5 models

We analyze models with a well-resolved stratosphere (high-top models) and models with a poorly-resolved stratosphere (low-top models) in the CMIP5 pre-industrial control experiments (Taylor et al., 2012). The pre-industrial control experiments are forced with only natural forcings, i.e. solar radiation, natural aerosols and greenhouse gas concentrations that imitate the conditions prior to 1850 and do not have

Table 2.2.  
Horizontal resolution, model top height and vertical resolution of the low-top models from CMIP5 archive analyzed in this study.

Number	Models	Resolution (lat $\times$ lon)	Lid Heights	Vertical Levels
1	bcc-csm1.1	$2.7906^\circ \times 2.8125^\circ$	2.917 hPa	26
2	CCSM4	$0.9424^\circ \times 1.25^\circ$	2.19 hPa	27
3	CNRM-CM5	$1.4008^\circ \times 1.40625^\circ$	10 hPa	31
4	CSIRO-Mk3.6.0	$1.86^\circ \times 1.87^\circ$	4.5 hPa	18
5	INM-CM4	$1.5^\circ \times 2^\circ$	10 hPa	21
6	GFDL-ESM2M	$2.02^\circ \times 2.5^\circ$	3 hPa	24
7	GFDL-ESM2G	$2.02^\circ \times 2^\circ$	3 hPa	24
8	HadGEM2-ES	$1.25^\circ \times 1.875^\circ$	3 hPa	38
9	MIROC5	$1.4008^\circ \times 1.406^\circ$	3 hPa	40
10	NorESM1-M	$1.8947^\circ \times 2.5^\circ$	3.54 hPa	26

anthropogenic contributions, which would allow us to solely examine the impact of natural variability. In addition, significantly long span of model integrations in pre-industrial control experiments helps to improve the signal to noise ratio (Furtado et al., 2015). We select the models based on the availability of all variables, including monthly zonal and meridional wind, geopotential height and surface air temperature, and follow Charlton-Perez et al. (2013) to divide the models into high-top and low-top groups. The 10 high-top models are listed in Table 2.1 and the 10 low-top models are listed in Table 2.2. The two groups of models differ significantly in model top height and vertical resolution but not in horizontal resolution (as shown in Tables 2.1 and 2.2). We compare the average of the high-top and low-top models over the whole available time period.

The classification into two groups is solely based on Charlton-Perez et al. (2013), where the model lid height at 1 hPa is the threshold between the high-top and low-top.

Previously, Sassi et al. (2010), using two versions of a state-of-the art climate model with different resolution of the middle atmosphere, documented that both models simulate similar zonal mean zonal wind and temperature during winter, except that the low-top model has a stronger zonal wind and a colder polar vortex at middle stratosphere compared to the observations (see their Fig. 2). They suggested that the difference in zonal mean circulation is primarily due to the reflection of planetary waves from the lid of the low-top model. Charlton-Perez et al. (2013) also found that the two groups simulate similar mean state climate and similar biases characterized with warm biases near the tropical tropopause (around 100 hPa) and cold biases near the extratropical tropopause (near 250 hPa), except at the region near the model top. Additionally, they revealed that the difference between the two groups maximizes in the extratropical middle stratosphere when the stratosphere is dynamically active (i.e. winter). Specifically, in a multi-model ensemble study, Lee and Black (2015) showed that the general structure of winter climatology of the zonal-mean zonal wind in the two groups resembles the observations although the intensity of both subtropical jet and polar night jet is stronger in the CMIP5 models (see their Fig. 1). They also found that the vertical extent of the polar vortex in the low-top models are shallow which may alter the refractive index for planetary wave propagation due to weaker lower stratospheric winds. In contrast to the mean climate, the stratospheric variability on daily and inter-annual time scale is weaker in the low-top model group, which can affect the troposphere-stratosphere coupling (Charlton-Perez et al., 2013).

### 2.2.3 Diagnostics

We focus on the late autumn and early winter SIC variability over the BKS region ( $70^{\circ}$ – $82^{\circ}$ N,  $15^{\circ}$ – $100^{\circ}$ E), specifically during November and December (ND) following previous studies (Hoshi et al., 2017; Kim et al., 2014; Yang et al., 2016; Zhang et al., 2017). We define BKS SIC index using the standardized SIC anomaly averaged during ND, area-averaged over the BKS region. Here we reverse the sign of the

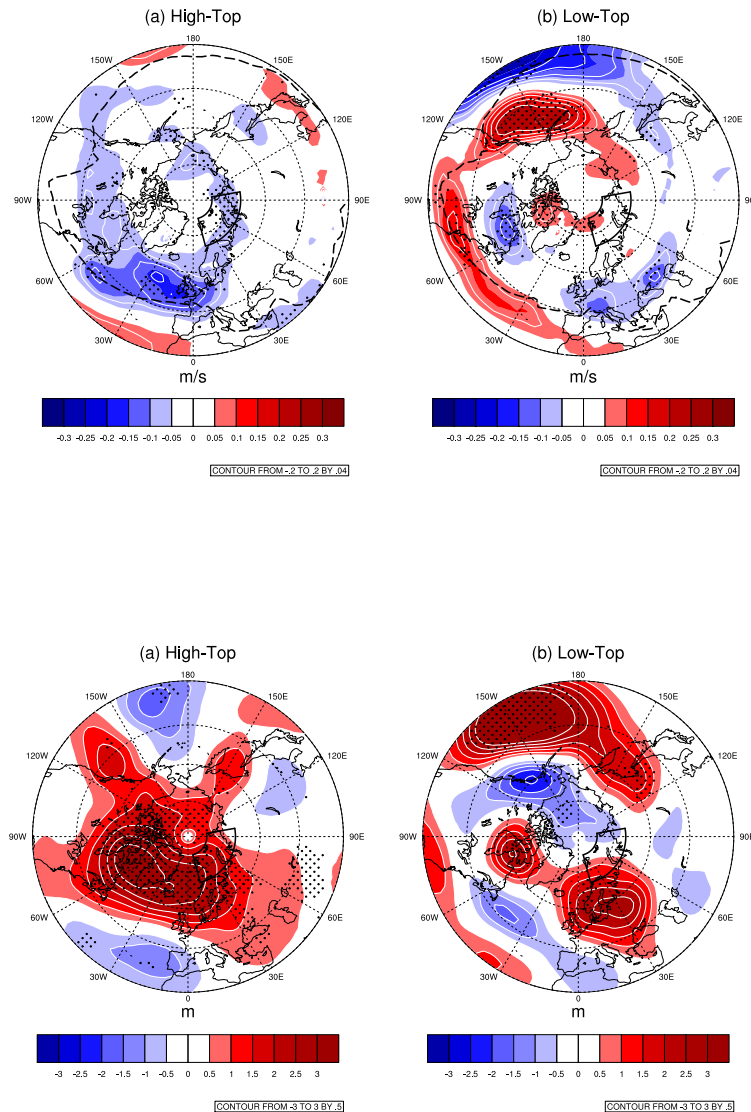


Figure 2.1. Regression of 700 hPa zonal wind anomaly (in m/s per 1 standard deviation of BKS SIC loss) during February on the normalized BKS SIC variability in the previous November and December in (a) high-top models and (b) low-top models (color shadings and white contours with contour interval of 0.04 m/s), respectively. The dashed black line indicates the climatological jet position. The BKS region is highlighted in thick black box. The dots imply that at least 80% of the models agree on sign of change. (c) and (d) are similar to (a) and (b) but for 500 hPa geopotential height (color shadings and white contour with contour interval of 0.5m) during February in lower panel.

SIC index to emphasize the effect associated with sea ice loss. We perform lagged regression analysis between the BKS SIC index and winter time atmospheric variables to identify the possible impact of SIC loss on the atmospheric circulation in the subsequent months. We note that the variations of the monthly simulated BKS SIC among different models are comparable between the two groups and the models can approximately reproduce the observed detrended BKS SIC variability within the multi-model spread (Fig. A.1). We find that the regression results remain robust while using October-November BKS SIC (not shown) instead of ND BKS SIC index.

In order to further diagnose the two-way troposphere-stratosphere coupling, we examine the variability of polar cap zonal mean zonal wind, area-averaged between  $50^{\circ}$ – $70^{\circ}$ N. In addition, we examine the zonal mean eddy heat flux  $[v^*T^*]$  at 100 hPa to diagnose the upward wave propagation (Hoshi et al., 2017; Polvani and Waugh, 2004; Simpson et al., 2009). Here,  $v$  and  $T$  are monthly meridional wind and air temperature, respectively, and the bracket and asterisk denote zonal mean and deviation from zonal mean, respectively.

We interpolate each model into a common grid of horizontal resolution of  $2^{\circ}$  longitude  $\times$   $2^{\circ}$  latitude to calculate multi-model mean. We estimate the agreement among models by examining if at least 80% of the models agree on the sign of the response. The statistical significance in observations is calculated using the students  $t$ -test at the 95% confidence level. We also find that the differences between the two groups of the models remain unchanged by varying the subsample of the models from the two groups (not shown). Additionally, we find that normalizing both the BKS SIC and the atmospheric variables does not change the conclusion (not shown).

## 2.3 Results

### 2.3.1 Prolonged response in tropospheric circulation

First, we examine the mid-latitude circulation response associated with BKS SIC variability in the observations (Fig. A.2). The observations show a long-lasting im-

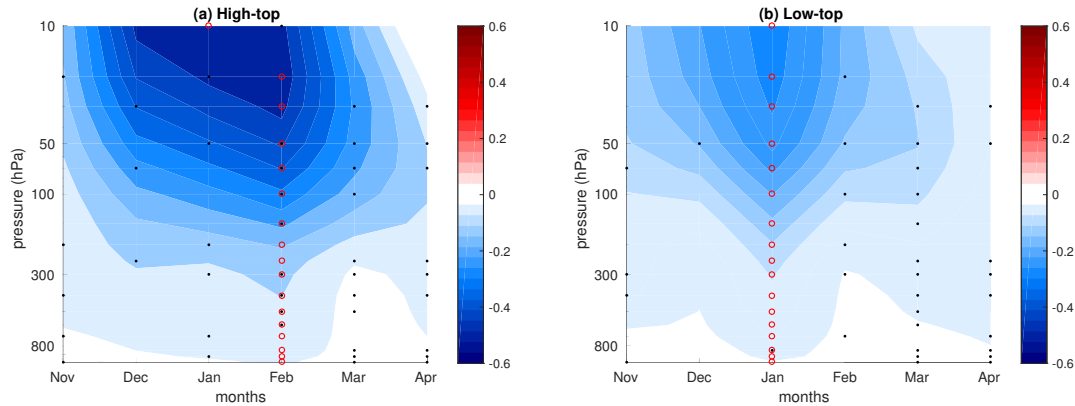


Figure 2.2. Monthly evolution of zonal mean zonal wind (in m/s per 1 standard deviation of BKS SIC loss) averaged between  $50^{\circ}$ – $70^{\circ}$ N from November to April, due to BKS SIC loss in November and December in (a) high-top models and (b) low-top models (color shadings). The red circles represent minimum value for each pressure level. The black dots indicate that at least 80% models agree on sign of change.

impact of late autumn early winter SIC variability on the atmospheric circulation well into mid winter (January to March). Figure A.2 shows the regression of observed detrended 700 hPa zonal wind onto the BKS SIC index from December to subsequent April. We find an equatorward shift of the tropospheric jet associated with a pronounced weakening on the poleward flank of the climatological jet. The signal is more pronounced over the North Atlantic-European sector from January to March and disappears in April. We note that the response in tropospheric jet, is not synchronized with the SIC variability, but rather maximizes in the subsequent January to March. Next we explore whether state-of-the-art coupled climate models can simulate the lead-lag relationship and whether there is any significant difference between high-top and low-top models.

Figure 2.1 shows the mid-latitude circulation response associated with BKS SIC variability in CMIP5 multi-model mean during February, as an example. The high-top models show a long-lasting impact that the atmospheric circulation associated with late autumn early winter SIC variability persists well into mid winter (February).

Figure 1ab show the regression of 700 hPa zonal wind onto the BKS SIC during February, for two groups of models, respectively. We find a weakening on the poleward flank of the climatological jet for both groups. In addition, more importantly, the high-top multi-model mean (Fig. 2.1a), with well resolved stratosphere, shows a stronger weakening of the tropospheric jet over the North Atlantic-Europe sector, however, the deceleration of the tropospheric jet in this region in low-top multi-model mean (Fig. 2.1b) is much weaker. It is difficult to compare the model simulations with the observations due to the differences in the length of the time series and forcings, but the pattern of the high-top multi-model mean shows a closer resemblance to the observations, especially the jet weakening response over the North Atlantic sector (Fig. A.2c), as compared to the low top multi-model mean.

In addition, we also show the regressed 500 hPa geopotential height field and find similar differences between the two groups of models (see Fig. 2.1c and 2.1d). A negative NAM-like pattern is seen with positive geopotential height anomaly over the Arctic and negative geopotential height anomaly over the North Atlantic region for both groups. However, high-top models (Fig. 2.1c) show a more pronounced geopotential height anomaly compared to low-top models (Fig. 2.1d), especially over the polar region of the North Atlantic sector. A similar negative NAM-like pattern is found in observations (not shown).

Previously, Furtado et al. (2015) studied the dynamical linkage between October snow cover over Eurasia and Arctic Oscillation (AO) in winter and found that CMIP5 models lack a robust lagged response compared to observations. Following Charney and Drazin (1961), they argued that the background zonal mean state in models may be responsible for the weaker propagation of the vertical component of wave activity flux that is proportional to the meridional heat flux and the subsequent stratospheric variability. It is possible that the circulation response can be sensitive to the basic state of the model (Bader et al., 2011; Kidston and Gerber, 2010), which can result in high-top and low-top differences. For example, Kidston and Gerber (2010) mentioned that an equatorward bias in climatological jet-position can result in enhanced

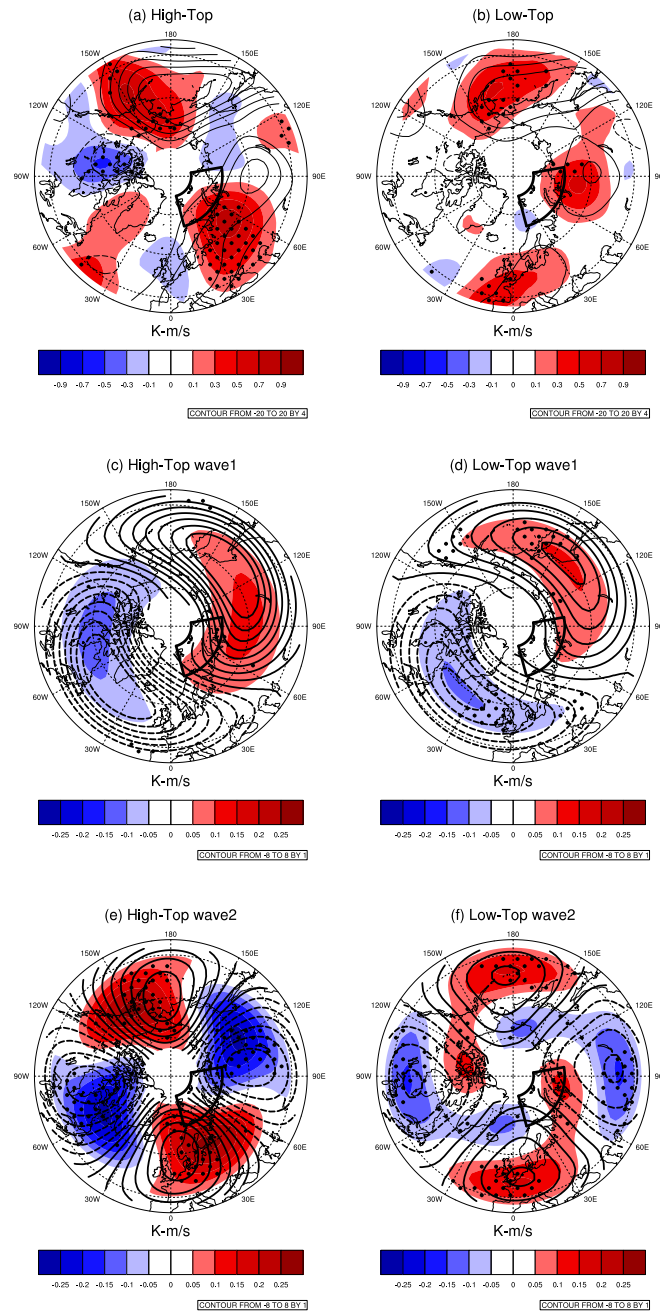


Figure 2.3. Similar to Fig. 2.1 but for 100mb eddy heat flux (color shadings, in  $K \cdot m/s$  per 1 standard deviation of SIC loss) in December in (a) high-top models and (b) low-top models, respectively. The black contours (with a contour interval of  $4 K \cdot m/s$ ) indicate climatological poleward heat flux where positive values are solid while negative values are dashed. (c), (d) and (e), (f) are similar to (a) and (b) but for wave-1 and wave-2 100mb eddy heat flux response (color shadings), respectively. The black contours have an interval of  $1 K \cdot m/s$  in (c), (d), (e) and (f).

poleward shift of the jet. Therefore, here we examine whether differences in climatological jet latitude and jet speed in models affect the anomalous zonal wind over the North Atlantic and the inter-model spread. We define the jet response as the change of jet speed over the region ( $45^{\circ}$ – $90^{\circ}$ N and  $315^{\circ}$ – $360^{\circ}$ E) with the strongest weakening of the jet in the North Atlantic sector. To calculate climatological jet statistics, we zonally average the 700 hPa zonal wind over the North Atlantic sector ( $45^{\circ}$ – $90^{\circ}$ N and  $270^{\circ}$ – $360^{\circ}$ E), interpolate into a finer latitudinal grid of  $0.05^{\circ}$  and define the maximum zonal wind speed as the jet speed and the corresponding latitude as the jet latitude. We find that neither group of models shows any significant correlation between the jet response and the climatological jet-latitude (Fig. A.3a). Although, we find a moderate yet statistically insignificant negative correlation between the jet response and the climatological jet speed in low-top models which suggests that low-top models with a faster climatological jet are more likely to produce a larger slowdown of the jet speed to sea ice variability (Fig. A.3b). However, lack of robustness in this relationship is in contrast with the statistically robust circulation response as shown in Figure 2.1. Hence, we argue that the differences in circulation response between high-top and low-top models are not likely related to differences in climatology, but instead, are attributed to the representation of the stratospheric pathway (to be discussed next).

### 2.3.2 Dynamics of troposphere-stratosphere coupling

The previous section presented the differences between CMIP5 high-top and low-top models in simulating the impact associated with the BKS SIC variability on the midlatitude circulation. In this section, we attribute the differences between high-top and low-top models to the stratospheric pathway. Figure 2.2 shows the monthly evolution of polar cap zonal mean zonal wind from November to April associated with BKS SIC variability. We find that both groups of models simulate a weakening of the stratospheric polar vortex but with different strength. In the high-top multi-model mean, the weakening of the stratospheric polar vortex starts in Decem-

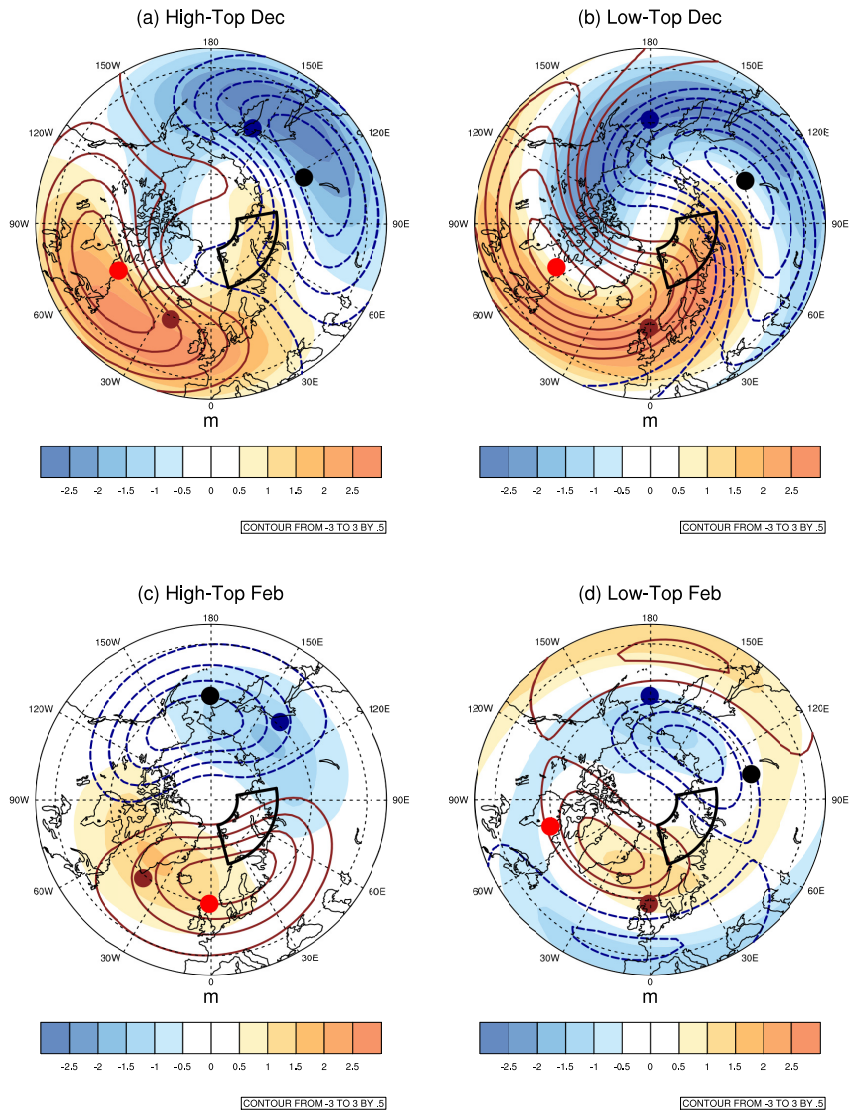


Figure 2.4. Wave-1 geopotential height regression (per 1 standard deviation of BKS SIC loss) at 500 mb (color shadings) and 50 mb (black contours with contour interval of 0.5 m) during December (a and b) and February (c and d), respectively. Contour interval is 0.5 m. Positive values in contours are solid brown while negative values are dashed blue and the zero contour is omitted. The solid brown dot and solid blue dot represent the maxima and minima at 60°N, as an example, at 500mb. The solid red dot and solid black dot represent the corresponding maxima and minima at 50mb, respectively.

ber, maximizes in January at 10 hPa and gradually migrates downward reaching the lower troposphere in February (Fig. 2.2a). The downward descent of the stratospheric circulation response indicates possible stratosphere-troposphere coupling in mid-winter. However, in the low-top multi-model mean, the weakening of zonal wind is weaker and the tropospheric response is short-lived and disappears after January (Fig. 2.2b). Previously, Charlton-Perez et al. (2013) documented that the key reason behind short-lived tropospheric response in low-top models is the lack of stratospheric dynamical variability which results in reduced e-folding time scale of NAM-like signal.

To better understand the stronger weakening of the stratospheric polar vortex in high-top models compared to low-top models, we study the eddy heat flux at 100 hPa, which provides a diagnostic measurement of troposphere-stratosphere coupling (Kim et al., 2014; Polvani and Waugh, 2004; Sun et al., 2015). We choose December as the upward propagation phase, which is during the forcing period (ND) and coincides with the onset of the weakened polar vortex (Fig. 2.2). In the multi-model mean, an anomalous upward heat flux is seen in December in both high-top and low-top models (Fig. 2.3ab). It primarily occurs in the vicinity of Eastern Eurasia (EE) region ( $50^{\circ}$ - $80^{\circ}$ N,  $140^{\circ}$ - $160^{\circ}$ W) and Central Eurasia (CE) region ( $50^{\circ}$ - $80^{\circ}$ N,  $50^{\circ}$ - $90^{\circ}$ E), which collocates with the climatological maxima of eddy heat flux. These two regions were also found as two important centers of action for linear constructive interference and troposphere-stratosphere coupling in Hoshi et al. (2017). Following an enhanced upward heat flux anomaly, the weakening of the stratospheric polar vortex reaches its maximum during January (Fig. 2.2). We closely compare this chain of events between the two groups of models, to explore the reason behind the stronger response in high-top models. In December, prior to the maximum stratospheric response in January, we find a stronger positive anomaly in eddy heat flux in the vicinity of CE and EE regions in high-top models (Fig. 2.3a) compared to low-top models (Fig. 2.3b), consistent with the more pronounced weakening of the stratospheric polar vortex in high-top models compared to low-top.

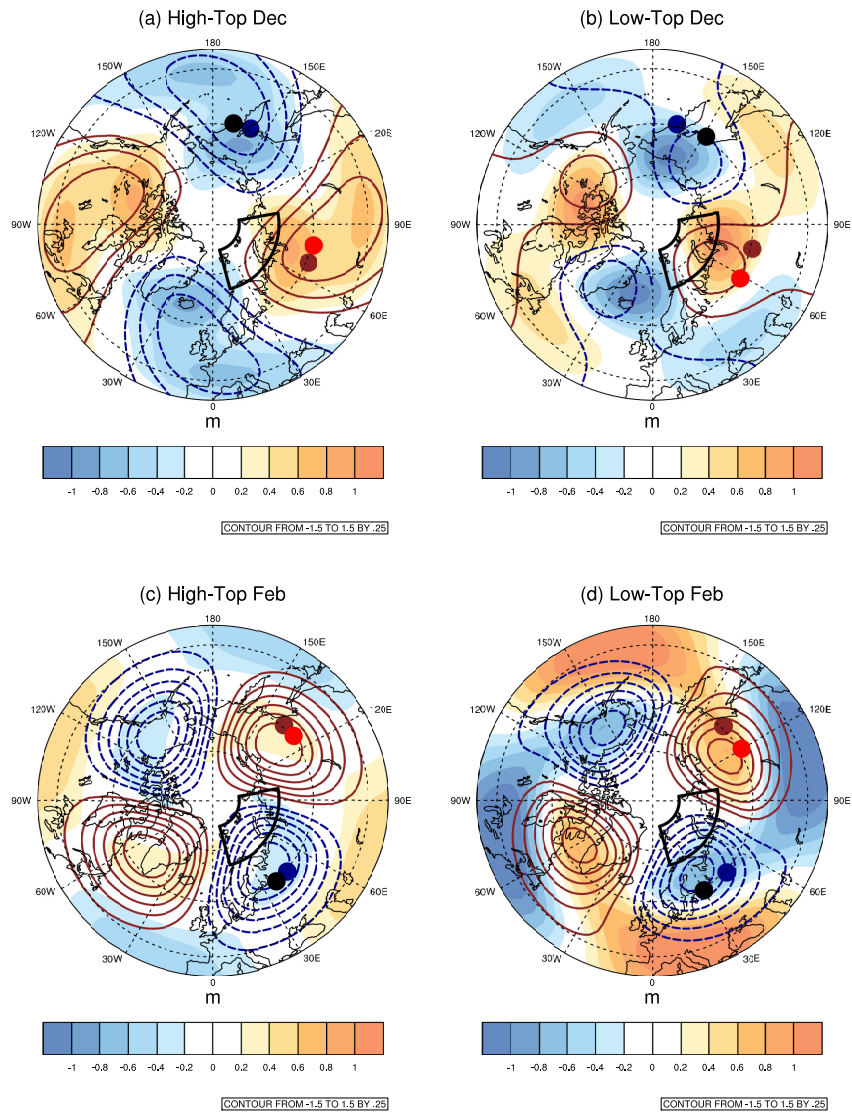


Figure 2.5. Similar to Fig. 2.4 but for wave-2 geopotential height regression (in color shadings and black contours with contour interval of 0.25 m). Note the difference in colorbar from Figure 2.4.

Further decomposition of 100 hPa eddy heat flux into zonal wave-1 and wave-2 components shows that the key difference between the two groups of models can be mainly attributed to wave-2 component (Fig. 2.3e and 2.3f) as the contributions from wave-1 component are almost identical (Fig. 2.3c and 2.3d). This results in stronger linear interference mechanism where the anomaly of wave-2 component is mostly in phase with the climatological wave and thus leads to larger upward wave-2 flux into the lower stratosphere in high-top models (Fig. 2.3e) (Garfinkel et al., 2010; Smith et al., 2010; Zhang et al., 2017). In contrast, for low-top models, the weaker response in wave-2 component results in reduced upward wave-2 flux into lower stratosphere from interference with climatological waves (Fig. 2.3f).

To further examine the wave propagation between the two groups, we study the wave-1 (Fig. 2.4) and wave-2 (Fig. 2.5) components of geopotential height at 500 hPa and at 50 hPa during upward propagation phase in December and during downward migration phase in February, respectively. In Figure 2.2, we found that the downward descent of weakened zonal wind dies off after January in low-top models while the high-top models show long-lasting response up to February. Hence, we consider February as the downward migration phase to explicitly distinguish the persistence of stratosphere-troposphere coupling between the two groups. We choose two vertical levels to determine the phase tilt with height of the wave patterns and the wave propagation (following Shaw et al., 2014). We expect a west-ward phase tilt for troposphere-stratosphere coupling during upward wave propagation phase and an east-ward phase tilt for stratosphere-troposphere coupling during downward wave migration phase. In wave-1 component, for both groups, we find a west-ward phase tilt with height between the two vertical levels during December (Fig. 2.4a and 2.4b). However, in contrast to the high-top models (Fig. 2.4c), the low-top models do not show the east-ward phase tilt with height during February (Fig. 2.4d) which is an indication of no downward coupling. This is consistent with Figure 2 where we find that the downward coupling disappears after January for low-top models. In contrast

to wave-1, the wave-2 component (Fig. 2.5) shows a much weaker response and the two levels mostly overlap each other.

Therefore, the key difference between the two groups of models is a stronger stratospheric response due to stronger eddy heat flux and a longer-lived tropospheric signal following a stronger two-way coupling in high-top multi-model mean compared to low-top. However, as for why stratospheric wave propagation is distinct between the two groups of models, is beyond the scope of this study. As suggested in previous studies (Garfinkel et al., 2012; Sun et al., 2015), the weaker vertical wave propagation in low-top models could possibly be associated with a stronger polar vortex due to more wave reflection near the model lid (Sassi et al., 2010; Shaw and Perlwitz, 2010; Sun et al., 2015). In addition, Shaw and Perlwitz (2010) found that different stratospheric states can also alter tropospheric wave climatology that may lead to different tropospheric wave interference in the two groups of models.

### 2.3.3 Missing mid-winter Eurasian cooling

Another possible consequence of SIC loss that has been discussed extensively in recent studies is the Eurasian cold air outbreaks. However, the evidence of the linkage between the Arctic and mid-latitude extremes is doubtful due to limited period of observations and poor understanding of how the dynamics works (e.g. see review papers by Cohen et al., 2014; Shepherd, 2016). But several studies have suggested that a prominent warm Arctic cold Eurasia pattern (as found in Overland et al., 2011) is attributable to BKS SIC loss and an associated intensified Siberian high that advects cold air from the Arctic to the south (e.g. Kug et al., 2015; Mori et al., 2014; Vihma, 2014).

In CMIP5 multi-model mean, however, the cold temperature anomaly over Eurasia during February is almost absent: there is a very small and statistically insignificant cold anomaly over Eurasia in high-top models (Fig. 2.6a) whereas the cold anomaly is absent in low-top models (Fig. 2.6b). We note that following previous discussions,

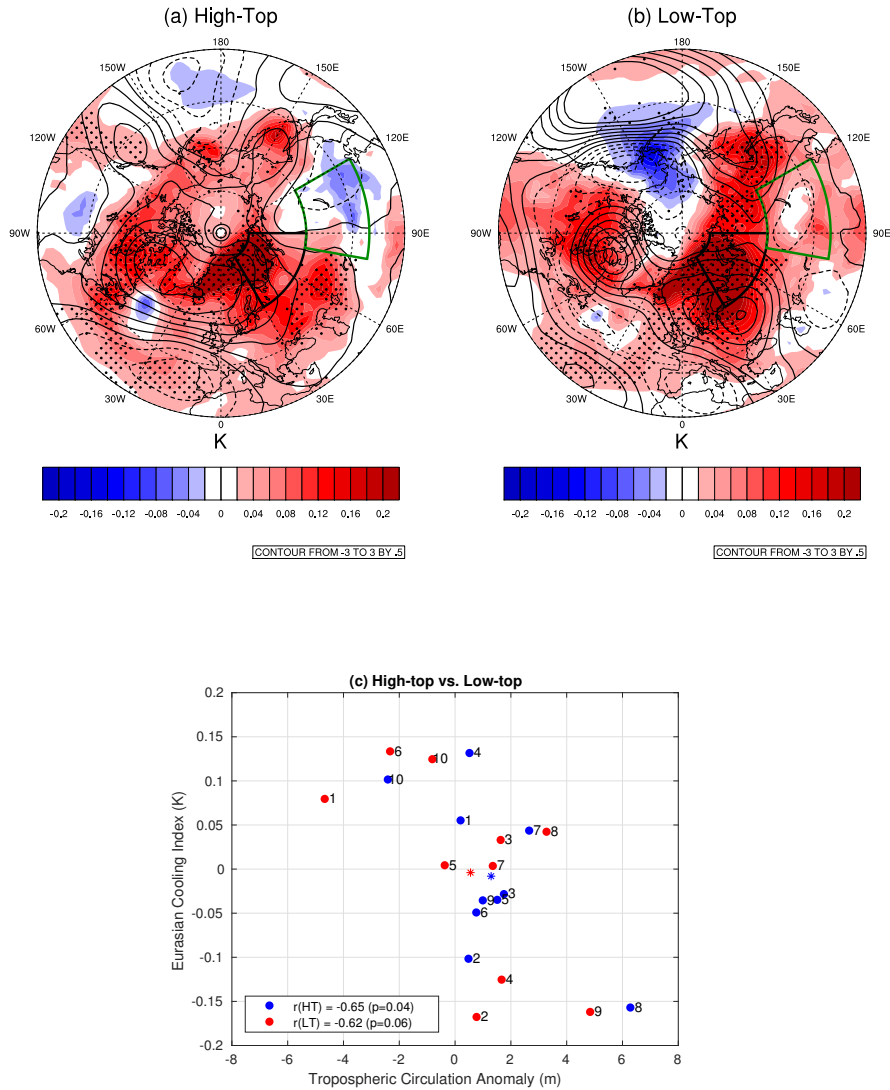


Figure 2.6. Similar to Fig. 2.1 but for surface air temperature (color shadings) and 500 hPa geopotential height (black contours) during February in (a) high-top and (b) low-top models. Positive values in geopotential height are solid while negative values are dashed. Contour interval is 0.5 m. The regions to construct the Ural mountain ridge anomaly and the Eurasia cold anomaly are highlighted in thick black and green boxes, respectively. (c) Scatter plot of 500 hPa geopotential height anomaly over  $60^{\circ}$ – $80^{\circ}$ N and  $30^{\circ}$ – $90^{\circ}$ E versus Eurasia SAT (ECI) over  $40^{\circ}$ – $60^{\circ}$ N and  $80^{\circ}$ – $120^{\circ}$ E during February associated with BKS SIC loss in the previous November and December in high-top models (in blue) and low-top models (in red). The numbers represent the corresponding models listed in Tables 2.1 and 2.2. The multi-model mean is shown as asterisk in blue for high-top and red for low-top, respectively. The correlation coefficient ( $r$ ) and  $p$ -value are shown in the legend for high-top and low-top models, respectively.

here we focus on the prolonged Eurasian temperature response during February. Despite the missing Eurasian cooling in models during mid-winter, both high-top and low-top models can simulate the Eurasian cooling during early-winter (not shown), which possibly does not include a stratospheric pathway.

We argue, this is possibly due to inability of the models to simulate an intensified ridge near the Ural Mountains and a trough over Eastern Eurasia (Zhang et al., 2018). To further examine that, we investigate the relation between the mid-tropospheric circulation anomaly and Eurasian surface air temperature (SAT) anomaly among all the models. More specifically, we define the anomalous mid-tropospheric ridge as the weighted area averaged 500 hPa geopotential height anomaly over  $60^{\circ}$ – $80^{\circ}$ N  $30^{\circ}$ – $90^{\circ}$ E and construct an Eurasian Cooling Index (ECI) as the weighted area averaged SAT anomaly over  $40^{\circ}$ – $60^{\circ}$ N and  $80^{\circ}$ – $120^{\circ}$ E associated with BKS SIC variability. Although the multi-model mean is not able to simulate Eurasian cooling, there is a statistically significant negative correlation between the tropospheric circulation anomaly and ECI among the models (Fig. 2.6c), which suggests that the models that simulate a stronger intensified ridge near the Ural Mountains are likely to simulate a stronger Siberian cooling.

One possibility underlying the missing Eurasian cooling may be due to air-sea interaction in the coupled models, where oceanic feedbacks can impact the magnitude of the temperature response (Deser et al., 2016, 2015; McCusker et al., 2016). In a modeling study of Deser et al. (2016), they showed that an elevated global sea surface temperature (SST) associated with sea ice loss warms the troposphere by a combination of local and remote processes, which leads to strong thermodynamically induced warming over the high-latitude continents and dominates over the dynamically induced intensified Siberian high and associated cooling over Eurasia. In particular, Deser et al. (2016) argued that in response to the Arctic sea ice loss, warm SST is confined near the edge of the Arctic in the atmospheric models, whereas the warming spreads to lower latitudes of the ocean basins in the coupled model simulations (note positive SST anomaly over lower latitudes in Fig. 2.6ab). Consequently, the

dynamically-induced cooling might be weakened or even eliminated by the thermodynamically induced warming (Screen et al., 2018b).

Therefore, even though we find robust responses in tropospheric circulation associated with SIC variability via the stratospheric pathway, the resulting surface air temperature anomaly over Eurasia, especially in the coupled model experiments, remains an open question.

## 2.4 Conclusions and Discussion

Through multi-model analysis of coupled climate models, this study reveals the robustness of the prolonged impact of the stratospheric pathway in linking BKS SIC variability and mid-latitude circulations. In this study we examine how CMIP5 models simulate the mid-latitude circulation response as a result of BKS SIC variability and whether models with well-resolved stratosphere outperform models with poorly-resolved stratosphere.

In the first part of the study, we find that high-top multi-model mean simulates a stronger circulation response than low-top counterpart during mid winter, especially in zonal wind and geopotential height. The results also exhibit that the largest circulation responses are evident over the North-Atlantic region which weaken earlier in the low-top models but persist in the high-top models. In the second part of the study, we attribute the differences in mid-latitude circulation response between high-top and low-top models to the representation of the stratospheric pathway. Compared to low-top models, we find a stronger and longer-lived negative NAM-like response in high-top models. During upward propagation phase, a stronger vertical wave propagation is found in high-top models, which leads to a stronger response in stratospheric polar vortex. In particular, we show that the wave-2 eddy heat flux plays the dominant role for enhanced upward vertical wave propagation following constructive linear interference with climatological waves in high-top models. During downward migration phase, on the other hand, the phase-tilt of wave-1 geopotential height be-

tween two vertical levels supports the long-lasting stratosphere-troposphere coupling in high-top models. However, the multi-model mean in neither high-top or low-top is capable of simulating intensified Siberian High and associated dynamically induced cooling over Siberia during mid-winter. Therefore, we find significant differences in atmospheric circulation response between high-top and low-top models which suggests an important role of the representation of the stratosphere in linking the Arctic to the mid-latitudes.

Previously, only a few studies examined the connection between the Arctic and the mid-latitudes using CMIP5 multi-model ensemble, however, the mechanism remained inconclusive due to contrasting results and methodologies. For example, Zappa et al. (2018) found the largest mid-latitude circulation response during late winter due to future projected sea ice loss, however, Boland et al. (2017) found no support for a linkage between sea ice and atmospheric circulation in CMIP5 future projection. In contrast to them, our study investigates the impact of Arctic sea ice variability in pre-industrial control experiments, particularly in high-top versus low-top models. It should be also noted that, in contrast to another study by Kelleher and Screen (2018), we solely examine the impact of BKS SIC variability and do not consider the dynamical mechanisms leading to the SIC loss.

Overall, this multi-model analysis has clearly demonstrated the robustness of the prolonged circulation responses over mid-latitude due to BKS SIC variability and a critical role of the stratospheric pathway. In particular, our study includes: 1. an assessment of the stratospheric pathway in a multi-model ensemble using diverse models from different modeling groups. 2. a detailed analysis of stratosphere-troposphere coupling which helps to distinguish the dynamics and its impact between high-top and low-top models. More specifically, we explicitly identify the zonal wave-2 eddy heat flux as the key for different dynamical coupling between the two groups of models.

While high-top and low-top multi-model mean show differences in the simulation of tropospheric circulation to BKS sea ice loss, there are a few caveats that we should consider. Firstly, the collective performance of the two model groups is not necessarily

true when we examine each individual model. Instead, we find a considerable spread in the model response in each group (Fig. 2.6c and S2). Secondly, in addition to model lid height, high-top and low-top model groups also have different model physics that could possibly cause the difference and inter-model spread. For example, in an assessment of troposphere-stratosphere coupling in CMIP5 future projections, Manzini et al. (2014) argued that the division of high-top and low-top models in future warming scenarios may not be reliable due to inter-model difference in climate sensitivity. Therefore, to unambiguously distinguish the role of the stratospheric pathway, “nudging” might be a better methodology. But previous studies using nudging method (e.g. Nakamura et al., 2016; Wu and Smith, 2016; Zhang et al., 2017) have found consistent conclusions that troposphere-stratosphere coupling is largely responsible for the prolonged tropospheric circulation response. Third point concerns that using daily variables instead of monthly may be a better way to assess the chain of events involving the troposphere-stratosphere coupling, especially for identifying peak eddy heat flux and following stratospheric response. Lastly, we acknowledge that correlation does not necessarily imply causation, and the lead-lag regression may not be the best way to identify the consequences of sea ice loss on the mid-latitude circulation response. For example, McGraw and Barnes (2018) used a “Granger Causality” approach to better establish the causality by ensuring that the results are not due to memory in data. Barnes and Simpson (2017) also took the “Granger Causality” to quantify the response of zonal wind to variability of Arctic temperature on sub-seasonal time scale. They found a robust impact but only a small additional percentage of variance of jet position and speed can be attributed to Arctic Amplification.

In summary, our results complement the conclusions of previous studies (Kim et al., 2014; Nakamura et al., 2016; Sun et al., 2015; Wu and Smith, 2016; Zhang et al., 2017) that suggests the stratospheric pathway plays an important role for a persistent and amplified mid-latitude circulation response due to BKS SIC variability. We explicitly demonstrate that CMIP5 high-top models, collectively, better simulate a

stronger vertical wave propagation and long-lasting downward coupling that produces a teleconnection between the Arctic and the mid-latitude via a “stratospheric bridge”. This study also suggests possible issues in low-top global climate models, especially for understanding NH weather and climate conditions. The results may be helpful for further improvement of global climate models by incorporating a well-resolved stratosphere.

In this chapter, our main focus is to investigate the robustness of the stratospheric pathway in driving the impact of BKS SIC loss on to mid-latitude circulation in a multi-model ensemble. However, the difference between CMIP5 multi-model ensemble is not a very clean comparison to explicitly distinguish the importance of the Barents-Kara Sea SIC loss on the regional weather via stratospheric pathway. Therefore, in order to understand the underlying mechanism of the observed “Warm Arctic Cold Siberia” pattern, targeted modeling experiment is necessary. This is the motivation for the work to be presented in Chapter 3.

### 3. ROLE OF THE STRATOSPHERIC PATHWAY IN LINKING THE BARENTS-KARA SEA SEA ICE LOSS TO A COLDER SIBERIA

A part of this chapter has been published in Science Advances Journal.

Reference: Zhang, P., Wu, Y., Simpson, I. R., Smith, K. L., Zhang, X., De, B., Callaghan, P. (2018). A Stratospheric Pathway Linking a Colder Siberia to Barents-Kara Sea Ice Loss. *Science Advances*, 4

DOI: 10.1126/sciadv.aat6025

#### 3.1 Introduction

Dramatic sea ice retreat accompanied with amplified warming over the Arctic has been observed in the recent decades (Screen and Simmonds, 2010). At the same time, an increasing frequency of extreme weather events across Europe and North America, particularly extreme cold snaps and enhanced snow fall, has gained a lot of socio-economic attention. Additionally, a cooling trend has emerged over Northern Hemisphere (NH) mid-latitude continents in winter (Shepherd, 2016), which has been referred as the “Warm Arctic Cold Siberia (or Continents)” (WACS) patterns (Overland et al., 2011). A group of previous studies have suggested a potential linkage between the rapid sea ice decline and Arctic warming and the cold winter events (Kug et al., 2015; Mori et al., 2014; Vihma, 2014). Alternatively, other studies have argued that extreme cold events are likely associated with the atmospheric natural variability (McCusker et al., 2016; Screen et al., 2015, for example). The conflicting results suggest that the relation between the Arctic and colder Siberia is still inconclusive due to poor understanding of how the interaction mechanism works.

Previous observational and modeling studies have suggested that sea ice variability, especially over the Barents and Kara Sea (BKS), could significantly influence the mid-latitude circulation in NH winter (see review papers by Barnes and Screen, 2015; Cohen et al., 2014, and references therein). More importantly, previous modeling studies have explicitly examined the role of the stratosphere in linking the BKS sea ice retreat to large-scale atmospheric circulation anomalies (Screen et al., 2015; Sun et al., 2015; Zhang et al., 2017). A weakening of the stratospheric polar vortex and a subsequent downward propagation of the stratospheric circulation anomaly, associated with an equatorward shift of mid-latitude jet have been identified (Hoshi et al., 2017; Jaiser et al., 2013; Kim et al., 2014; Zhang et al., 2017). However, to what extent the stratospheric pathway contributes to the Siberian cooling has not been well explored. This motivates us to further assess whether the stratosphere-troposphere coupling and the associated mid-latitude circulation anomalies due to BKS SIC retreat play a critical role to induce the cold temperature response over Siberia.

In this study, we examine the relationship between the BKS sea ice loss and Siberian cold temperature anomaly using a comprehensive Atmospheric General Circulation Model (AGCM), with well resolved stratosphere. We aim to critically demonstrate the underlying dynamical and thermodynamical adjustment as a result of BKS sea ice loss. Additionally, we conduct targeted experiments to quantitatively distinguish the influence of the troposphere and the stratosphere in driving the Siberian cold anomalies. In particular, we aim to address the following:

1. Can BKS SIC retreat lead to a colder Siberia?
2. What is the contribution of thermodynamical and dynamical components in driving the temperature response over Siberia?
3. What role does stratosphere-troposphere coupling play?

Previous studies have recommended the use of climate models with well resolved stratospheric dynamics (Charlton-Perez et al., 2013; Screen et al., 2018b; Sun et al., 2015) to study the impacts of sea ice loss. Therefore, the AGCM with well-resolved

stratosphere, will allow us to fully explore the stratosphere-troposphere coupling in this study. The study is organized as follows. Section 3.2 describe the methodology and experimental design. In Section 3.3, we present the relationship between Siberian cold temperature and BKS sea ice retreat and describe the underlying physical mechanism. Section 3.4 concludes the chapter.

This work is conducted as a part of a collaborative study and the results presented here have been incorporated towards a publication (Zhang et al., 2018). The insights from the investigation of the temperature budget associated with BKS SIC loss, presented here, contributed to Zhang et al. (2018). However, since the paper was designed to focus on the underlying dynamical mechanisms associated with extreme cold events over Eurasia and due to the limitation of the number of figures in the publication, the figures shown in this chapter were not included in Zhang et al. (2018).

## **3.2 Data and Methodology**

### **3.2.1 Numerical Model**

We perform a set of numerical experiments using Specified Chemistry Whole Atmosphere Community Climate Model version 4 (SC-WACCM4), a comprehensive AGCM with well resolved stratosphere (i.e. a “high-top” model), developed at National Center for Atmospheric Research (NCAR). The model is a component of Community Earth System Model version 1.2 (CESM1), with specified chemistry rather than interactive chemistry version WACCM4 (Smith et al., 2014). Note that the two versions has nearly identical climatology and atmospheric variability except low computational cost in SC-WACCM4 is useful to explore stratosphere-troposphere coupling (Smith et al., 2014). The model has a horizontal resolution of  $1.9^\circ$  latitude by  $2.5^\circ$  longitude, 66 vertical levels with a lid height at  $5.1 \times 10^{-6}$  hPa (approximately 140 km).

### 3.2.2 Experimental design

We conduct a control (CTRL) and three perturbation experiments, as described below. The surface boundary condition of the model is defined by prescribed sea surface temperature (SST) and sea ice concentration (SIC). The long CTRL experiment is performed with a repeating climatological seasonal cycle of SST and SIC, averaged over 1980-1999, obtained from the twentieth century historical simulation of the CESM1-WACCM4 (average of seven ensembles) in Coupled Model Intercomparison Project phase 5 (CMIP5) experiments.

In the first perturbation experiment, referred as BKS\_FL (full response), the settings are identical to the CTRL except the SIC over BKS is replaced by that in CMIP5 CESM1-WACCM4 simulation forced by Representative Concentration Pathway (RCP) 8.5 radiative forcing and averaged over the period of 2080-2099. The SST in BKS region over the open water areas that used be covered by sea ice in the CTRL is also replaced by RCP8.5 SST. The second perturbation experiment (named as BKS\_TP) is identical to the first perturbation experiment (i.e. BKS\_FL) except a nudging method is applied in the stratosphere to numerically shut down the stratosphere-troposphere coupling and isolate the tropospheric pathway. Specifically, in the nudging experiment, the zonal mean temperature, zonal wind, meridional wind, and specific humidity in the stratosphere are nudged towards a reference state obtained from the CTRL. The fields are fully nudged above 54 hPa with a nudging coefficient 1, no nudging is applied below 90 hPa with a nudging coefficient 0 and the nudging strength is linearly decreased in between. The nudging is performed at every time step of the model integration but the reference state from the CTRL is obtained at every 6 hours. The nudging time-scale is chosen to be 6 hours. In order to distinguish the contribution of the stratospheric pathway, we conduct third perturbation (i.e. second nudging) experiment (named as BKS\_SP). The BKS\_SP run is identical to the CTRL run, except that the zonal mean state in the stratosphere is

nudged toward that in the BKS\_FL run using the same nudging coefficients as in the BKS\_TP run.

The difference between BKS\_FL run and CTRL run examines the impact of BKS SIC loss on Siberian temperature. The difference between BKS\_TP and the CTRL can explicitly quantify the contribution due to the tropospheric adjustment within itself. The comparison between the BKS\_SP and CTRL assess the importance of an active stratospheric pathway to induce Siberian cooling. Since the most significant mid-latitude response occurs during the following two months of the largest SIC forcing (not shown), we focus on January-February (JF) response. Previous studies also suggested that early winter sea ice loss results in a prolonged mid-latitude circulation response in the subsequent winter (Koenigk et al., 2016; Zappa et al., 2018; Zhang et al., 2017).

The experiments are integrated for 60 model years, with the first 10 years discarded as spin-up. Thus 49 whole winters from the last 50 years are analyzed in each run.

### 3.2.3 Observations

We analyze observed monthly sea ice concentration (SIC) data with a resolution of  $25km \times 25km$  obtained from passive microwave satellite measurements with NASA team algorithm (Cavalieri et al., 1996) from 1982 to 2015 period. ERA-Interim re-analysis data produced by the European Center for Medium-Range Weather Forecasts (ECMWF) (Dee and Coauthors, 2011) has been used to examine observed temperature and atmospheric circulation response to BKS SIC loss. We use the monthly 500hPa geopotential height in  $1.5^\circ$  longitude  $\times$   $1.5^\circ$  latitude horizontal resolution for the period of 1982-2015.

### 3.2.4 Diagnostics

We perform lagged regression analysis between the BKS SIC loss in late autumn (November) and atmospheric circulation variables in the following winter months

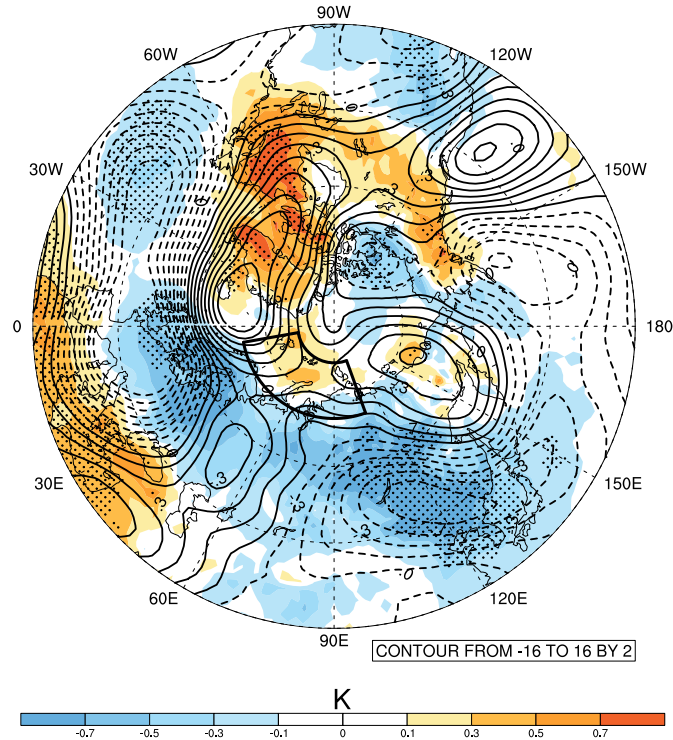


Figure 3.1. Regression of surface air temperature (color shadings, units: K/1 standard deviation of BKS SIC loss) and geopotential height at 500 hPa (contours, units: m/1 standard deviation of BKS SIC loss) during JF onto normalized BKS SIC index in November. Positive values in contours are solid black while negative values are dashed black and the zero contour is omitted. The black box highlights the BKS area over 70°–82°N and 10°–110°E. The stipplings indicate that the temperature response is significant at 95% confidence level using the students  $t$ -test.

(JF). We calculate a SIC index using standardized SIC anomalies, area averaged over the BKS region (70°–82°N, 15°–100°E), during November. Here we reverse the sign of the SIC index to emphasize the effect associated with sea ice loss. Our aim is to identify the possible impacts of late-autumn SIC loss on the atmospheric circulation and temperature in subsequent winter. We focus on the year-to-year variability by removing the long-term linear trend and the contribution from the ENSO (as linear regression on the Nino 3.4 index) from observations for all variables. The statistical

significance in observations and in model response is calculated using the students  $t$ -test at the 95% confidence level.

In order to calculate temperature budget, we vertically interpolate the simulated data in hybrid sigma coordinate into pressure level. We do not perform extrapolation when the pressure level is outside of the range of surface pressure. Therefore, we choose 850 hPa pressure level for the analysis (that provides maximum near surface area with no extrapolation), and thus to understand the underlying mechanism of surface air temperature (SAT) anomaly.

### 3.3 Results

#### 3.3.1 Colder Siberia in response to BKS SIC retreat

First, we examine the impacts of late-autumn BKS SIC variability on Siberian temperature and associated large-scale circulation anomalies in JF, using observations. Figure 3.1 shows the regression of observed detrended surface air temperature (color shading) and geopotential height (contours) onto BKS SIC index. We find a pronounced cold anomaly over the Siberia/northern Eurasia sector associated with a localized surface warming over the BKS, which resembles the WACS pattern. The corresponding tropospheric circulation anomaly is represented by an increase of geopotential height over the Arctic and a decrease over the northern continents with a prominent ridge near the Ural Mountains and a downstream trough over the Siberia. The anomalous ridge/trough pattern suggests a possible northerly advection of cold Arctic air into the continents that can favor a colder Siberian temperature.

Figure 3.2a shows the surface temperature and large-scale circulation response as simulated in the BKS\_FL experiment. We find a localized BKS surface warming induced by SIC melting and a surface cooling located over Siberia/northern Eurasia sector (highlighted in purple box). The corresponding large-scale tropospheric circulation anomaly is characterized by a positive ridge near the Ural Mountains and

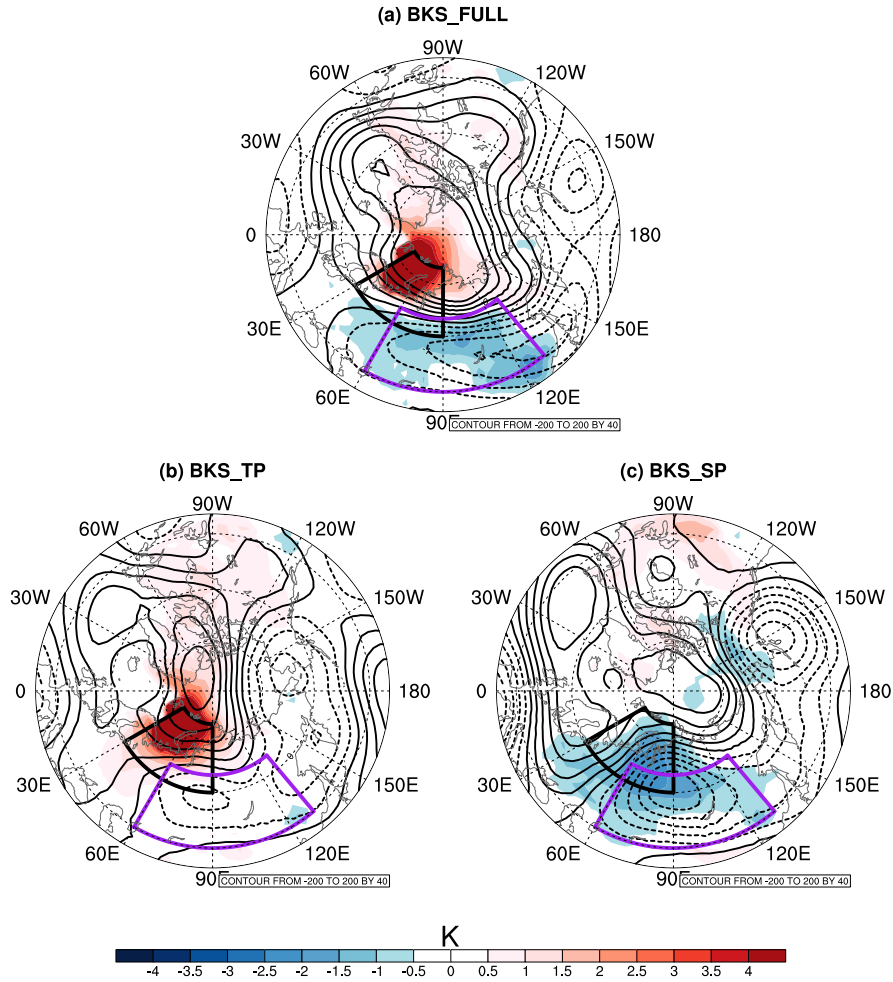


Figure 3.2. Responses of surface air temperature (color shadings, units: K) and geopotential height at 500 hPa (contours, units: gpm, contour interval 40gpm) in (a) BKS\_FL, (b) BKS\_TP and (c) BKS\_SP experiments, respectively. Positive values in contours are solid black line while negative values are dashed black line and the zero contour is omitted. The black box highlights the area corresponding to the ridge near the Ural mountains over 60°–80°N and 30°–90°E and the purple box highlights the area corresponding to maximum Siberia cooling over 48°–65°N and 60°–130°E. No extrapolation is performed when the pressure level is outside of the range of surface pressure.

a downstream trough over the Siberia. Additionally, Fig. 3.3a explicitly shows an enhanced northerly wind advection into the Siberia due to the amplified ridge/trough

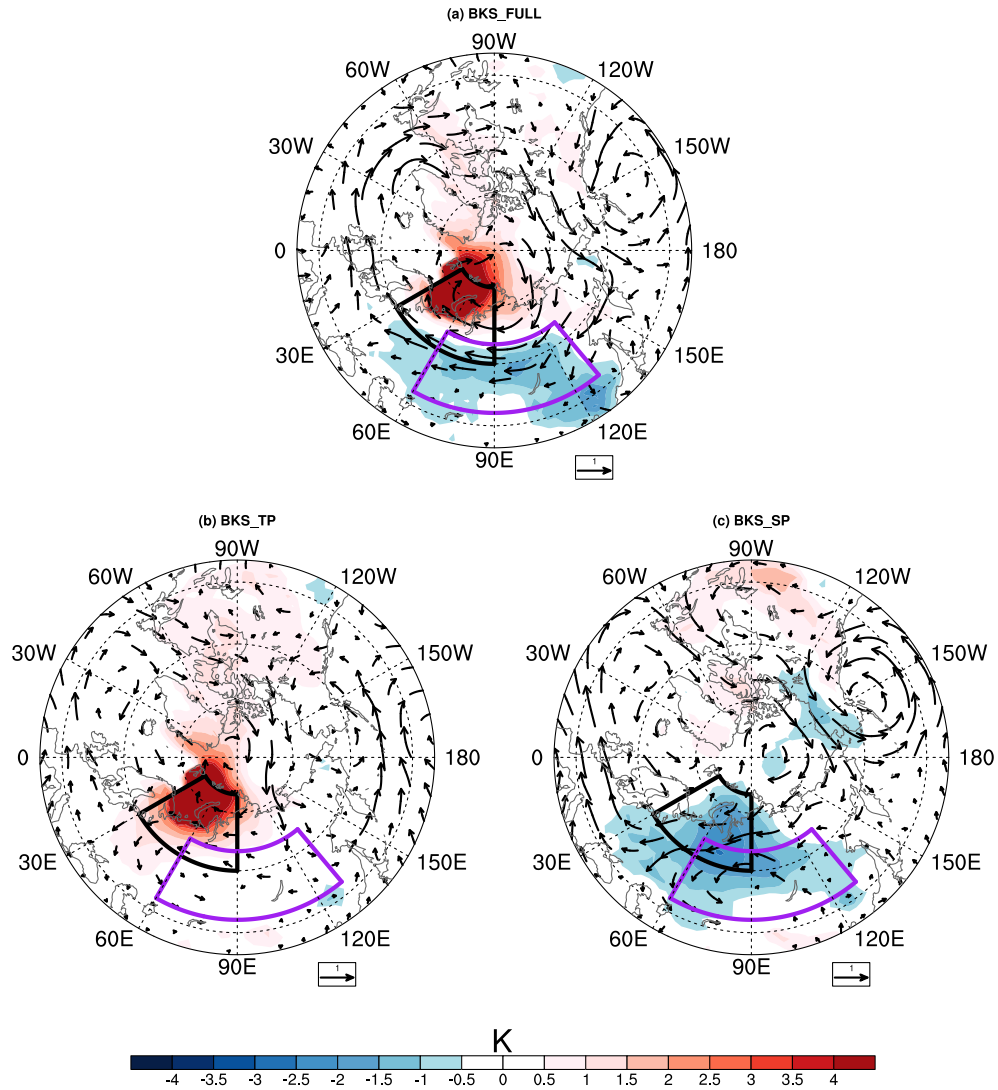


Figure 3.3. Same as Fig. 3.2 except wind vectors at 850 hPa are shown instead of geopotential heights.

patterns. The simulated responses to BKS SIC loss complements the statistical analysis using the observations (Fig. 3.1). Therefore, the findings reinforce our confidence to further explore the origin of Siberian cooling.

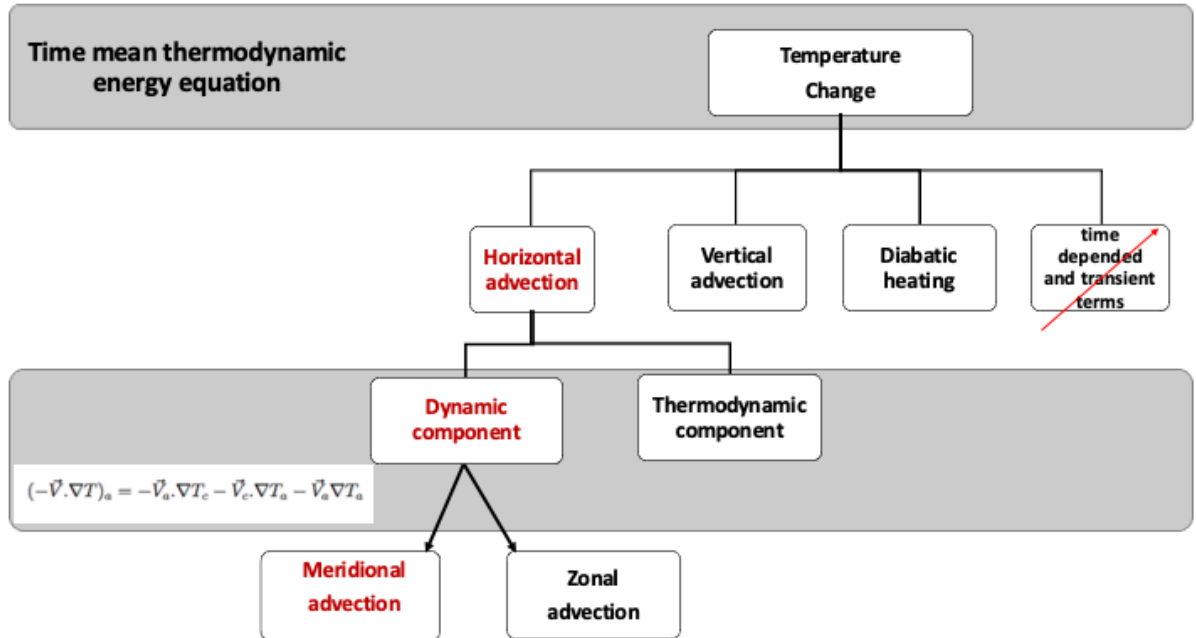


Figure 3.4. Decomposition of temperature budget analysis following Rodwell and Hoskins (2001). Red text indicates the dominate terms.

### 3.3.2 Mechanism of Siberian cooling

We decompose the simulated temperature response into each term of the temperature tendency equation (i.e., time mean thermodynamic energy equation), following the Equation (1) of Rodwell and Hoskins (2001), in order to explicitly assess the mechanism underlying the Siberian cold anomaly. The schematic in Fig. 3.4 shows the decomposition of the temperature budget. In particular, we examine the balance among diabatic forcing, vertical advection and horizontal advection, since on a seasonal time scale the time dependence term is negligible (Rodwell and Hoskins, 2001). The comparison reveals that the horizontal advection term dominates in driving the simulated temperature response over Siberia (not shown).

Furthermore, we decompose the horizontal temperature advection (Fig. 3.5a) into dynamic and thermodynamic components, following Equation (3.1), and compare

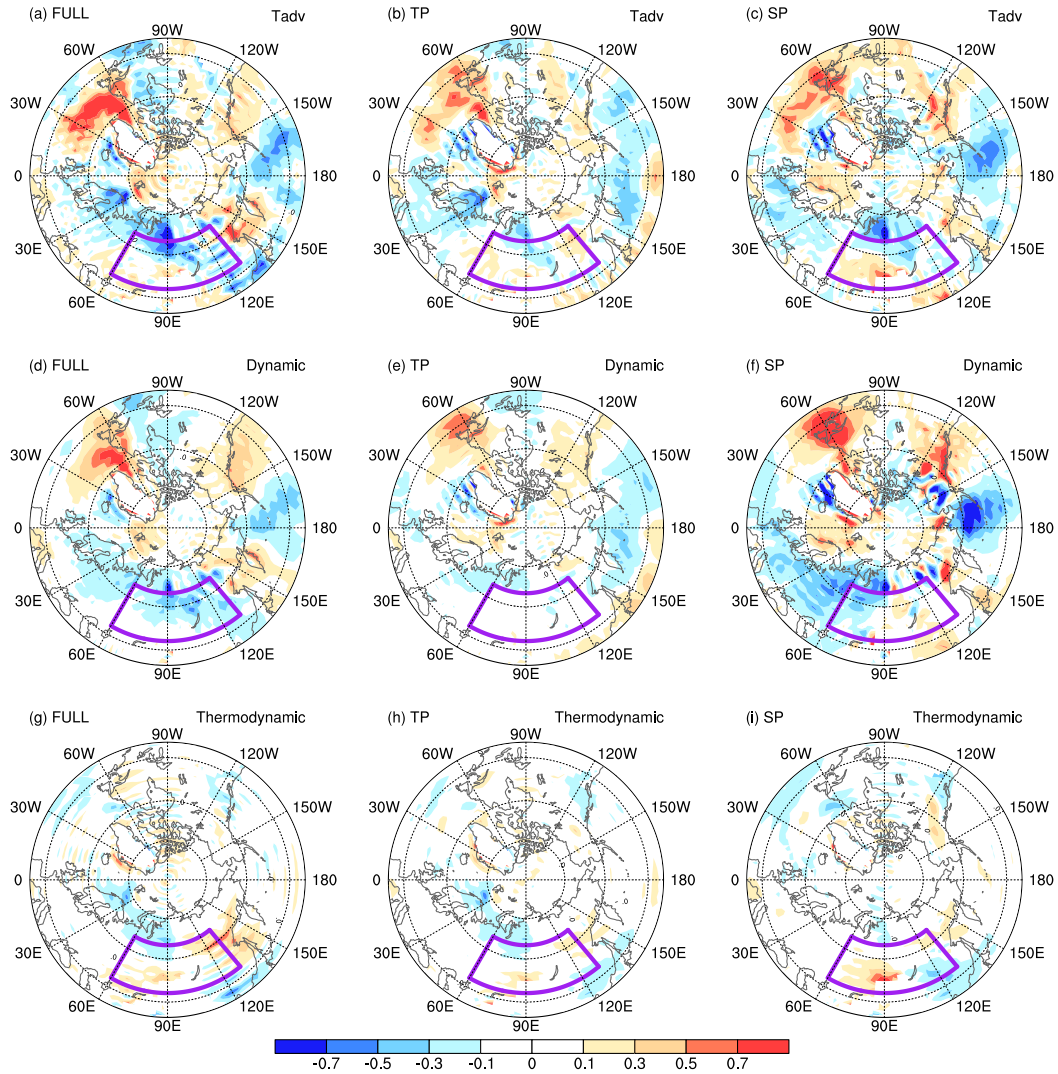


Figure 3.5. Horizontal temperature advection response at 850 hPa in BKS\_FL run (a), and its dynamic (d) and thermodynamic components (g). (b, e, h) and (c, f, i) are the same as (a, d, g) but for BKS\_TP run and BKS\_SP run, respectively. The area, where the pressure level is outside of the range of surface pressure, is masked.

their contribution over  $48^{\circ}$ – $65^{\circ}$ N and  $60^{\circ}$ – $130^{\circ}$ E, the area that experiences the most pronounced cooling due to BKS SIC loss (highlighted in purple box in each figure).

$$(-\vec{V} \cdot \nabla T)_a = -\vec{V}_a \cdot \nabla T_c - \vec{V}_c \cdot \nabla T_a - \vec{V}_a \nabla T_a \quad (3.1)$$

We find a larger contribution of the dynamic component (the first RHS term of Equation 3.1 and Fig. 3.5d) compared to the thermodynamic component (the second RHS term of Equation 3.1 and Fig. 3.5g). This suggests that the Siberian cooling is dynamically induced rather than a result of thermodynamical adjustment. Further decomposition of the dynamic component of the horizontal temperature advection (Fig. 3.6a), into zonal (Fig. 3.6d) and meridional terms (Fig. 3.6g) shows that the meridional advection of temperature dominates over the zonal advection. The results, therefore, robustly support that northerly wind anomaly from the Arctic into the continents is the key for a colder Siberia.

### 3.3.3 Role of stratosphere-troposphere coupling

We conduct two sets of nudging experiments in order to numerically isolate the role of the troposphere only and the stratosphere-troposphere coupling in driving a colder temperature response over Siberia. The Siberian cooling is almost gone when we numerically deactivate the stratosphere in BKS\_TP run (Fig. 3.2b) despite the identical SIC forcing as in the BKS\_FL run. The tropospheric circulation pattern, characterized by a positive geopotential height anomaly over the Arctic and negative anomaly over the continents with a pronounced ridge near the Ural mountains and a downstream trough, also weakens in BKS\_TP run than in the BKS\_FL run. Correspondingly, the dynamical cold air advection from the Arctic is reduced and results in less Siberia cooling (Fig. 3.3b). In contrast, surface cold temperature anomaly and the intensified trough over Siberia are found in BKS\_SP run (Fig. 3.2c), when we isolate the contribution of the troposphere-stratosphere coupling associated with BKS SIC loss. Concurrent cold air advection from the Arctic into the Siberia causes dynamically induced cold temperature anomaly (Fig. 3.3c).

The nudging experiments explicitly show that, the Siberian cooling, in the BKS\_FL experiment is comparable to the BKS\_SP response, but almost vanishes in the BKS\_TP run. Therefore, stratosphere-troposphere coupling has an important role in driving

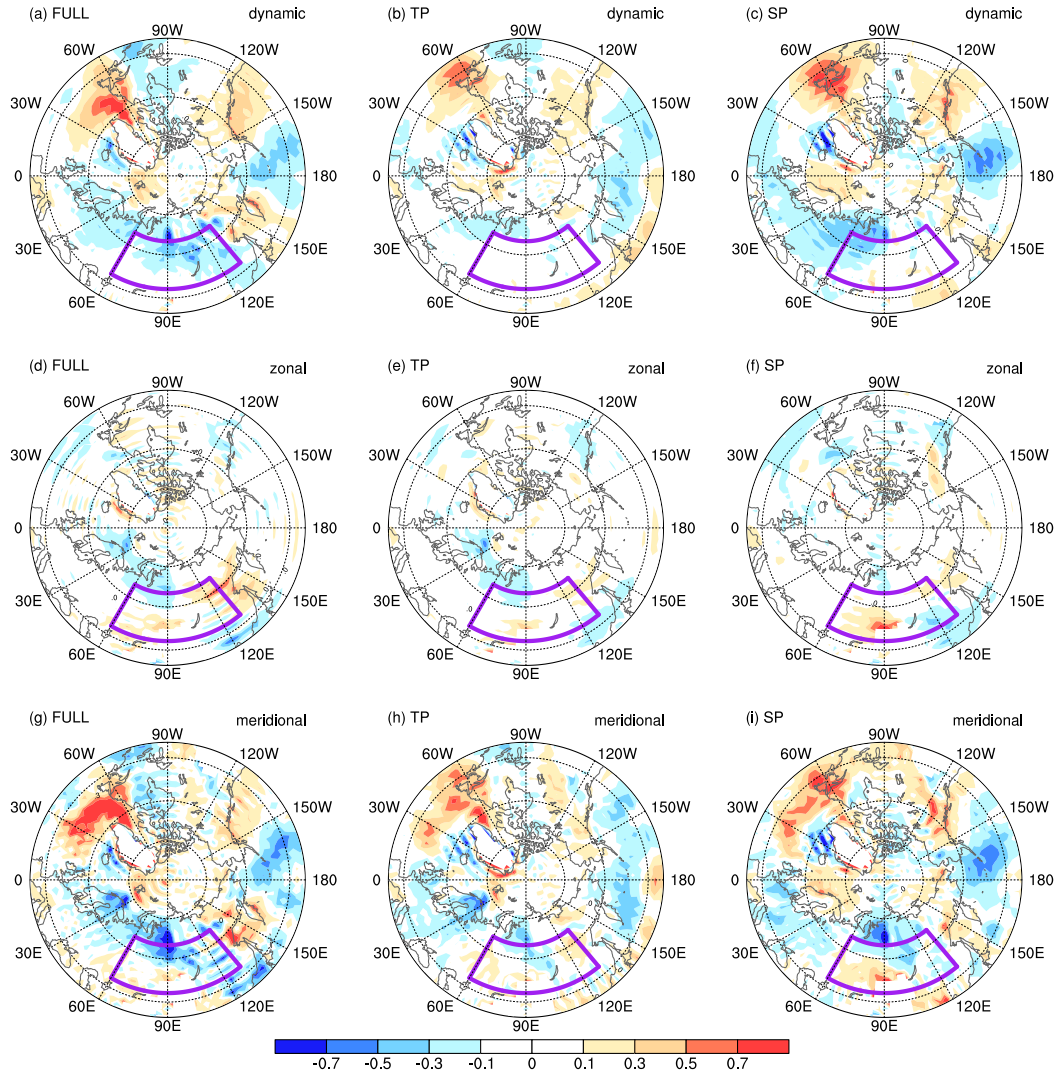


Figure 3.6. Dynamic component of horizontal temperature advection response at 850 hPa in BKS\_FL run (a), and its zonal (d) and meridional components (g). (b, e, h) and (c, f, i) are the same as (a, d, g) but for BKS\_TP run and BKS\_SP run, respectively. The area, where the pressure level is outside of the range of surface pressure, is masked.

the Siberian cooling due to BKS SIC loss. Isolating the tropospheric pathway weakens the circulation anomaly and as a result, reduces the dynamically induced temperature

response.

Next, we explicitly examine the influence of stratosphere-troposphere coupling in driving the horizontal temperature advection from the Arctic into the Siberia using the nudging experiments. The horizontal advection term, over Siberia  $48^{\circ}$ – $65^{\circ}$ N and  $60^{\circ}$ – $130^{\circ}$ E, is reduced in BKS\_TP experiment (Fig. 3.5b) compared to that in BKS\_FL (Fig. 3.5a) but returns in BKS\_SP (Fig. 3.5c), . We further decompose the horizontal temperature advection into the dynamic and thermodynamic components in BKS\_TP run and BKS\_SP, following the Equation (3.1). Fig. 3.5e shows that the dynamic component of the horizontal temperature advection from the Arctic almost vanishes over Siberia when we shut down the stratosphere-troposphere coupling in BKS\_TP but causes cooling over Siberia in BKS\_SP run (Fig. 3.5f). The thermodynamic component of the horizontal temperature advection (Fig. 3.5h) does not have a major change due to shutting down the stratospheric pathway.

Further decomposition of the horizontal temperature advection into zonal and meridional terms, in absence of stratospheric pathway in the BKS\_TP run, shows a significant reduction in the meridional component (Fig. 3.6h) compared to the zonal (Fig. 3.6e). Fig. 3.6i shows that meridional term of the dynamic component, in BKS\_SP run, contributes more in driving cold anomaly in BKS\_FL run (Fig. 3.6g). Thus, we demonstrate that less Siberia cooling in BKS\_TP experiment is largely attributable to reduced cold temperature advection from the Arctic. Targeted nudging experiments explicitly show an important contribution of the stratospheric pathway to induce the dynamical teleconnection between the BKS SIC loss and Siberia temperature.

### 3.4 Conclusions and Discussion

The present study, through targeted modeling experiments, reveals the contribution of the dynamical processes linking the BKS SIC loss and colder Siberia. We

show that a comprehensive AGCM with a well-resolved stratosphere can simulate the observed relation between the BKS SIC loss and Siberian cooling. The results from the thermodynamic and dynamic decomposition find that the key mechanism for the linkage is the large-scale dynamical adjustment due to BKS SIC loss, characterized with an amplified Ural High and a downstream trough over Siberia. Consequently, the meridional temperature advection from the Arctic into the continent dominates in driving the Siberian cooling.

Furthermore, we demonstrate that an active stratospheric pathway contributes significantly in driving the dynamically induced cooling. It has been documented that the dynamical linkage between BKS sea ice retreat and Siberian cooling, via a stratosphere-troposphere coupling, can be attributable to a weakening of the stratospheric polar vortex due to BKS SIC loss (Kim et al., 2014; Sun et al., 2015; Zhang et al., 2017). The prolonged downward effect from the weakened stratospheric polar vortex leads to a negative North Atlantic Oscillation (NAO) like pattern, characterized by a positive geopotential height anomaly over the Arctic and a negative geopotential height anomaly over the adjacent continents, and the downstream ridge/trough anomaly over Atlantic-Eurasia section. We identify that the resultant northerly flow and cold air advection from the Arctic is responsible for the surface cooling over Siberia.

The analysis emphasizes on the stratospheric pathway to explain the linkage between the BKS SIC and a colder Siberia. The finding suggests that the discrepancies in the previous studies, as mentioned in the introduction, could be partly due to different stratospheric representation in the models. For example, the modeling studies that can not reproduce the Siberia cooling used low-top models without a fully resolved stratosphere (McCusker et al., 2016; Sun et al., 2016). Thus, our study advocates to incorporate a well-resolved stratosphere in the climate models to better understand the impacts of the Arctic sea ice loss and obtain a realistic projection of regional weather. Additionally, the finding will contribute towards an improved seasonal weather forecast in winter.

## 4. ARE MID-LATITUDE CIRCULATION RESPONSES LINEARLY ADDITIVE TO REGIONAL ARCTIC AMPLIFICATION? INSIGHTS FROM AN IDEALIZED ATMOSPHERIC GENERAL CIRCULATION MODEL

A version of this chapter is soon to be submitted for publication

### 4.1 Introduction

Dramatic sea ice loss and amplified warming over the Arctic (AA) has been observed in the recent decades (Screen and Simmonds, 2010). Previous observational and modeling studies have suggested a potential influence of the Arctic sea ice loss on the mid-latitude circulation in Northern Hemisphere (NH) winter (see review papers by Cohen et al. (2014), Barnes and Screen (2015) and references therein). Nevertheless, how and to what extent the AA contributes to modulate the mid-latitude circulation remains inconclusive due to the incomplete understanding of the underlying mechanisms (Screen et al., 2018b).

It has been suggested that the atmospheric circulation response is sensitive to the geographical location and spatial pattern of the Arctic sea ice loss (McKenna et al., 2018; Screen, 2017; Screen et al., 2018b; Sun et al., 2015; Zhang et al., 2017). However, majority of the previous works focused on the impacts of the sea ice melting over either the pan-Arctic (McCusker et al., 2016; Ogawa et al., 2018; Screen et al., 2015) or the Barents-Kara Sea (BKS) (De and Wu, 2018; Kim et al., 2014; Mori et al., 2014; Zhang et al., 2018). Circulation responses including a weakening of the stratospheric polar vortex and an equatorward shift of the mid-latitude jet were commonly found. Only a few studies highlighted the opposing impacts on the stratospheric polar vortex

associated with the sea ice loss over different Arctic regions (McKenna et al., 2018; Sun et al., 2015). For instance, Sun et al. (2015) found a stratospheric polar vortex weakening with sea ice loss inside the Arctic Circle (primarily over the BKS) while a strengthening with sea ice loss outside the Arctic Circle (mainly over the Bering Sea, Sea of Okhotsk, and Hudson Bay).

In a recent study, Screen (2017) divided the whole Arctic into nine sub-regions to study the regional impacts and further compared with the pan-Arctic response, using the comprehensive Atmospheric General Circulation Model (AGCM) HadGEM2. In each of the perturbation experiments, Screen (2017) imposed the sea ice forcing over individual region by subtracting two standard deviations of monthly sea ice concentration (SIC) from the climatology at each ice covered grids and adding two standard deviations of monthly sea surface temperature to the climatology over partially ice-covered grids. The study showed that the response to pan-Arctic sea ice loss cannot be obtained by simple linear addition of the responses to regional sea ice loss. Specifically, a nonlinear interaction among the responses to regional sea ice loss was suggested, however, the underlying dynamical mechanism remains unexplained. This motivates us to further investigate the linear additivity problem but using a simple AGCM. Comparing to the comprehensive AGCM, the idealized AGCM has the advantage in isolating the dynamics from uncertainties that arise due to complex physical parameterizations in comprehensive atmospheric model, sea ice model and their coupling. In this way, the idealized model would serve as a useful testbed for the robustness of the results as found in comprehensive AGCMs. In addition, the computational efficiency of idealized AGCM would also facilitate the exploration of the sensitivities of the responses to forcing magnitude. Targeted experiments can also be easily implemented to aid the interpretation of the underlying dynamical mechanism.

In this study, we focus on three regions over the Arctic, i.e. BKS, Baffin Bay-Davis Strait-Labrador Sea (BDL) and East Siberia-Chukchi sea (ESC), and the reasons are the following. In the recent decades, the Arctic has warmed up the most over the BKS and BDL regions (Shepherd, 2016, see their Fig. 2). Possible influences on

Eurasia cooling associated with BKS sea ice loss (Mori et al., 2014; Zhang et al., 2018) and on North America cooling following ESC and BDL sea ice loss (Chen and Luo, 2017; Kug et al., 2015; Overland and Wang, 2018) were suggested in previous studies. Therefore, these three regions play a crucial role in affecting the mid-latitude circulation and weather extremes.

With the simple AGCM experiments, we aim to address the following questions:

1. What are the impacts of the regional AA, separately and simultaneously, on the stratospheric polar vortex and the tropospheric circulation?
2. Are these responses linearly additive? If not, what is the underlying dynamical mechanism?
3. How do the results vary with forcing magnitude?

This chapter is organized as follows. In section 4.2, we describe the methodology and experimental design using the simple AGCM. In section 4.3, we present the zonal mean zonal wind response to regional AA and investigate the linear additivity, its underlying mechanism and sensitivity to forcing magnitude. Section 4.4 concludes this study.

## 4.2 Data and Methods

### 4.2.1 Observations

We analyze monthly SIC data obtained from passive microwave satellite measurements with NASA team algorithm (Cavalieri et al., 1996) during 1982–2015. The monthly atmospheric variables from the ERA Interim reanalysis data produced by the European Center for Medium-Range Weather Forecasts (ECMWF) are used during the same period (Dee and Coauthors, 2011). We define monthly SIC index using detrended and standardized SIC anomaly, area averaged over the BKS ( $70^{\circ}$ – $80^{\circ}$ N,  $10^{\circ}$ – $110^{\circ}$ E), BDL ( $55^{\circ}$ – $75^{\circ}$ N,  $270^{\circ}$ – $310^{\circ}$ E) and ESC ( $65^{\circ}$ – $82^{\circ}$ N,  $160^{\circ}$ – $210^{\circ}$ E) regions,

respectively, from November to subsequent February. Each region is highlighted by black boxes in Fig. A4. In order to identify the responses in surface air temperature and circulation associated with regional SIC variability, we perform lagged regression analysis between monthly SIC indices and atmospheric variables during boreal winter. Both the long-term trend and contribution from the El Niño-Southern Oscillation (or ENSO, derived as linear regression on Niño 3.4 index) are removed from the atmospheric variables prior to the regression analysis. We also reverse the sign of the SIC indices to emphasize the response associated with SIC loss. Note that we define SIC index for BKS using November SIC and for BDL and ESC using December and January SIC. This is because the concurrent surface warming associated with the SIC loss is maximized in those respective months for each region (not shown).

#### 4.2.2 Numerical Model

We perform a set of numerical experiments using a dry dynamical core, developed at the Geophysical Fluid Dynamics Laboratory (GFDL). The model integrates the primitive equations driven by idealized physics (Held and Suarez, 1994) and includes a simple representation of the stratospheric polar vortex (Polvani and Kushner, 2002) and a realistic topography to excite stationary waves (Smith et al., 2010). As found previously, this model simulates a tropospheric jet located at about  $40^{\circ}\text{N}$  that is close to the observed winter climatology (Wu and Smith, 2016) and a fairly realistic stationary wave climatology (Zhang et al., 2017). The model has a spectral T42 horizontal resolution, 40 sigma levels in the vertical with a model top at 0.02 hPa. To simplify the analysis, we integrate the model under perpetual winter conditions.

#### 4.2.3 Experimental Design

For each forcing region (ESC, BDL, BKS and ALL), we perform a perturbation experiment (referred to as FULL) and compare it against a long control (CTRL)

integration. In the FULL experiment, we impose an additional heating,  $\Delta Q$ , to the temperature tendency equation as follows:

$$\frac{\partial T}{\partial t} = .. - \kappa_T [T - T_{eq}] + \Delta Q \quad (4.1)$$

where  $\kappa_T$  is the Newtonian relaxation time scale and is 40 days,  $T_{eq}$  is the original radiative equilibrium temperature profile and is a function of latitude  $\phi$  and sigma level  $\sigma$ . The imposed heating rate,  $\Delta Q$ , as a function of longitude  $\lambda$ , latitude  $\phi$ , and sigma level  $\sigma$ , is designed to mimic the structure of the observed temperature anomaly associated with sea ice loss over ESC, BDL and BKS regions.

Figure A.4 shows the regressed surface air temperature on SIC index for the three Arctic regions in observations. We choose the zonal and meridional profile of the prescribed heating based on Fig. A.4. The regressed temperature profile also penetrates to the mid-troposphere, with slightly varying altitudes for each region (not shown). For simplicity, the vertical depth of the prescribed heating is chosen to be identical for each region.

Accordingly, here is the imposed heating rate:

$$\Delta Q = Q_0 \cos^k\left(\frac{5}{2}(\phi - \phi_0)\right) e^{m(\sigma-1)} \sin^n\left(\frac{3}{2}\lambda - \lambda_0\right), \quad (4.2)$$

for ESC run,  $\phi \geq 50^\circ N$ ,  $\phi_0 = 64^\circ N$ ,  $150^\circ < \lambda < 250^\circ E$ ,  $\lambda_0 = 193^\circ E$ ,

for BDL run,  $\phi \geq 55^\circ N$ ,  $\phi_0 = 67^\circ N$ ,  $250^\circ < \lambda < 350^\circ E$ ,  $\lambda_0 = 0$ ,

for BKS run,  $\phi \geq 65^\circ N$ ,  $\phi_0 = 75^\circ N$ ,  $10^\circ < \lambda < 110^\circ E$ ,  $\lambda_0 = 0$ ,

where  $k = 12$ ,  $m = 5$ ,  $n = 4$  are chosen to mimic the observed heating profile (as shown in Fig. A.4). The ALL run is conducted with imposed heating over all three regions simultaneously. In section 4.3, as a primary example, we use a heating rate  $Q_0 = 3.5$  K/day. The horizontal structure of the prescribed heating profile is shown in Fig. 4.1 and the corresponding vertical profile is shown in Fig. A.5 for  $Q_0 = 3.5$  K/day. To examine the sensitivity to forcing magnitude, we also perform experiments with  $Q_0 = 2.5, 3.0, 4.0, 4.5$  K/day. Forcing magnitude smaller than 2.5 K/day is found to result in insignificant response in the stratosphere and thus is not included.

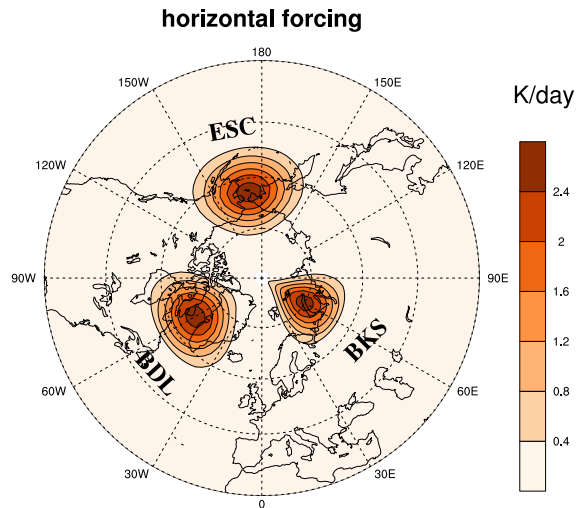


Figure 4.1. Spatial structure of the prescribed heating rate (color shadings and black contours, with contour interval 0.4 K/day) at the lowest model level for  $Q_0 = 3.5$  K/day.

To aid the interpretation of the underlying dynamical mechanisms, especially the contributions from the stratosphere-troposphere coupling dynamics, we perform another set of experiments (namely no-vortex). The no-vortex experiments are identical to the standard configuration introduced before except that the lapse rate is set to zero in the stratosphere and no topography is imposed. The no-vortex experiments are employed to remove the influence of the stratosphere-troposphere coupling and thus to isolate the tropospheric dynamics alone. We integrate the model for 18,000 days (equivalent to 50 years under perpetual winter conditions) in CTRL and FULL runs and for 12,000 days in no-vortex runs.

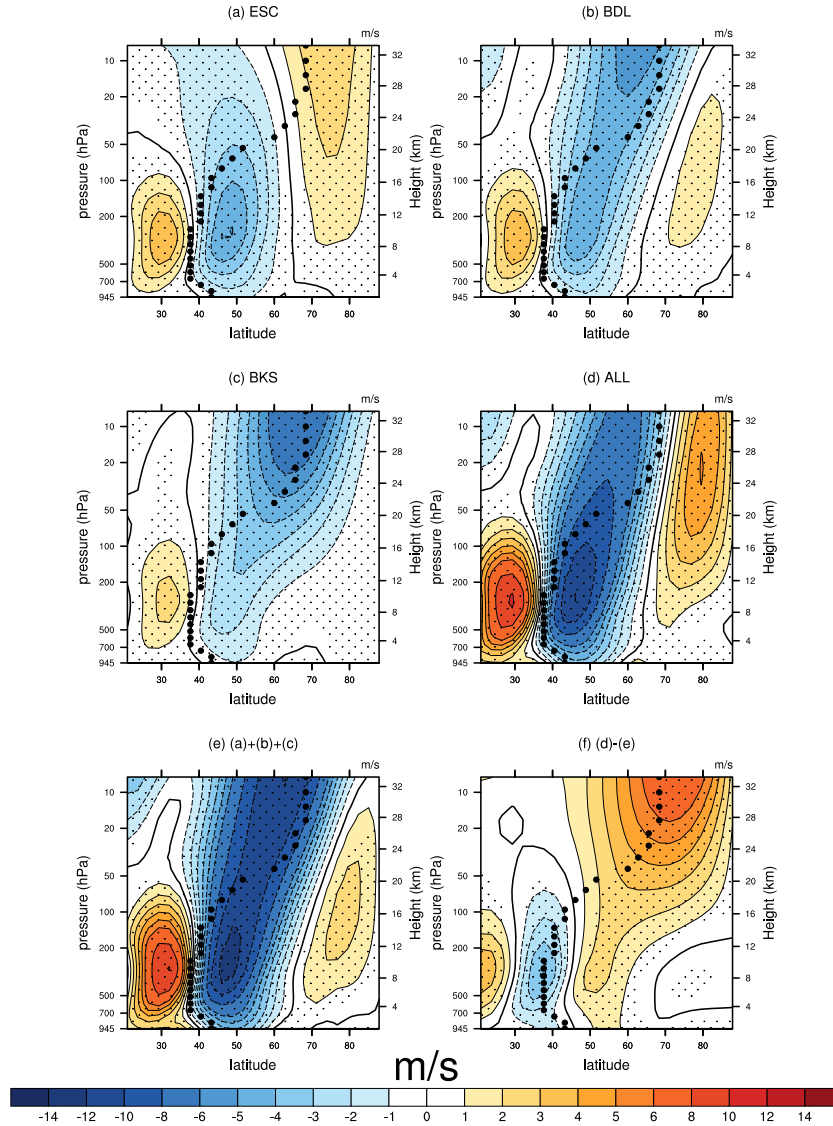


Figure 4.2. Response of zonal mean zonal wind (color shadings and contours, with contour interval of 1 m/s upto  $\pm 6$  m/s and 2 m/s beyond that) in the FULL runs with a heating magnitude of 3.5 K/day in (a) ESC, (b) BDL, (c) BKS, (d) ALL experiments. (e) is the sum of the circulation responses to individual regional forcings and (f) is the difference between (d) and (e). Black dots represent the climatological location of jet maximum. Stippling denotes the regions that are statistically significant at the 95% confidence level using a two-sided  $t$ -test.

## 4.3 Results

### 4.3.1 Simulated atmospheric circulation response to regional AA

First, we present the zonal mean zonal wind response in the idealized AGCM experiments with imposed heating over ESC, BDL, BKS regions, separately, in Fig. 4.2a-c. In response to ESC heating, the simulated atmospheric circulation shows an equatorward shift of the NH mid-latitude tropospheric jet characterized by a strengthening on the equatorward flank of the climatological jet and a weakening on the poleward flank (Fig. 4.2a). The stratospheric polar vortex shows a strengthening above 50hpa while a weakening below that. This response is qualitatively similar to the regression results in observations (Fig. A.6a), except that the observations show a stronger and more equatorward located jet increase in the stratosphere, and the modeling results in McKenna et al. (2018). Analysis of the Eliassen-Palm (EP) flux (Fig. 4.3a) shows that the strengthening of the stratospheric polar vortex poleward of 60°N is primarily associated with a downward wave propagation anomaly, which is due to a destructive interference in zonal wave-1 (not shown). The weakening of the stratospheric zonal mean zonal wind over the mid-latitudes is due to the convergence of EP flux anomaly, dominated by its meridional component (not shown).

The circulation response in the other two runs, with prescribed heating over BDL (Fig. 4.2b) and BKS (Fig. 4.2c), shows an equatorward shift of the NH mid-latitude tropospheric jet and a general weakening of the stratospheric polar vortex. Comparing the two runs, the weakening of the stratospheric polar vortex is slightly stronger in the BKS run than the BDL run. These patterns also qualitatively resemble the observed results in the regression analysis except in the low-latitude stratosphere for the BDL case (Fig. A.6bc). We find that the enhanced EP flux convergence, dominated by the meridional component over the mid-latitudes (not shown) and vertical component over the high-latitudes (Fig. 4.3b), is responsible for the weaker stratospheric polar vortex due to BDL warming. The widespread weakening of the stratospheric polar

vortex associated with BKS warming is primarily due to the enhanced upward wave propagation (Fig. 4.3c), similar to McKenna et al. (2018); Zhang et al. (2017).

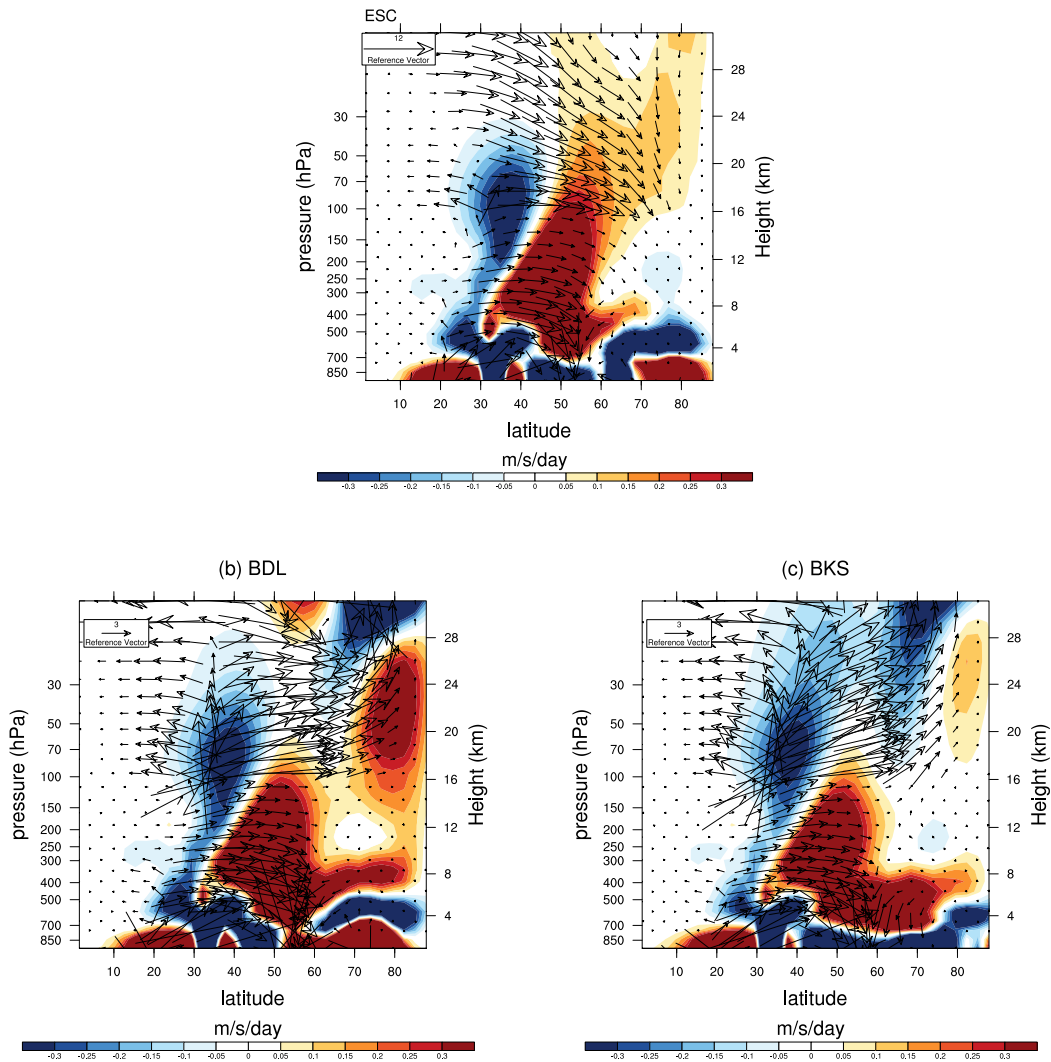


Figure 4.3. Response of EP flux (vector) and EP flux divergence (color shading, units: m/s/day) for the vertical component in (a) ESC, (b) BDL, (c) BKS, respectively. The EP flux is multiplied by the square root of  $1000/\text{pressure (hPa)}$  to better demonstrate the waves in the stratosphere. Note that the vectors above 100hPa have been further magnified by a factor of 8 in ESC and by a factor of 6 for BDL and BKS.

The perturbation experiment ALL, with imposed heating over all three regions simultaneously, shows a stronger equatorward shift of the tropospheric jet and a dipole structure in the stratospheric polar vortex with a strengthening poleward of  $70^{\circ}\text{N}$  and a weakening over the mid-latitudes (Fig. 4.2d). Interestingly, the linear addition of the zonal mean zonal wind response to regional AA (Fig. 4.2e), as obtained from the first three FULL runs, is not identical to the response obtained from ALL (Fig. 4.2d). In particular, the sum of the responses to regional AA actually over-estimates the response to simultaneous forcing in most regions in the midlatitudes. As a result, the difference between Fig. 4.2d and Fig. 4.2e, as shown in Fig. 4.2f, resembles a positive Northern Annular Mode (NAM)-like structure with a stronger polar vortex in the stratosphere and a poleward shift of the mid-latitude jet in the troposphere. The pattern remains robust over a range of imposed forcing magnitudes (to be discussed later). Additionally, we find that the circulation response to regional AA is not linearly additive either if we have two regions instead of three regions (not shown).

### 4.3.2 Non-linearity and stratosphere-troposphere coupling

Here we further explore the non-linearity and the underlying dynamical mechanism. The vertically coherent non-linear structure, as shown in Fig. 4.2f, likely suggests a possible role of the stratosphere-troposphere coupling. To examine the contribution of stratosphere-troposphere coupling, we make use of the no-vortex experiments.

First, we quantify the percentage of non-linearity by calculating the absolute value of the ratio between the residual and response to ALL. Figure 4.3a shows the percentage ratio between Fig. 4.2f and Fig. 4.2d, and non-linearity of about 10–60% can be seen in the midlatitude troposphere and stratosphere. This contribution of non-linearity to the total response is certainly non-negligible. In order to assess the stratospheric influence, we examine the corresponding results in the no-vortex runs. Since no-vortex configuration has no climatological stratospheric polar vortex and

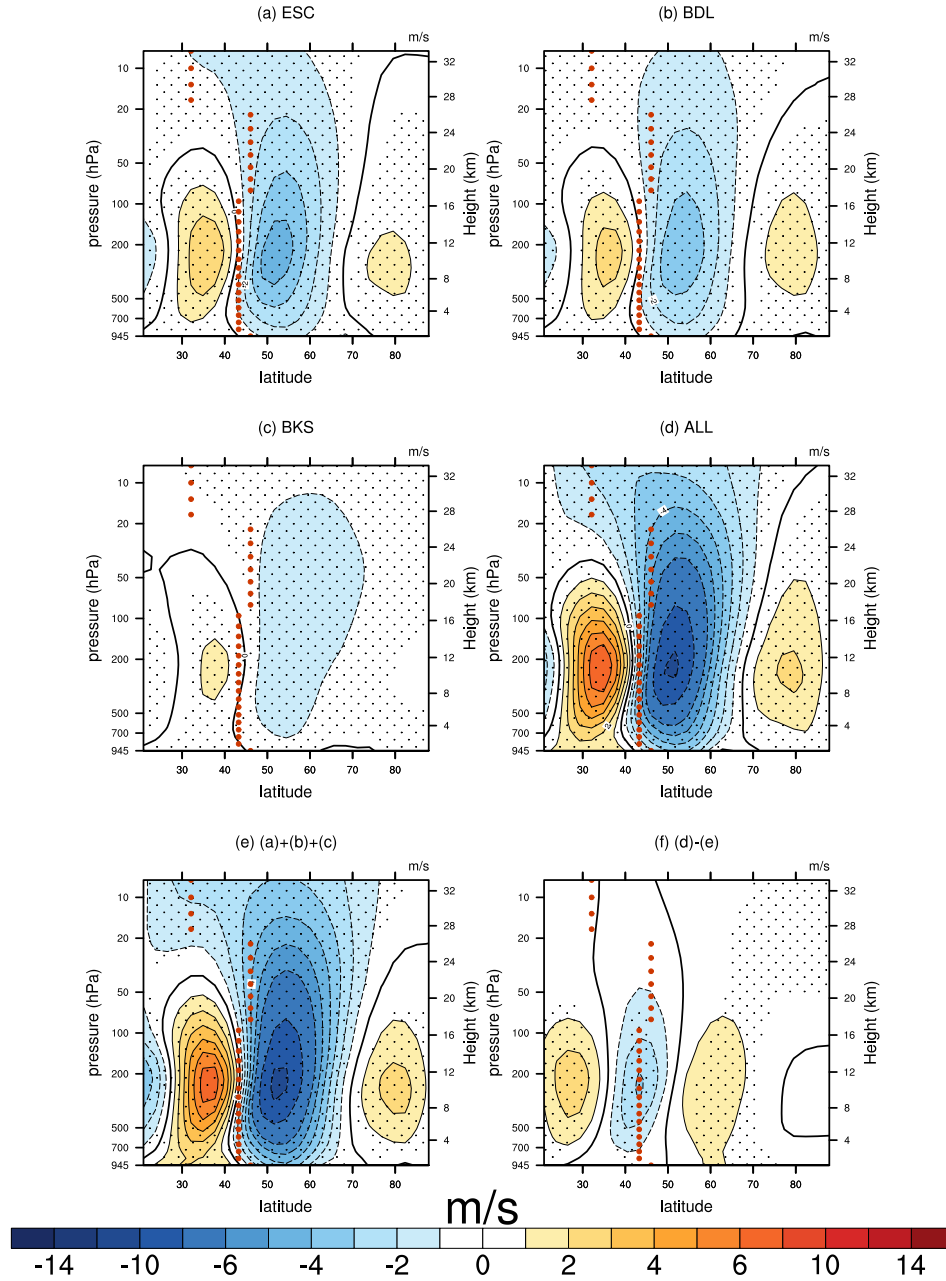


Figure 4.4. Similar to fig. 4.2 but for no-vortex configuration.

thus no stratosphere-troposphere coupling, only the tropospheric dynamics is in effect. Figure 4.4a-f is similar to Fig. 4.2 but in the no-vortex configuration. When

comparing the percentage of non-linearity between the standard and no-vortex configuration (Fig. 4.5a and Fig. 4.5b), the amount of non-linearity in the troposphere is significantly reduced in the latter. Therefore, the results confirm that stratosphere-troposphere coupling plays an important role in amplifying the non-linearity in the troposphere.

### 4.3.3 Variation of non-linearity with forcing magnitude

Next, we quantify how non-linearity varies with forcing magnitude. The resulting warming over the Arctic, area averaged temperature at 945 hPa over the Arctic region ( $67.5^{\circ}$ – $90^{\circ}$ N) in ALL runs, lies between 8.2 K–12.8 K. The AA values are comparable with the projected annual mean AA that is likely to exceed  $8.3^{\circ}$ C during 2080–2099 in the representative concentration pathway 8.5 (RCP8.5) scenario with respect to the historical scenario during 1980–1999 as reported in the Intergovernmental Panel on Climate Change (IPCC) Fifth Assessment (AR5) report (Collins et al., 2013).

As discussed above, Fig. 4.5a shows the percentage of non-linearity at the heating rate of 3.5 K/day. Qualitatively similar patterns are found over a range of forcing magnitude, however, the percentage ratio generally tends to increase with forcing magnitude in both the troposphere and stratosphere (Fig. A.7). To summarize the results, as an example, we show the relation between the forcing magnitude and non-linearity at two grid points, one at 700hPa,  $50^{\circ}$ N to represent the mid-latitude troposphere and the other at 20hPa,  $50^{\circ}$ N to represent the mid-latitude stratosphere, respectively (see red and blue dots in Fig. 4.5a). We choose  $50^{\circ}$ N because it approximately collocates with the maximum jet anomaly over the midlatitudes (Fig. 4.2d). We find that the percentage of non-linearity in the troposphere first decreases from 2.5 to 3.0 K/day heating rate and then increases steadily from about 22% to 32% when heating rate increases from 3.0 to 4.5 K/day. In the meanwhile, the non-linearity in the stratosphere is about the same with heating rate of 2.5 and 3.0 K/day and increases significantly from about 21% to 43% with increasing heating rate. As a

comparison, the no-vortex results are also shown but the non-linearity ratio is below 10% and is much smaller than the counterparts in the standard configuration with 3.5 K/day heating rate.

#### 4.4 Conclusions and Discussion

In this study, we have explored the linear additivity of the mid-latitude circulation response to regional AA, the underlying dynamical mechanism and sensitivity to forcing magnitude using a simplified AGCM. Specifically, we have found that:

- Regional AA has similar impacts on the tropospheric zonal mean zonal wind with an equatorward shift of the mid-latitude tropospheric jet. But differences in the response are seen in the stratosphere. While the stratospheric polar vortex generally weakens with imposed heating over the BKS and BDL regions, the stratospheric polar vortex strengthens above 50hPa when the forcing is imposed over the ESC region.
- The zonal mean zonal wind responses to regional AA are not linearly additive and the sum of the responses to regional AA over-estimates the response to simultaneous AA forcing in most midlatitude regions. As a result, a positive NAM-like vertically coherent response is found in the residual term.
- The stratosphere-troposphere interaction plays an important role in amplifying the non-linearity in the troposphere.
- For an amplified warming of about 10K over the Arctic (corresponding to imposed heating rate of 3.5 K/day), non-linearity could contribute about 10–60% to the total response in the midlatitude troposphere and stratosphere and is not negligible. In addition, the non-linearity also generally increases with forcing magnitude.

We would like to emphasize, as mentioned in the introduction, that considerable diversities exist among model responses to Arctic sea ice loss, part of which can be

attributable to different spatial patterns of the prescribed forcing (Screen et al., 2018b, and references therein). As found in this study, responses to sea ice loss over different regions can interact non-linearly to affect the mid-latitude circulation response. The results suggest that, because of this non-linearity, studying the regional sea ice loss might not provide the full picture of the consequences of pan-Arctic sea ice loss in decadal timescale. And pan-Arctic sea ice forcing, rather than regional sea ice forcing, should be implemented in studies whose focus is the impact of decadal sea ice melting.

In addition, we find that the stratosphere-troposphere coupling plays a critical role in understanding not only response to regional AA but also the non-linearity of the tropospheric circulation response to regional AA. In particular, the non-linearity is amplified by active stratosphere-troposphere coupling through downward influence. It's therefore important to fully and correctly represent the stratospheric circulation response in sea ice loss model experiments.

In summary, the results demonstrated using idealized AGCM experiments agree qualitatively with the results found in Screen (2017) using a comprehensive AGCM. In both Screen (2017) and our study, non-linearity is found and in particular, the sum of responses to regional forcing tends to over-estimate the response to simultaneous forcing. Our study also complements Screen (2017) and examines the role of stratosphere-troposphere coupling and sensitivity to forcing magnitude. However, we note that the model, used by Screen (2017), does not have a well resolved stratosphere (“low-top”), so the non-linearity found in Screen (2017) could possibly be under-estimated. Therefore, it is worth extending the study but using with a well resolved stratosphere comprehensive AGCM (“high-top”) and re-assessing the contribution of non-linearity in the large-scale atmospheric circulation and regional extremes. For the mechanism underlying the non-linearity, it's possible that regional circulation response is more prone to develop with regionally confined forcing than extended forcing and therefore causes an over-estimation of the circulation response. But more work is needed to better understand it.

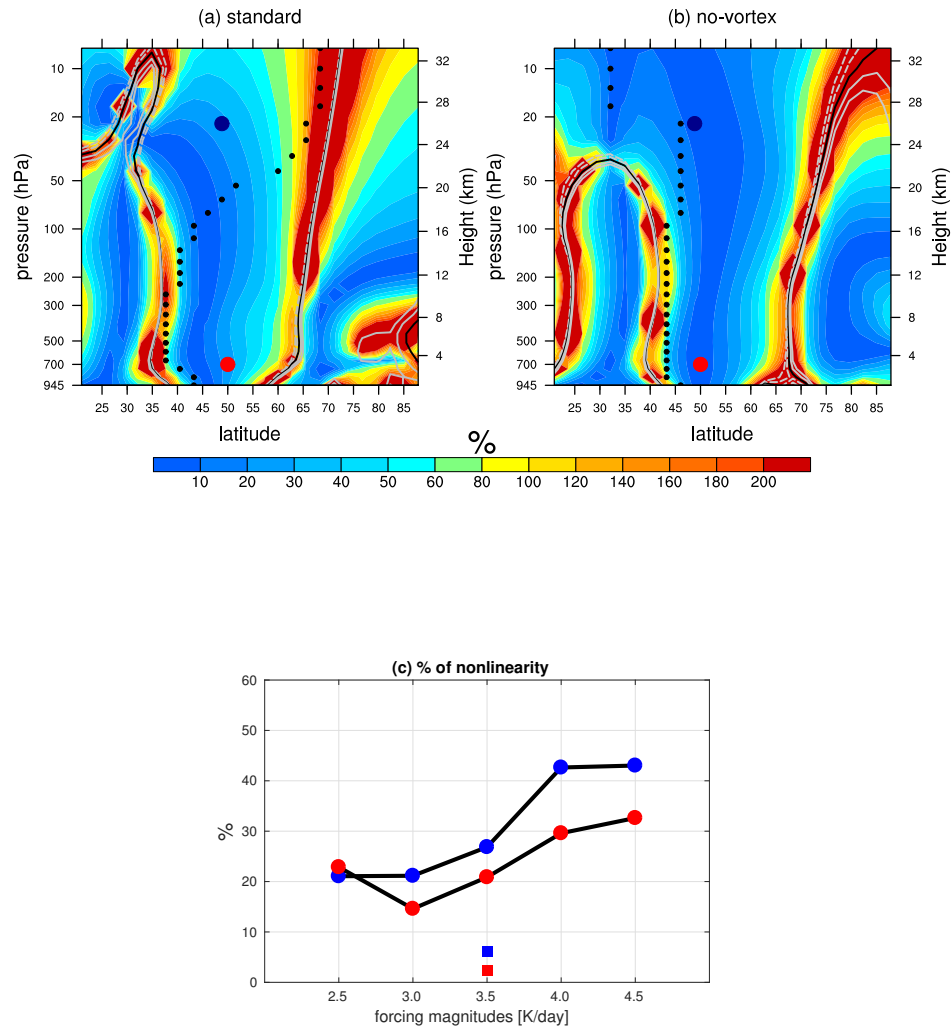


Figure 4.5. (a) Absolute value of percentage of non-linearity in zonal mean zonal wind response as obtained with 3.5 K/day forcing magnitude in FULL run. The ratio percentage is calculated as residual (Fig. 2f) divided by ALL (Fig. 2d). The values in the denominator (ALL) that lie between  $-0.2$  and  $+0.2$  m/s are shown in gray contours with contour interval of  $0.1$  m/s, where negative values are shown in dashed line, positive values are shown in solid line and zero value is shown in black. Black dots represent the climatological location of the jet maxima. (b) Similar to (a) except for the no-vortex runs. (c) Relation between the forcing magnitude and non-linearity ratio at 700hPa,  $50^\circ\text{N}$  (red dots, also in Fig. 3ab) and 20hPa,  $50^\circ\text{N}$  (blue dots, also in Fig. 3ab in dark blue dots), respectively, in FULL run. The corresponding values using no-vortex configuration are shown in squares.

## 5. CONCLUSIONS AND FUTURE DIRECTIONS

In this dissertation, we investigate the influences of the Arctic sea ice loss on the mid-latitudes by using a combination of observations and a hierarchy of climate models. The specific goal of our study is to explore and to quantify the role of stratosphere-troposphere coupling in linking the Arctic to the mid-latitudes during boreal winter. Throughout this thesis we aim to elucidate the chain of events linking the sea ice loss and its resulting responses in the surface warming, stratospheric polar vortex and tropospheric eddy driven jet, as summarized below.

In chapter 2, we examine the robustness of the hypothesis that Arctic sea ice variability can impact the mid-latitude wintertime circulation via the stratosphere, using a multi-model ensemble framework. We explore whether the comprehensive climate models that participated in the CMIP5 experiments are able to reproduce the observed delayed circulation response to Arctic sea ice loss and warming. We analyze two groups of coupled global climate models, with different model top heights and vertical resolutions, from the CMIP5 experiments. It is found that the models with well resolved stratosphere (high-top) simulate a stronger and prolonged circulation response compared to the models with poorly resolved stratosphere (low-top) in mid-winter as a result of autumn BKS SIC variability. In order to attribute the different circulation responses to the stratospheric dynamics, we systematically diagnose the dynamical pathway of the stratosphere-troposphere linkage in the two groups. The chain of events, that connects the autumn sea ice loss to the mid-latitude circulation in winter via a two-way stratosphere-troposphere interaction, shows consistent differences in responses between the two groups. Specifically, analysis of eddy heat flux suggests an enhanced upward propagation of planetary waves following constructive linear interference in the high-top models. Consequently a stronger weakening of the stratospheric polar vortex is found. During downward migration phase, the

phase-tilt of wave-1 geopotential height shows a long lasting stratosphere-troposphere coupling in the high-top models. The results demonstrate an important role of the stratosphere-troposphere interaction in establishing teleconnection between the Arctic and the mid-latitudes. Furthermore, the multi-model ensemble framework, using coupled models from the diverse modeling groups, minimizes the biases due to model physics and provides a robust assessment of the prolonged and remote impacts of the BKS SIC loss and the underlying dynamical pathway. The results suggest possible limitations in the low-top climate models, especially in understanding the NH weather and climate, that may be accountable for conflicting conclusions in the previous studies. Our study advocates to incorporate a well-resolved stratosphere in the global climate models for future improvement.

In Chapter 3, we further extend the study to explore the influence of the BKS SIC loss on the surface temperature budget using targeted modeling experiments. Specifically, we investigate the pattern of the Warm Arctic Cold Siberia and the underlying mechanism. We perform numerical model experiments using a comprehensive AGCM, with a well-resolved stratosphere, forced with BKS sea ice decline only. The model experiments produce a colder Siberia as a result of BKS sea ice decline. Furthermore, we identify that the temperature response is driven adiabatically by the large-scale dynamical adjustment due to the BKS SIC loss. It is the intensification of the meridional temperature advection from the Arctic, following an amplified ridge near the Ural Mountains and a downstream trough, that causes anomalous cold temperature over the Siberia. We find that the Siberia cooling is almost gone, following a weaker circulation anomaly, when we numerically suppress the influence of the stratosphere and isolate the tropospheric pathway in the AGCM experiment. Alternatively, the contribution from the stratospheric pathway only, largely simulates the intensified Ural ridge and downward trough associated with the Siberian cooling. The targeted experiments allow us to compare between relative contributions of the tropospheric and the stratospheric pathways, that suggests an important role of the stratosphere-troposphere coupling. Our study demonstrates that the colder Siberian winters are

consequence of the large-scale circulation changes driven by the BKS SIC loss via a “stratospheric bridge”. Therefore, we suggest that a strong autumn sea ice retreat over the BKS has important influence on the Siberian winter on an inter-annual timescale.

The key finding from the first two projects, using ensemble of coupled climate models and experiments in a comprehensive GCM, shows an important role of the stratospheric pathway in extending and amplifying the influence of the BKS SIC loss. In chapter 4, we were intrigued to extend the above diagnoses on the different regions of the Arctic such as East Siberia and Chukchi Sea (ESC) and Baffin Bay-David Strait and Labrador Sea (BDL). We assess whether the contributions of regional sea ice loss and AA on the atmospheric circulation are linearly additive using a simplified AGCM. We find that the regional AA has similar impacts on the tropospheric circulation with an equatorward shift of the mid-latitude tropospheric jet but differences are seen in the stratospheric responses. In particular, the stratospheric polar vortex weakens due to warming over BKS and BDL but strengthens due to warming over the ESC.

It is found that the stronger (weaker) stratospheric circulation response is consistent with the reduced (enhanced) vertical wave propagation following a destructive (constructive) linear interference between the wave responses with the climatology. More importantly, we identify that the zonal mean zonal wind responses to regional AA are not linearly additive and the sum of the regional responses over estimates the response to simultaneous forcing. As a result, a positive NAM-like vertically coherent response in mid-latitude circulation is seen in the residual term. Additional targeted experiments show that the non-linearity reduces significantly when we isolate the tropospheric dynamics only. Therefore, the stratosphere and its interaction with the troposphere plays a significant role in contributing to the non-linearity in atmospheric circulation responses to regional Arctic sea ice loss. The key finding from the idealized AGCM experiments suggest that studying the regional sea ice loss may not provide the full picture of the consequences of pan-Arctic sea ice loss especially in the decadal time scale. The pan-Arctic sea ice loss should be implemented in the studies where

the focus is the consequences of long-term SIC loss. Alternatively, because of the non-linearity, it is possible that the regional circulation responses are more sensitive to the regional sea ice loss on inter-annual time scale.

The major contributions in the thesis are summarized in the following:

- We show robust impacts of the Arctic sea ice loss on the mid-latitude circulation during boreal winter characterized by an equatorward shift of the tropospheric jet. The response is consistent for AA over different regions over the Arctic.
- We demonstrate that the stratosphere and its coupling with the troposphere plays an important role to establish teleconnection between the Arctic sea ice loss and the mid-latitudes. Specifically, we find a weaker (stronger) stratospheric polar vortex is associated with an increase (decrease) in vertical wave propagation following a constructive (destructive) linear wave interference between the wave responses with the climatology due to regional sea ice loss (Smith et al., 2010). More importantly, the stratospheric circulation anomaly descends into the troposphere that results in an intensified tropospheric circulation anomaly. The hypothesis is consistent for different regions of the Arctic using observations and a hierarchy of climate models.
- The results suggest that strong regional sea ice anomaly can affect the regional circulation and weather patterns on inter-annual time scale. For example, in comprehensive modeling experiment, we find that the autumn sea ice loss over the BKS can result in a colder Siberian winter. The finding is important for an improved seasonal forecast.
- Our study, in simplified AGCM experiment, suggests that the sea ice loss confined over different regions can non-linearly interact with each other and thus, result in different mid-latitude responses. Therefore, it is likely that the recently emerged temperature trend over Siberia is due to natural variability and not a result of BKS sea ice loss (Ogawa et al., 2018). More importantly, the

results advocate studying pan-Arctic sea ice loss to understand the long term consequences.

- Our study suggests that the representation of the stratospheric dynamics can be a major source of discrepancies in the existing modeling studies. For example, we explicitly quantify that the high-top multi-model mean from CMIP5 experiments can simulate an amplified and a prolonged tropospheric circulation response due to autumn BKS sea ice loss compared to the low-top counterpart. Additionally, the targeted experiments using comprehensive AGCM shows that an absence of a realistic stratosphere-troposphere coupling inhibits the model's ability to simulate the observed Siberian cooling. We also note that most of the modeling studies that can not reproduce Siberian cooling used a low-top model (McCusker et al., 2016, for example) in contrast with the studies that simulated Siberian cooling in a high-top model (Mori et al., 2014, for example). Therefore, our findings advocate to incorporate well resolved stratospheric dynamics for further improvement of the global climate models.
- The non-linear interaction among the regional AA suggests that different spatial patterns of the prescribed sea ice forcing in the previous modeling studies can be accountable for conflicting conclusions (Pedersen et al., 2016; Screen, 2017; Sun et al., 2015). Therefore, the studies should exercise caution in studying the regional cases which may not provide the full consequences of the pan-Arctic sea ice loss.

Overall, the thesis contributes towards an improved understanding of the underlying mechanism of the remote impacts of the Arctic on the mid-latitude circulation. We suggest more future work is needed to diagnose the complex dynamics and achieve a better understanding of how and to what extent the rapidly changing Arctic is important for the climate system. Some of the future directions and possible extension from our work is described below:

- It is interesting that, in chapter 2, we do not find Siberian cooling using multi-model ensemble of CMIP5 models. Alternatively, the warm ocean basins that extends upto the lower latitudes of the North Atlantic suggest that a thermodynamic effect, due to ocean coupling, may compensate the dynamical cooling in the coupled models (Deser et al., 2016, 2015). Although the Siberian cooling remains about the same with or without an ocean coupling in Deser et al. (2016), it would be worth extending the AGCM experiment, presented in chapter 3, using a coupled model. In particular, an assessment of the contributions of the stratosphere in presence of an active ocean component would be an important step forward.
- The work presented in chapter 4, using a dry dynamical core, complements the previous finding by Screen (2017) in comprehensive AGCM experiments. An important extension of the analysis would be to investigate how the non-linear interaction among regional AA affects the regional weather, using a comprehensive AGCM with prescribed SIC forcing. In particular, it would be worth checking how the Arctic can influence the North American weather and the underlying dynamics for that.
- Several other factors, such as ENSO and sea surface temperature (SST), contribute to influence the stratospheric circulation and regional weather in winter. In addition, the weakening and equatorward shift of the mid-latitude jet due to AA could be offset by upper tropospheric warming in response to enhanced greenhouse gas. Therefore, a major step forward would be to disentangle the relative contributions of the AA, from the non-Arctic factors, on the mid-latitude circulation and weather.

## REFERENCES

- Ahn, J., Hong, S., Cho, J., Lee, Y.-W., and Lee, H. (2014). Statistical modeling of sea ice concentration using satellite imagery and climate reanalysis data in the barents and kara seas, 1979-2012. Remote Sensing, 6:5520–5540.
- Bader, J., Mesquita, M. D. S., Hodges, K. I., Keenlyside, N., Sterhus, S., and Miles, M. (2011). A Review on Northern Hemisphere Sea-ice, Storminess and the North Atlantic Oscillation: Observations and Projected Changes. Atmos. Res., 101:809–834.
- Baldwin, M. P. and Dunkerton, T. J. (2001). Stratospheric Harbingers of Anomalous Weather Regimes. Science, 294:581–584.
- Barnes, E. A. and Screen, J. A. (2015). The Impact of Arctic Warming on the Midlatitude Jet-Stream: Can it? Has it? Will it? Wiley Interdiscip Rev Clim Change, 6.3:277–286.
- Barnes, E. A. and Simpson, I. R. (2017). Seasonal Sensitivity of the Northern Hemisphere Jet-Streams to Arctic Temperatures on Subseasonal Timescales. J. Clim., 30(24):10117–10137.
- Boland, E. J. D., Bracegirdle, T. J., and Shuckburgh, E. F. (2017). Assessment of Sea ice-Atmosphere Links in CMIP5 Models. Clim Dyn, 49:683–702.
- Cai, D., Dameris, M., Garny, H., and Runde, T. (2012). Implications of All Season Arctic Sea-Ice Anomalies on the Stratosphere. Atmos. Chem. Phys., 12:11819-11831.
- Cassano, E. N., Cassano, J. J., Higgins, M. E., and Serreze, M. C. (2014). Atmospheric Impacts of an Arctic Sea Ice Minimum as Seen in the Community Atmosphere Model. International Journal of Climatology, 34:766–779.

- Cavalieri, D. J., Parkinson, C. L., Gloersen, P., and Zwally, H. J. (1996). Sea ice concentrations from nimbus-7 smmr and dmsp ssm/i-ssmis passive microwave data, version 1. [NASA National Snow and Ice Data Center Distributed Active Archive Center](#).
- Charlton-Perez, A. J., Baldwin, M. P., Birner, T., Black, R. X., Butler, A. H., Calvo, N., Davis, N. A., Gerber, E. P., Gillett, N., Hardiman, S., Kim, J., Krger, K., Lee, Y., Manzini, E., McDaniel, B. A., Polvani, L., Reichler, T., Shaw, T. A., Sigmond, M., Son, S., Toohey, M., Wilcox, L., Yoden, S., Christiansen, B., Lott, F., Shindell, D., Yukimoto, S., and Watanabe, S. (2013). On the lack of stratospheric dynamical variability in low-top Versions of the CMIP5 Models. [J. Geophys. Res. Atmos.](#), 118:2494–2505.
- Charney, J. G. and Drazin, P. G. (1961). Propagation of Planetary-Scale Disturbances From the Lower Into the Upper Atmosphere. [J. of Geophys. Res.](#), 66:83–109.
- Chen, X. and Luo, D. (2017). Arctic Sea Ice Decline and Continental Cold anomalies: Upstream and Downstream Effects of Greenland Blocking. [Geophysical Research Letters](#), 44:3411–3419.
- Cohen, J., Foster, J., M.Barlow, Saito, K., and Jones, J. (2010). Winter 2009-2010: A Case Study of an Extreme Arctic Oscillation Event. [Geophys. Res. Lett.](#), 37:L17707.
- Cohen, J., Screen, J. A., Furtado, J. C., Barlow, M., Whittleston, D., Coumou, D., Francis, J., Dethloff, K., Entekhabi, D., Overland, J., and Jones, J. (2014). Recent Arctic Amplification and Extreme Mid-latitude Weather. [Nat. Geosci.](#), 7:627–637.
- Collins, M. and Coauthors (2013). Long-term Climate Change:Projections, Commitments and Irreversibility. [Climate Change 2013: The Physical Science Basis](#), pages 1029 –1136.
- Collins, M., Knutti, R., Arblaster, J., Dufresne, J.-L., Fichet, T., Friedlingstein, P., Gao, X., Gutowski, W. J., Johns, T., Krinner, G., Shongwe, M., Tebaldi, C.,

- Weaver, A. J., and Wehner, M. (2013). Long-term climate change: Projections, commitments and irreversibility, pages 1029–1136. Cambridge University Press, Cambridge, UK.
- Comiso, J. C. (2000). Bootstrap Sea Ice Concentrations from Nimbus-7 SMMR and DMSP SSM/I-SSMIS, Version 2, [1979-2013]. Boulder, Colorado USA. NASA DAAC at the National Snow and Ice Data, page <http://dx.doi.org/10.5067/J6JQLS9EJ5HU>.
- De, B. and Wu, Y. (2018). Robustness of the Stratospheric Pathway in Linking the Barents-Kara Sea Sea Ice Variability to the Mid-latitude Circulation in CMIP5 Models. Climate Dynamics.
- Dee, D. P. and Coauthors (2011). The ERA-Interim Reanalysis: Configuration and Performance of the Data Assimilation System. Q.J.R. Meteorol. Soc., 137:553–597.
- Deser, C., Sun, L., Tomas, R. A., and Screen, J. (2016). Does Ocean Coupling Matter for the Northern Extratropical Response to Projected Arctic Sea Ice Loss? Geophys. Res. Lett., 43:2149–2157.
- Deser, C., Tomas, R. A., and Sun, L. (2015). The Role of OceanAtmosphere Coupling in the Zonal-Mean Atmospheric Response to Arctic Sea Ice Loss. J Clim, 28:2168–2186.
- Edmon, H. J., Hoskins, B. J., and McIntyre, M. E. (1980). Eliassen-Palm Cross Sections for the Troposphere. J. Atmos. Sci., 37:2600–2616.
- Francis, J. A. (2017). Why are arctic linkages to extreme weather still up in the air? Bulletin of the American Meteorological Society, 98:2551–2557.
- Francis, J. A., Skific, N., and Vavrus, S. J. (2018). North american weather regimes are becoming more persistent: Is arctic amplification a factor? Geophysical Research Letters, 45:11,414–11,422.

- Francis, J. A. and Vavrus, S. J. (2012). Evidence Linking Arctic amplification to Extreme Weather in Mid-latitudes. Geophys. Res. Lett., 39:L06801.
- Furtado, J. C., Cohen, J. L., Butler, A. H., Riddle, E. E., and Kumar, A. (2015). Eurasian Snow Cover Variability and Links to Winter Climate in the CMIP5 Models. Clim Dyn, 45:2591–2605.
- Garfinkel, C. I., Hartmann, D. L., and Sassi, F. (2010). Tropospheric Precursors of Anomalous Northern Hemisphere Stratospheric Polar Vortices. J Clim, 23:3282–3299.
- Garfinkel, C. I., Shaw, T. A., Hartmann, D. L., and Waugh, D. W. (2012). Does the Holton-Tan Mechanism Explain How the Quasi-Biennial Oscillation Modulates the Arctic Polar Vortex? J. of the Atmos. Sci., 69:1713–1733.
- Gerber, E. P., Butler, A., Calvo, N., Charlton-Perez, A., Giorgetta, M., Manzini, E., Perlwitz, J., Polvani, L. M., Sassi, F., Scaife, A. A., Shaw, T. A., Son, S. W., and Watanabe, S. (2012). Assessing and understanding the impact of stratospheric dynamics and variability on the earth system. Bulletin of the American Meteorological Society.
- Gong, T., Feldstein, S., and Lee, S. (2017). The Role of Downward Infrared Radiation in the Recent Arctic Winter Warming Trend. J Clim, pages 4937–4949.
- Held, I. M. and Suarez, M. J. (1994). A Proposal for the Intercomparison of the Dynamical Cores of Atmospheric General Circulation Models. Bull. Amer. Meteor. Soc., 75:1825–1830.
- Hoshi, K., Ukita, J., Honda, M., Iwamoto, K., Nakamura, T., Yamazaki, K., Dethloff, K., Jaiser, R., and Handorf, D. (2017). Poleward Eddy Heat Flux Anomalies Associated with Recent Arctic Sea Ice Loss. Geophys. Res. Lett., 44:446–454.

- Jaiser, R., Dethloff, K., and Handor, D. (2013). Stratospheric Response to Arctic Sea Ice Retreat and Associated Planetary Wave Propagation Changes. Tellus, 65A:19375.
- Kelleher, M. and Screen, J. (2018). Atmospheric Precursors of and Response to Anomalous Arctic Sea Ice in CMIP5 Models. Advances in Atmospheric Sciences, 35:27–37.
- Kidston, J. and Gerber, E. (2010). Intermodel Variability of the Poleward Shift of the Austral Jet stream in the CMIP3 Integrations Linked to Biases in 20th Century Climatology. Geophys. Res. Lett., 37:L09 708.
- Kim, B.-M., Son, S.-W., Min, S.-K., Jeong, J.-H., Kim, S.-J., Zhang, X., Shim, T., and Yoon, J.-H. (2014). Weakening of the Stratospheric Polar Vortex by Arctic Sea Ice Loss. Nat. Commun., 5:4646.
- Koenigk, T., Caian, M., Nikulin, G., and Schimanke, S. (2016). Regional Arctic Sea Ice Variations as Predictor for Winter Climate Conditions. Clim Dyn, 46:317–337.
- Kug, J. S., Jeong, J. H., Jang, Y. S., Kim, B. M., Folland, C. K., Min, S. K., and Son, S. W. (2015). Two Distinct Influences of Arctic Warming on Cold Winters Over North America and East Asia. Nat Geosci, 8:759–762.
- Lee, Y.-Y. and Black, R. X. (2015). The structure and dynamics of the stratospheric northern annular mode in cmip5 simulations. Journal of Climate, 28:86–107.
- Lu, J. and Cai, M. (2009). Seasonality of Polar Surface Warming Amplification in Climate Simulations. Geophys. Res. Lett., 36:L16704.
- Manzini, E., Karpechko, A. Y., Anstey, J., Baldwin, M. P., Black, R. X., Cagnazzo, C., Calvo, N., Charlton-Perez, A., Christiansen, B., Davini, P., Gerber, E., Giorggetta, M., Gray, L., Hardiman, S. C., Lee, Y.-Y., Marsh, D. R., McDaniel, B. A., Purich, A., Scaife, A. A., Shindell, D., Son, S.-W., Watanabe, S., and Zappa, G. (2014). Northern Winter Climate Change: Assessment of Uncertainty in

- CMIP5 Projections Related to Stratosphere-Troposphere Coupling. J. Geophys. Res. Atmos., 119:7979–7998.
- McCusker, K. E., Fyfe, J. C., and M, M. S. (2016). Twenty-Five Winters of Unexpected Eurasian Cooling Unlikely due to Arctic Sea-Ice Loss. Nat. Geosci., 9:838–842.
- McGraw, M. and Barnes, E. A. (2018). Memory Matters: A Case for Granger Causality in Climate Variability Studies. J. Clim.
- McKenna, C. M., Bracegirdle, T. J., Shuckburgh, E. F., Haynes, P. H., and Joshi, M. M. (2018). Arctic Sea Ice Loss in Different Regions Leads to Contrasting Northern Hemisphere Impacts. Geophysical Research Letters, 45:945–954.
- Mori, M., Watanabe, M., H., H. S., Inoue, J., M., and Kimoto (2014). Robust Arctic Sea-Ice Influence on the Frequent Eurasian Cold Winters in Past Decades. Nat. Geosci., 7:869–873.
- Nakamura, T., Yamazaki, K., Iwamoto, K., Honda, M., Miyoshi, Y., Ogawa, Y., Tomikawa, Y., and Ukita, J. (2016). The Stratospheric Pathway for Arctic Impacts on Midlatitude Climate. Geophys. Res. Lett., 43:3494–3501.
- Ogawa, F., Keenlyside, N., Gao, Y., Koenigk, T., Yang, S., Suo, L., Wang, T., Gastineau, G., Nakamura, T., Cheung, H. N., Omrani, N.-E., Ukita, J., and Semenov, V. (2018). Evaluating impacts of recent arctic sea ice loss on the northern hemisphere winter climate change. Geophysical Research Letters, 45:3255–3263.
- Overland, J. E., Dethloff, K., Francis, J. A., Hall, R. J., Hanna, E., Kim, S. J., Screen, J. A., Shepherd, T. G., and Vihma, T. (2016). Nonlinear Response of Mid-Latitude Weather to the Changing Arctic. Nature Climate Change, 6:992–999.
- Overland, J. E. and Wang, M. (2018). Arctic-Midlatitude Weather Linkages in North America. Polar Science, 16:1–9.

- Overland, J. E., Wood, K. R., and Wang, M. (2011). Warm Arctic-Cold Continents: Climate Impacts of the Newly Open Arctic Sea. Polar Research, 30(1):15787.
- Pedersen, R. A., Cvijanovic, I., Langen, P. L., and Vinther, B. M. (2016). The impact of regional arctic sea ice loss on atmospheric circulation and the nao. Journal of Climate, 29(2):889–902.
- Pithan, F. and Mauritsen, T. (2014). Arctic Amplification Dominated by Temperature Feedbacks in Contemporary Climate Models. Nat. Geosci, 7:181–184.
- Polvani, L. M. and Kushner, P. J. (2002). Tropospheric Response to Stratospheric Perturbations in a Relatively Simple General Circulation Model. Geophys. Res. Lett., 29:1114.
- Polvani, L. M. and Waugh, D. (2004). Upward Wave Activity Flux as Precursor to Extreme Stratospheric Events and Subsequent Anomalous Surface Weather Regimes. J. Clim, 17:3548–3554.
- Rodwell, M. J. and Hoskins, B. J. (2001). Subtropical anticyclones and summer monsoons. Journal of Climate, 14(15):3192–3211.
- Sassi, F., Garcia, R. R., Marsh, D., and Hoppel, K. W. (2010). The Role of the Middle Atmosphere in Simulations of the Troposphere During Northern Hemisphere Winter: Differences Between High- and Low-Top Models. J. of the Atmos. Sci., 67:3048–3064.
- Screen, J., C.Deser, , and Sun, L. (2015). Projected Changes in Rgional Climate Extremes Arising from Arctic Sea Ice Loss. Environ. Res. Lett., 10:084006.
- Screen, J. A. (2017). Simulated Atmospheric Response to Regional and Pan-Arctic Sea Ice Loss. J Clim, 30:3945–3962.
- Screen, J. A., Bracegirdle, T. J., and Simmonds, I. (2018a). Polar climate change as manifest in atmospheric circulation. Current Climate Change Reports, 4:383–395.

- Screen, J. A., Deser, C., Simmonds, I., and Tomas, R. (2014). Atmospheric Impacts of Arctic Sea-Ice Loss, 1979–2009: Separating Forced Change from Atmospheric Internal Variability. Clim Dyn, 43:333–344.
- Screen, J. A., Deser, C., Smith, D., Zhang, X., Blackport, R., Kushner, P. J., Oudar, T., McCusker, K., and Sun, L. (2018b). Consistency and Discrepancy in the Atmospheric Response to Arctic Sea-ice Loss Across Climate Models. Nat Geosci, 11:155–163.
- Screen, J. A. and Simmonds, I. (2010). The Central Role of Diminishing Sea Ice in Recent Arctic Temperature Amplification. Nature, 464:1334–1337.
- Screen, J. A., Simmonds, I., Deser, C., and Tomas, R. (2013). The Atmospheric Response to Three Decades of Observed Arctic Sea Ice Loss. J Clim, 26:1230–1248.
- Serreze, M. C. and Barry, R. G. (2011). Processes and impacts of arctic amplification: A research synthesis. Global and Planetary Change, 77:85 – 96.
- Shaw, T. A. and Perlwitz, J. (2010). The Impact of Stratospheric Model Configuration on Planetary-Scale Waves in Northern Hemisphere Winter. J. Clim, 23:3369–3389.
- Shaw, T. A., Perlwitz, J., and Weiner, O. (2014). Troposphere-Stratosphere Coupling: Links to North Atlantic Weather and Climate, Including Their Representation in CMIP5 Models. J. Geophys. Res. Atmos., 119:5864–5880.
- Shepherd, T. G. (2016). Effects of a Warming Arctic. Science, 353:989–990.
- Simpson, I., Hitchcock, P., Seager, R., and Wu, Y. (2019). The role of the stratosphere in future mid-latitude climate projections. USClivar Variations, 17:1–7.
- Simpson, I. R., Blackburn, M., and Haigh, J. D. (2009). The Role of Eddies in Driving the Tropospheric Response to Stratospheric Heating Perturbations. J. Atmos. Sci., 66:1347–1365.

- Smith, K. L., Fletcher, C. G., and Kushner, P. J. (2010). The Role of Linear Interference in the Annular Mode Response to Extratropical Surface Forcings. J Clim, 23:6036–6050.
- Smith, K. L., Neely, R. R., Marsh, D. R., and Polvani, L. M. (2014). The specified chemistry whole atmosphere community climate model (sc-waccm). Journal of Advances in Modeling Earth Systems, 6(3):883–901.
- Strey, S. T., Sara, T., Chapman, W. L., and Walsh, J. E. (2010). The 2007 Sea Ice Minimum: Impacts on the Northern Hemisphere Atmosphere in Late Autumn and Early Winter. J. of Geophys. Res., 115:D23103.
- Sun, L., Deser, C., and Tomas, R. (2015). Mechanisms of Stratospheric and Tropospheric Circulation Response to Projected Arctic Sea Ice Loss. J Clim, 28:7824–7845.
- Sun, L., Perlwitz, J., and Hoerling, M. (2016). What Caused the Recent Warm Arctic, Cold Continents Trend Pattern in Winter Temperatures? Geophys. Res. Lett., 43:5345–5352.
- Taylor, K. E., Stouffer, R., and Meehl, G. (2012). An Overview of CMIP5 and the Experiment Design. Bull. Amer. Meteor. Soc., 93:485–498.
- Thompson, D. W. J. and Wallace, J. M. (1998). The arctic oscillation signature in the wintertime geopotential height and temperature fields. Geophysical Research Letters, 25(9):1297–1300.
- Vihma, T. (2014). Effects of arctic sea ice decline on weather and climate: a review. Surv. Geophys., 35:1175–1214.
- Waugh, D. W., Sobel, A. H., and Polvani, L. M. (2017). What is the polar vortex and how does it influence weather? Bulletin of the American Meteorological Society, 98(1):37–44.

- Wu, Q. and Zhang, X. (2010). Observed Forcing-Feedback Processes Between Northern Hemisphere Atmospheric Circulation and Arctic Sea Ice Coverage. J. Geophys. Res. Atmos., 115:D14119.
- Wu, Y. and Smith, K. L. (2016). Response of Northern Hemisphere Midlatitude Circulation to Arctic Amplification in a Simple Atmospheric General Circulation Model. J. Clim., 29:2041–2058.
- Yang, X.-Y., Yuan, X., and Ting, M. (2016). Dynamical Link Between the Barents-Kara Sea Ice and the Arctic Oscillation. J. Clim., 29:5103–5122.
- Zappa, G., Pithan, F., and Shepherd, T. G. (2018). Multimodel Evidence for an Atmospheric Circulation Response to Arctic Sea Ice Loss in the CMIP5 Future Projections. Geophys. Res. Lett., 45:1011–1019.
- Zhang, P., Wu, Y., Simpson, I. R., Smith, K. L., Zhang, X., De, B., and Callaghan, P. (2018). A Stratospheric Pathway Linking a Colder Siberia to Barents-Kara Sea Ice Loss. Science Advances, 4.
- Zhang, P., Wu, Y., and Smith, K. L. (2017). Barents Kara Sea Sea Ice Variability to the Midlatitude Circulation in a Simplified Model. Clim Dyn., pages 1–13.

## A. SUPPLEMENTARY ILLUSTRATIVE MATERIAL

First three figures are for the second chapter and the following five figures are for the fourth chapter.

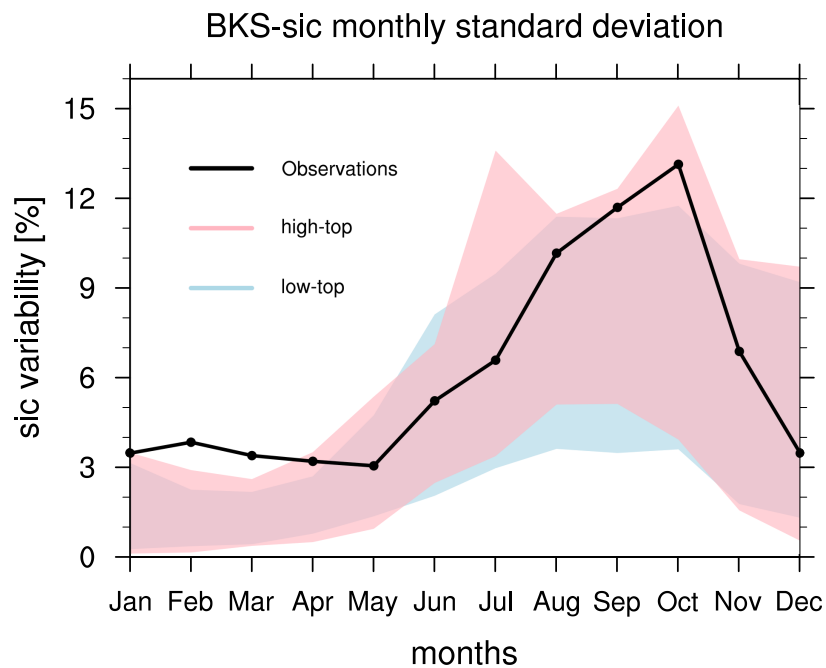


Figure A.1. Multi-model spread in monthly BKS SIC among the high-top (in light red) and low-top (in light blue) models and in the observations (black line).

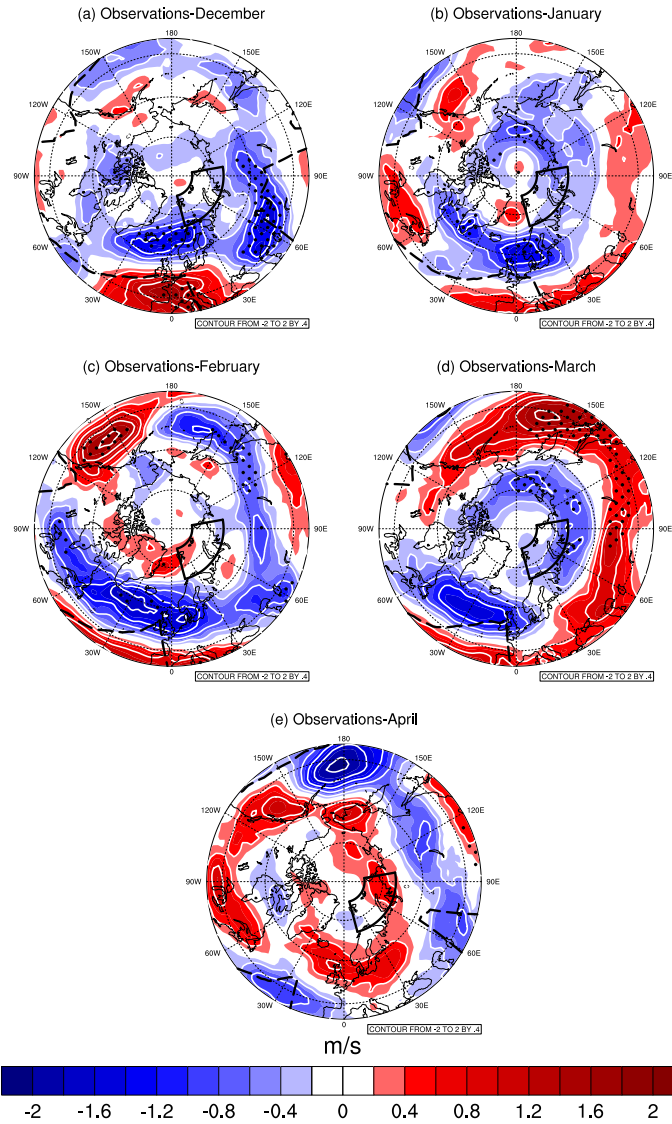


Figure A.2. Response of 700mb zonal wind anomaly (in m/s per 1 standard deviation of BKS SIC loss) in winter months in observations due to BKS SIC loss in the previous November and December. The sign is reversed for the normalized BKS SIC to emphasize the SIC loss. The dashed black line indicates the climatological jet position. The BKS region is highlighted in thick black box. The dots indicate that the responses are statistically significant at the 95% confidence level..

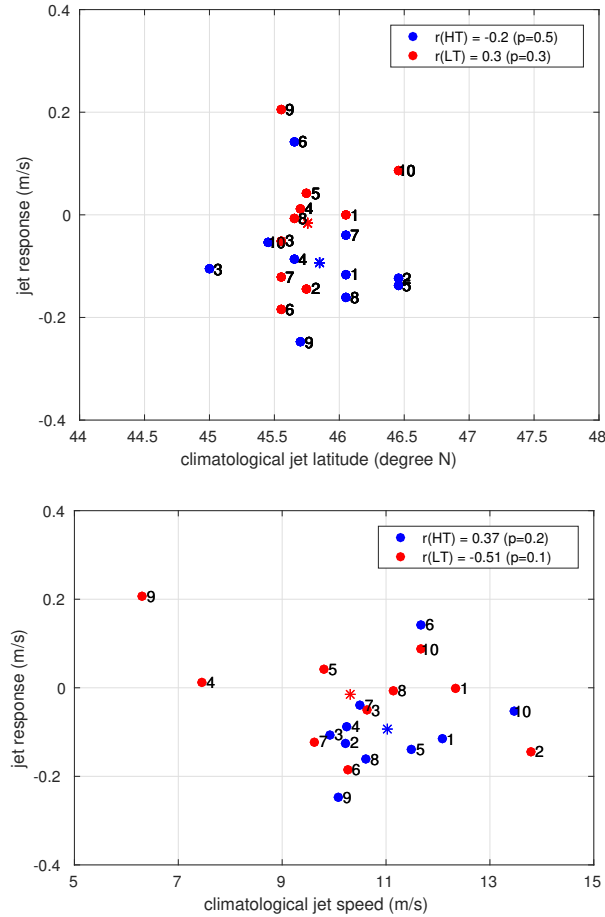


Figure A.3. Response in jet speed (in m/s per 1 standard deviation of BKS SIC loss) over the region with the strongest weakening (45° – 90°N and 315° – 360°E) vs. climatological jet latitude (in °N) and climatological jet speed (in m/s) over the North Atlantic sector (45° – 90°N and 270° – 360°E) in (a) upper panel and (b) lower panel, respectively. The numbers represent the corresponding high-top models (in blue) and low-top models (in red) listed in Tables 2.1 and 2.2. The multi-model mean is shown as star in blue for high-top and in red for low-top, respectively. The correlation coefficient ( $r$ ) and  $p$ -value are shown in the legend for high-top and low-top models, respectively

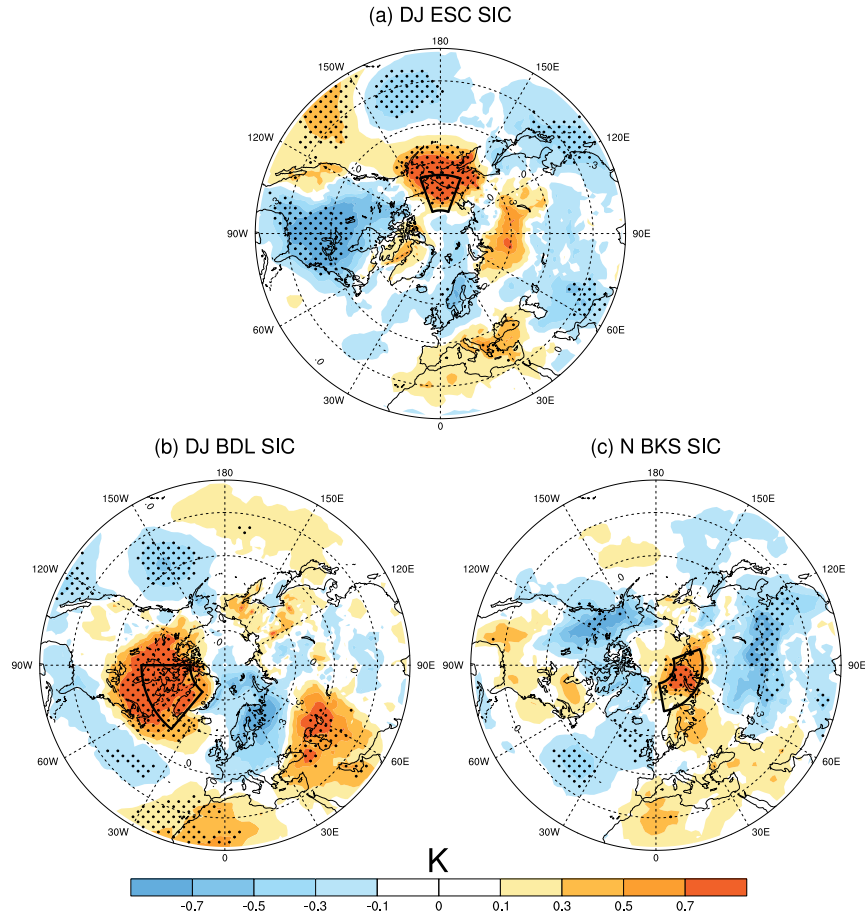


Figure A.4. Response of detrended surface air temperature (SAT) (in K per 1 standard deviation of SIC loss) during Dec. and Jan. associated with concurrent SIC loss in Dec. and Jan. (DJ) over the (a) ESC and (b) BDL regions, respectively. (c) shows the SAT response during Nov. due to SIC loss over BKS in Nov (N). The black box highlights the (a) ESC, (b) BDL and (c) BKS area, respectively. The dots indicate that the response is statistically significant at the 95% confidence level using t-test.

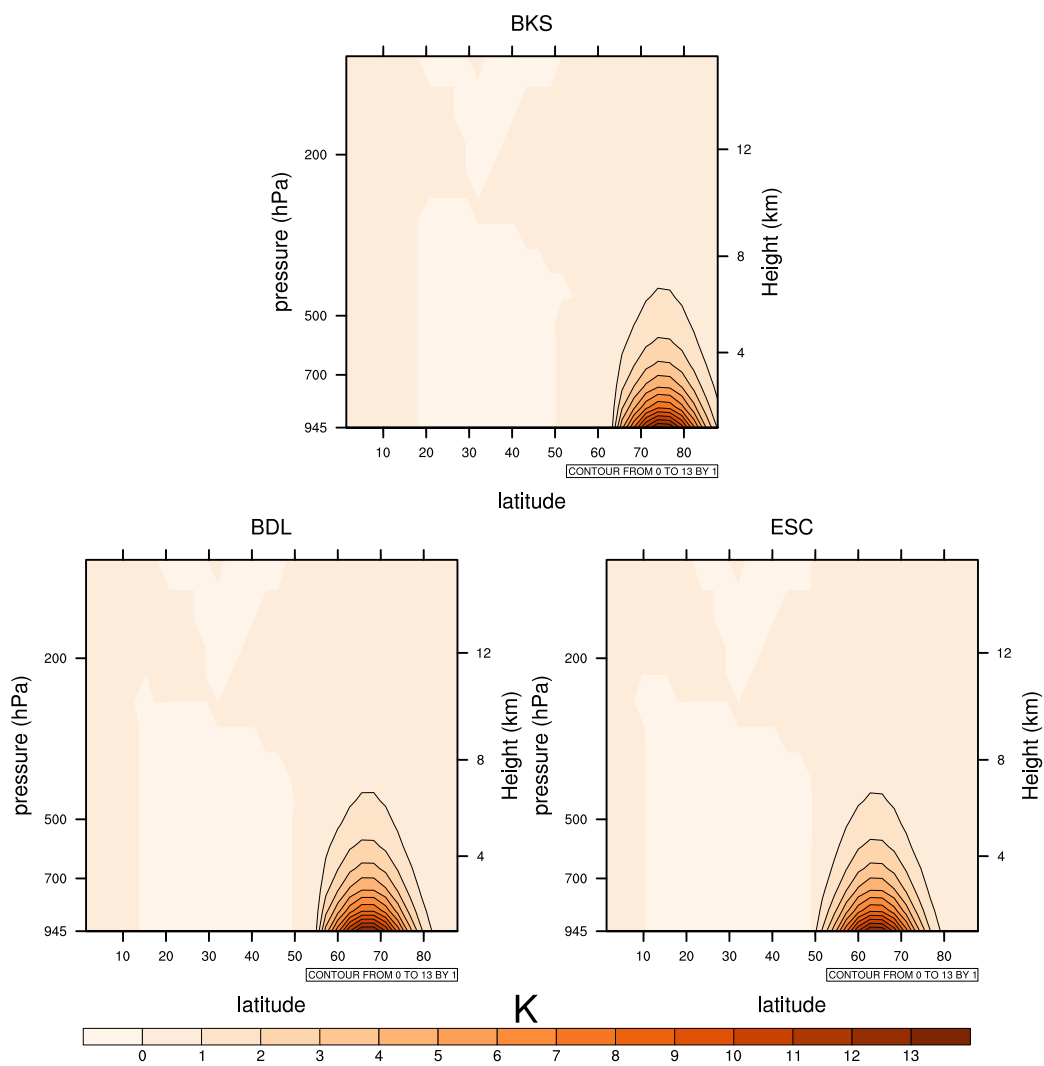


Figure A.5. Vertical profile of zonal mean of prescribed heating rate with a forcing magnitude of 3.5 K/day over ESC, BDL and BKS, respectively. Contour interval is 0.2 K/day.

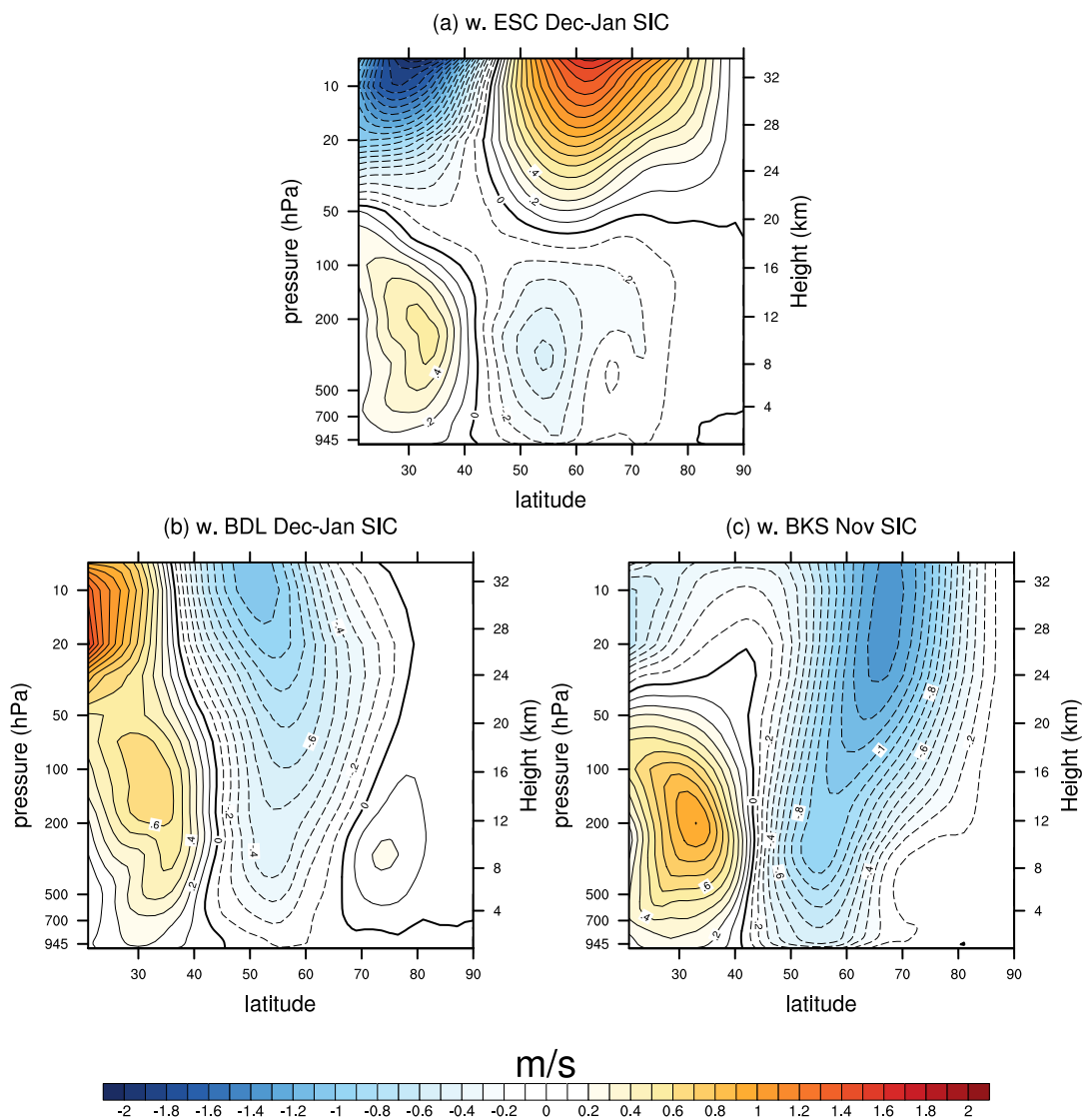


Figure A.6. Response of detrended zonal mean zonal wind anomaly (in m/s per 1 standard deviation of SIC loss) during Dec-Jan-Feb associated with SIC loss in (a) Dec-Jan over ESC, (b) Dec-Jan over BDL and (c) Nov over BKS, respectively, in both color shadings and contours.

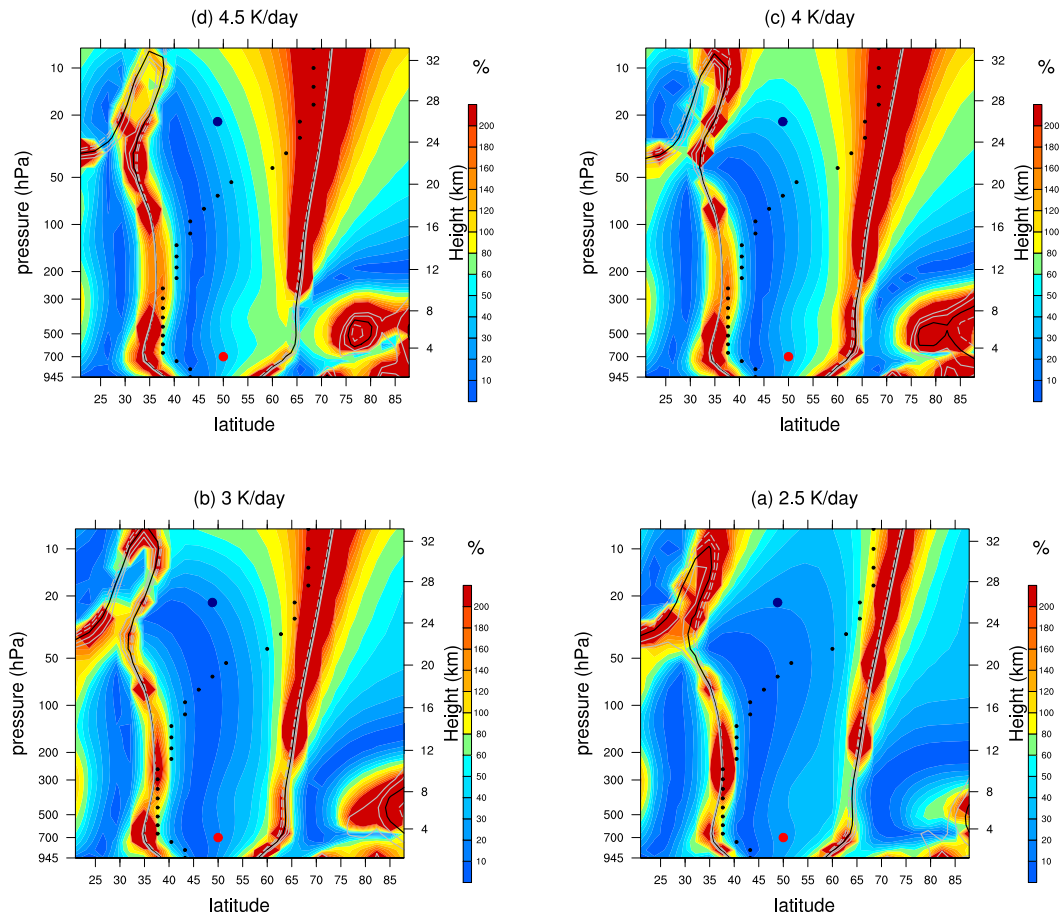


Figure A.7. Similar to Fig. 4.5 (a) except for forcing magnitude of (a) 2.5 K/day, (b) 3 K/day, (c) 4 K/day and (d) 4.5 K/day, respectively.